AD-779 856

STUDIES IN THE MARGINAL ICE ZONE OF THE CHUKCHI SEA: ANALYSIS OF 1972 DATA

Gerald R. Garrison, et al

Washington University

Prepared for:

Naval Undersea Center
Advanced Research Projects Agency

14 March 1974

Studies in the Marginal Ice Zone of the Chukchi Sea

Analysis of 1972 Data

by G. R. Garrison
E. A. Pence
H. R. Feldman
S. R. Shah

PREPARED FOR:

ARCTIC SUBMARINE LABORATORY, CODE 90
NAVAL UNDERSEA CENTER, SAN DIEGO, CALIFORNIA
UNDER CONTRACT N00123-71-C-1333, ARPA ORDER NO. 1782

APL-UW 7311
14 March 1974

CONTENTS

I. INTRODUCTION

The 1972 Pacific Marginal Ice Zone Study (MIZPAC-72) by the Applied Physics Laboratory was conducted in the Chukchi Sea between 20 July and 18 August from the USCGC STATEN ISLAND and a drifting ice floe. The objective of the study was to obtain useful data on the phenomena encountered during the previous summer--namely, the warm water intrusion from the south, the resulting thermal fine structure and its effect on acoustic transmissions, and the volume reverberation produced by biological scattering layers. Reference 1 describes the 1971 investigations in the Chukchi and Beaufort Seas.

A 1-day helicopter survey was made in April to observe spring oceanographic conditions. The work in the summer from the icebreaker consisted mainly of two cruises, conducted during the first and last weeks of the study, and was designed to obtain an overall description of the temperature and salinity distribution and the biological scattering layers in the marginal ice zone (MIZ) of the Chukchi Sea as well as some knowledge of the changes that occur during the summer.

The studies made from the ice floe required a stable platform from which measurements over fixed dimensions could be made. Temperature-depth profiles of the water under the floe were taken simultaneously from several stations to determine the outline of the thermal layers. In conjunction with the temperature profiles, underwater acoustic pulses were transmitted from one station to another to determine variations in acoustic propagation related to the thermal structure. The floe remained in the MIZ until the last day when it was carried into the Beaufort Sea by a strong current along the coast.

This report contains the analysis of the 1972 data which have been published in detail in Ref. 2. Most of the data required to substantiate the conclusions made in this report are repeated here. The remaining data in Ref. 2 may be of use to oceanographers and arctic investigators with interests in studies other than those conducted by the authors.

Local daylight time, Greenwich time less 9 hours, is used throughout this report.

II. SUMMARY

Spring Conditions

In late April, a helicopter was employed to land on various ice floes from which a temperature probe was lowered to the sea bottom to obtain temperature-depth profiles of the water. At the time, the 15-mile expanse of nearly open water off Barrow had a temperature near the freezing point. The only warmer water detected was a -1.4°C layer at a depth of 30 m near the shore-fast ice 20 miles southwest of Barrow. The origin of this layer is unknown.

Weather

During the August field studies hourly observations of the wind speed and direction, atmospheric pressure, air temperature and visibility were recorded manually while the ice floe was occupied. Floe orientation and water depth were also noted. The weather ranged from clear days with cold nights to rainy days with relatively warm nights. The air temperature varied between 32 and 53°F (0 and 11°C), the barometer reading had a high of 30.28 in. (76.7 cm) and a low of 29.28 in. (74.4 cm), and the wind speed ranged from 0 to 30 mph.

There had been continual easterly winds during July and it is likely this wind was the force keeping the intrusion of warm Pacific water in the western portion of the Chukchi Sea. The sunny days and light rains caused considerable surface melting, but this ablation appeared minor compared to the loss of ice beneath the surface.

Currents

The drift of the occupied ice floe, at first slowly southward and then rapidly to the northeast, indicates, as in 1971, a strong flow northeasterly along the coast which appears to create an eddy that carries the ice lying north of the stream southward into the main flow/current.

Current measurements relative to the floe, combined with floe drift records, show that the floe usually followed the main under-ice current at 60 to 80% of the speed of the water.

Warm Intrusions

In late July the intrusion of Pacific water from the Bering Strait appeared as a warm 10-m deep surface layer extending across the western portion of the Chukchi Sea. This intrusion corresponded to an absence of ice cover as far north as latitude 73°.

In the eastern Chukchi Sea the intrusion along the coast of Alaska was small compared to the previous summer and was mainly on the surface. The failure of the warm intrusion to spread northward allowed the heavy ice cover to exist a few miles north of Barrow in early August. In mid-August the intrusion along the coast reached 8°C but remained within 5 miles of the coast at Barrow.

Volume Reverberation

Extensive measurements of volume reverberation were made during two 1-week cruises in the Chukchi Sea before and after the ice floe occupation. The instrumentation consisted of two downward-looking, narrow-beamed, echo-sounding systems at frequencies of 38 and 105 kHz. System self-noise was such that the instrumentation could detect volume scattering strengths above -85 dB (ref. 1 m^{-1}). Biological samples were taken simultaneously to identify the scatterers. In all, 179 data files were taken at 100 different locations: 98 files at 105 kHz, of which 7 files were taken by helicopter, and 81 files at 38 kHz.

Examination of the data reveals that the acoustic scattering strength can vary greatly from location to location even within a few miles. Occasional scattering layers were observed at all depths, and many biological species were collected. An especially high scattering strength was observed in the warm surface layer resulting from the intrusion of Pacific water.

Scattering strengths as high as -40 dB were found. The scattering strength of a typical layer was -50 to -70 dB. Numerous single targets were also occasionally observed at all depths. The overall uncertainty in the measurement of the scattering strength in a depth interval was approximately ±3 dB. The measurements at 38 kHz often correlated well with those at 105 kHz, but sometimes they did not. These data have been augmented by data collected in 1973 at these frequencies and at 60 kHz. We plan to improve our biological sampling methods and to add a 250-kHz system for detecting smaller organisms.

Thermal Fine Structure

To measure thermal microstructure, a large ice floe was provided with four stations on the corners of a 140-m square, each station being equipped for taking temperature profiles. Profiles were taken simultaneously at the four stations every hour, except during the 2 days when profiles were taken at 15-min intervals for 6 hours.

For the first several days the floe drifted slowly southward through the transition region between the winter water and the warm intrusion along the coast. This transition region contained thermal microstructure with temperature excursions of ±0.1°C. As the floe moved southward into

the coastal current, a predominant warm layer appeared at the surface and larger microstructure, ±0.2° to ±0.3°C, appeared at the lower depths. This structure represents horizontal layers several hundred meters in extent with an average thickness of about 3 m.

Acoustic Transmissions

Transmissions of underwater sound pulses at 60 kHz were made between two stations on the ice floe at hourly intervals coincident with the temperature profile schedule. Variations of 5 to 10 dB were often observed in the region of the thermal microstructure at a range of 200 m. These variations occurred for low angle transmissions and are predictable from sound ray calculations.

Helicopter Oceanography

To demonstrate the feasibility of using helicopters to take measurements in the marginal ice zone, we often made use of a Coast Guard helicopter. After locating an open lead in the ice, the helicopter would hover for 5 to 10 min just above the water while a transducer or temperature probe was lowered beneath the surface. If equipment is kept light and measurements can be taken quickly, helicopters provide a rapid means of investigating a large area.

III. FIELD TRIP

The 1-month summer operation consisted of two 1-week cruises on an icebreaker across the Chukchi Sea and a 2-week drift on an ice floe. A summary of the activities is given in Table I.

Table I. Itinerary for MIZPAC-72.

20 July	Depart Barrow on STATEN ISLAND
20 July	Barrow Line
24 July	Wainwright Line
25 July	Icy Cape Line
26 July	Chukchi Sea Crossing
28 July	Wainwright Line
29 July	Search for Suitable Floe
30 July	To Barrow
31 July	Depart from Barrow
1 Aug	Ice Camp Established
4 Aug	Barrow Line
5 Aug	Wainwright Line
7 Aug	Wainwright to Ice Camp
12 Aug	Abandon Ice Camp
13 Aug	Barrow Line
14 Aug	Wainwright Line
15 Aug	Chukchi Sea Crossing
17 Aug	Southward Crossing
19 Aug	Arrive Nome

Support

The USCGC STATEN ISLAND (Figure 1) supplied the main support for the operation. Its NAVSAT equipment provided valuable navigational information throughout the project and ship's personnel took Nansen casts as requested to provide a check on the accuracy of the CTD measurements.

In addition to providing reconnaissance flights, the ship's two helicopters served as platforms for oceanographic measurements. One helicopter contained a temperature-depth probe with cable and recording equipment; as the helicopter hovered 3 m above the water, the probe was lowered slowly to a depth of 50 m and then recovered. The other helicopter carried the volume reverberation equipment; while the helicopter hovered, the transducer was suspended just below the surface for about 10 minutes to take volume reverberation measurements (see Figure 2). Before lowering any equipment into the sea, it was necessary to drop the helicopter's sling cable into the water to discharge the static electricity that had built up on the helicopter.

Figure 1. STATEN ISLAND alongside ice floe camp.

The Coast Guard radio station at the Naval Arctic Research Laboratory (NARL) gave considerable assistance to the project, providing radio communication between the ship and personnel at NARL.

Food, tents, gasoline, propane and clothing required for the ice camp were provided by NARL. NARL also served as a base of operations and provided food and lodging for personnel awaiting transportation to ship or airport.

Instrumentation aboard the icebreaker for measuring temperature and salinity profiles and volume reverberation was provided by the Applied Physics Laboratory. (This equipment has been described in Ref. 1, a report on 1971 MIZPAC studies.) Special equipment for taking plankton samples was provided by the University of Washington's Oceanography Department.

Two Omega receivers were provided by the U.S. Naval Oceanographic Office. One was operated at NARL and the other was installed at the ice floe camp. There were various problems with the Omega system, especially with operating procedures. For example, we were not aware of a 1 sec delay between station WWV and the start of the Omega cycle, nor that the Japanese station on channel H was operating on an experimental schedule. We were also confused about the time the New York Omega station was replaced by the North Dakota station in segment D. In addition, sun flare activity interfered with reception of both the Omega and WWV signals; even when reception improved and some of the confusing signals were properly interpreted, the few fixes obtained were still a few miles from the NAVSAT positions.

Figure 2. Helicopter hovering for underwater reverberation measurement.

Ice Floe Camp

The search for a suitable ice floe took place on 29 July. Two helicopters covered a 10-mile square, stopping briefly at each corner of the area to obtain a temperature profile. Several floes were found and one near the ship was selected for investigation (see Figure 3). The commanding officer of the STATEN ISLAND, along with APL representatives, walked over the floe and drilled several holes tc measure the ice thickness. The large smooth area along one side, an attractive feature, showed an ice thickness of 8 ft. The ridged area was assumed to be much thicker. Because the STATEN ISLAND had to pick up personnel and supplies at Barrow before a camp could be established, we built a 10-ft tower on the highest point of the floe, installed a 1.35-MHz radio beacon, and stretched a 400-ft antenna from the tower to anchors in the ice.

On 1 August the STATEN ISLAND returned from Barrow and proceeded to the position determined for the floe 3 days earlier. At first the radio direction finder gave some misleading information, but after repairs were made the floe was relocated easily. Much of the ice along the outer edge of the flat area had vanished but the floe appeared to be satisfactory for a 2-week camp.

All building materials, equipment and supplies were transferred from the ship to the floe. Four stations, at the corners of a square, were established on the floe and two APL representatives were assigned to each station. Each station contained a tent for living quarters and a work hut covered with a plastic tarp (see Figure 4). A central tent, supplemented by a plastic-covered hut, was used for preparing meals. Photographs of the individual camps are shown in Figure 5.

Each station was provided with a temperature probe, cable and recorder for measuring temperature profiles. Simultaneous temperature measurements were scheduled at all four stations every hour. In addition, a conductivity probe was included with the profiling equipment at Station 2, and a transducer and receiver were provided at Station 1 to record the sound level profile from a transmitter placed beyond Station 2. Equipment was also provided for measuring wind speed, floe orientation, water depth, air pressure and temperature, and current magnitude and direction.

Holes for the equipment were drilled with a 9-in. ice auger or melted with a propane-fueled hot-water ice melter (Ref. 1). Many of the holes passed through about 8 ft of ice into a 2 or 3 ft pocket of water followed by more ice. This type of ice structure caused difficulty for the drill and also for the ice melter since the hot water was flushed away through the cavity.

Figure 3. Ice floe selected for the ice camp.

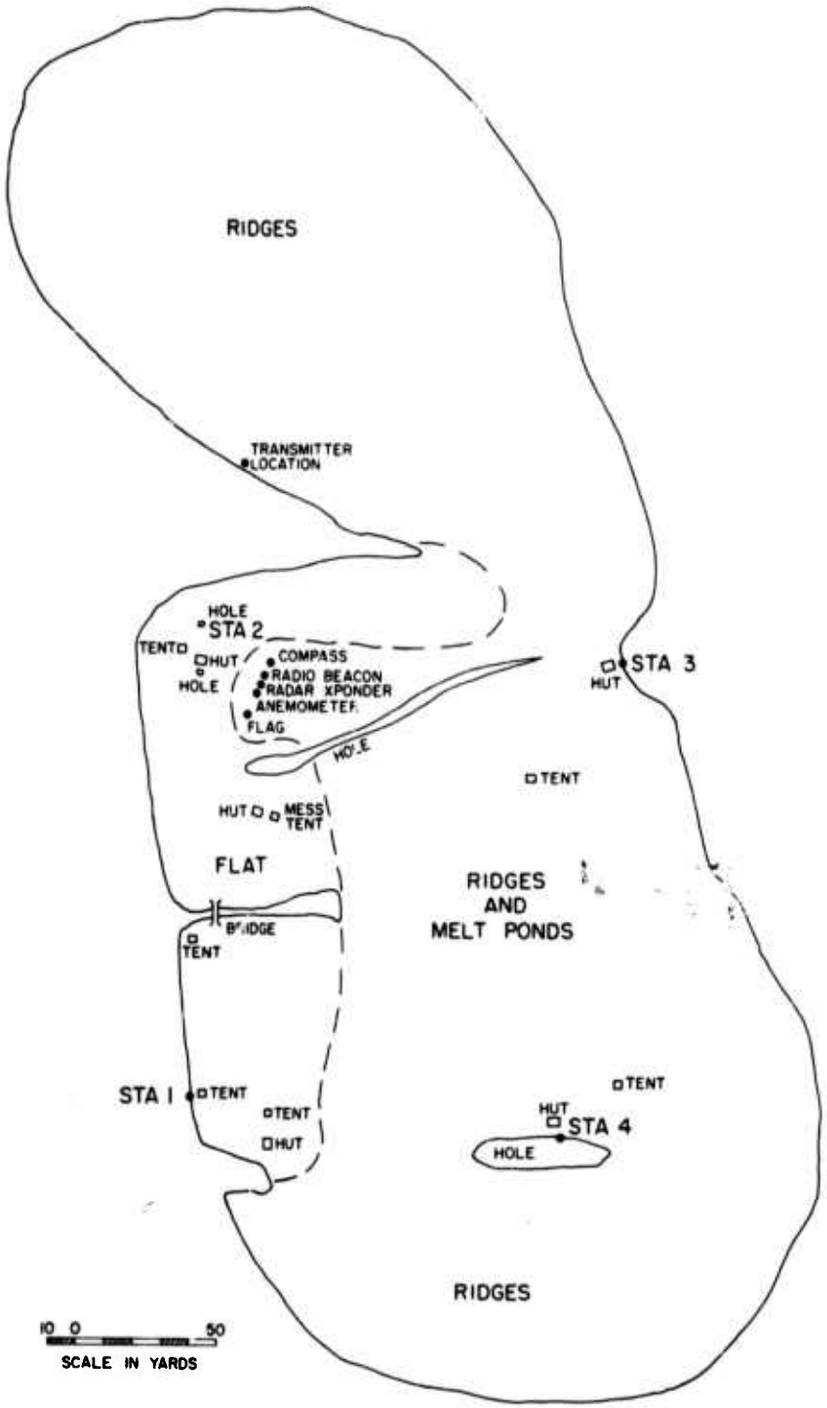

Figure 4. Sketch of the ice floe.

Station 2
Work Shelter

Station 1
Work Shelter

Central Cook Tent

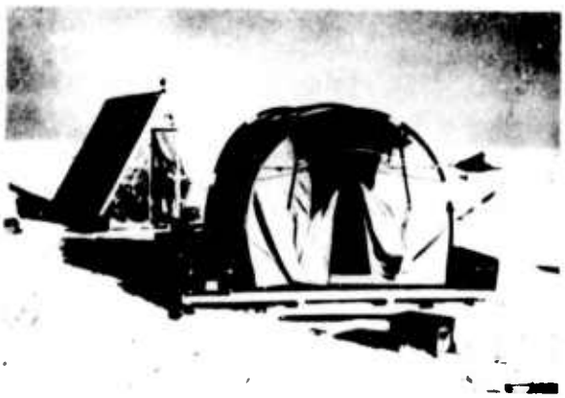

Station 1 Sleeping Tent
and Work Shelter

Station 4 Work Shelter

Figure 5. Ice camp structures.

Three stations were in operation by 3 August and the fourth by 5 August. Profile data were taken regularly until 11 August, when all gear was packed for loading on the icebreaker the next day.

Figure 6 is the track of the ice floe plotted from navigational fixes determined by the STATEN ISLAND, using NAVSAT to determine the ship's position and then radar or visual sightings to determine the relative position of the ice floe. In the figure a point represents every 6 hours of travel and a short cross line represents the start of each day. The drift speed increased to 0.8 kn on 10 August and to 1.3 kn on 11 August, causing considerable streaming of the profiling cables. Fortunately, most of the planned measurements were completed by this time.

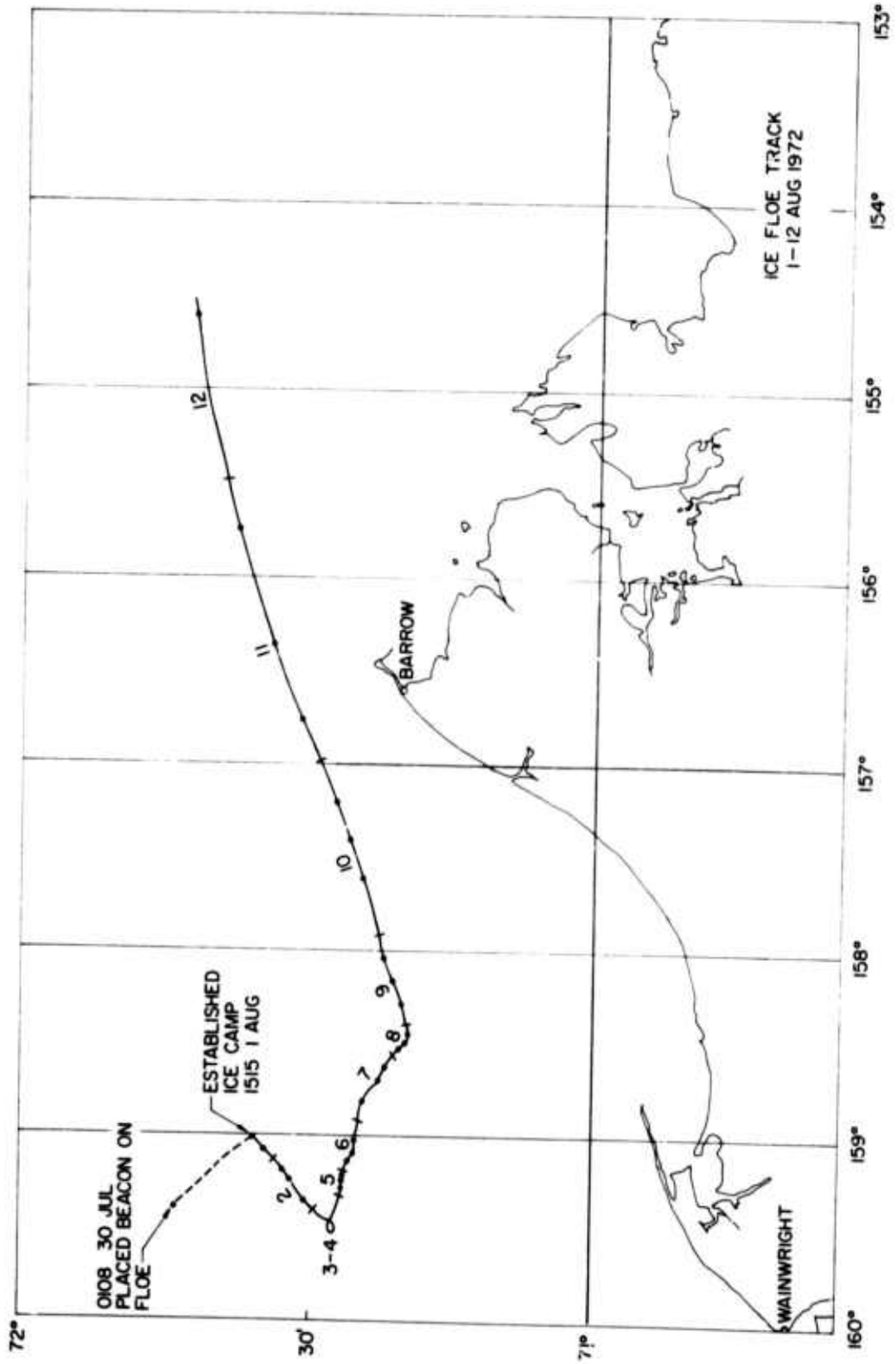

Figure 6. Drift track of the occupied ice floe.

IV. ENVIRONMENTAL DATA

Although measurements of the environment are highly desirable when studying any natural phenomenon, such measurements can also reduce the time and effort available for studying the variables of primary interest. As a compromise, environmental data-gathering was limited to current and weather measurements when personnel were available.

Current Measurements

Current-measuring probes were lowered by hand from the ice floe. The measurements were time consuming and had a low priority, so current data are sparse and irregular. A summary of the measurements is given in Table II.

Table II. Summary of current measurements, 1972.

Date	Number of Profiles: Speed	Direction	
3 Aug	3		
4 Aug	3	1	
5 Aug	3	2	
6 Aug	1		
7 Aug	3	3	
8 Aug	3	3	
9 Aug	2	1	
10 Aug	5	5	(20-40 m only)
11 Aug	1		

The equipment used to measure current speed consisted of a Savonius rotor and a Vibrotron® pressure transducer attached to the end of electrical cables that were married to a strain line. A 4-lb weight was suspended below the rotor. The pulses from the Savonius reed switch (actuated by the rotor magnets), along with the Vibrotron signal, were fed to counters at the surface where they were read and recorded manually. The direction unit consisted of a large vane and flux-gate compass, along with a Vibrotron, and was operated on a separate strain line. The outputs of the compass and Vibrotron were read and recorded manually at the surface.

From 3 to 7 August speed profiles were taken by lowering the instrument slowly while manually recording the Vibrotron output and rotor count. Later, the instrument was held at each depth long enough to get a stable reading. The current measurements are relative to the floe, which was usually moving. Direction profiles were taken separately. The instrument

was stopped at every meter of depth to record the magnetic direction of the current flow. The direction vane was then dragged along the bottom to obtain the direction of the floe's movement. These data are presented in Figures 7-9. The reading near the bottom is an indication of the actual speed of the floe with respect to the bottom. When both the speed and direction of the floe's movement are known, the current reading can be corrected.

Prior to 7 August the current speed was less than 10 cm/sec and the direction was fairly constant at depths below 10 m. On 7 August the floe picked up speed to 19 cm/sec in a southeasterly direction (Figure 6) and the current relative to the floe was about 15 cm/sec in a northerly direction (Figure 9). Adding the two vectors gives an absolute current of 24 cm/sec at 72° true. Later in the day the relative current and the floe drift speed decreased (Figure 10) with an indication at 1830 that the current had stopped and the floe was continuing, giving a relative current to the west. Near the end of the day the relative current dropped below 10 cm/sec in a southeasterly direction. Since the floe was nearly stationary, this indicates the speed and direction of absolute current.

On 8 August the floe was moving at about 8 cm/sec in the same direction as the relative current, which dropped to 5 cm/sec (see Figure 11).

On 9 August the floe picked up speed to 20 cm/sec at 70° true. With a relative current of 15 cm/sec at 46° true (see Figure 12), the computed absolute current was 34 cm/sec at 60° true. At this time the floe moved at 60% of the speed of the water.

On 10 August the floe moved east-northeast at 35 cm/sec and the relative current built up to 25 cm/sec in the same direction, indicating an absolute current of 60 cm/sec (see Figure 13). Again, the floe moved at 60% of the water speed.

On 11 August the floe drift track shows a speed of about 100 cm/sec. A relative current of 20 cm/sec was measured at 15 m, indicating an absolute current of 120 cm/sec if we assume the direction was parallel to the drift. At depths from 20 to 30 m the relative current was near zero (see Figure 14). The increase in relative speed below 30 m may indicate a current in the opposite direction, in which case it would represent water moving slower than the floe. Unfortunately, no direction measurements were made at that time.

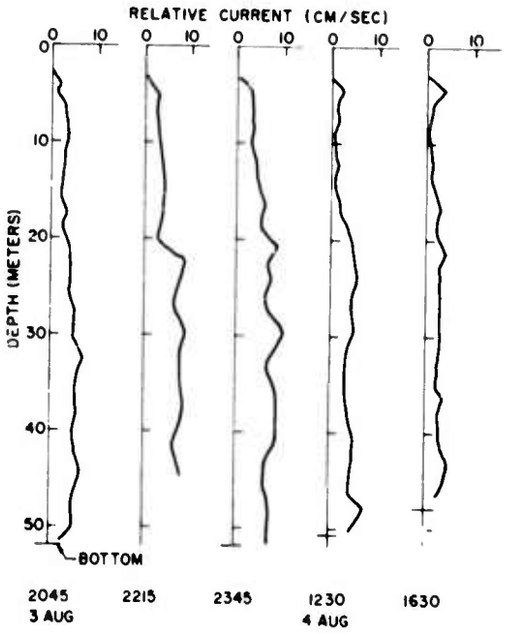

Figure 7. Current measurements from the ice floe on 3 and 4 August.

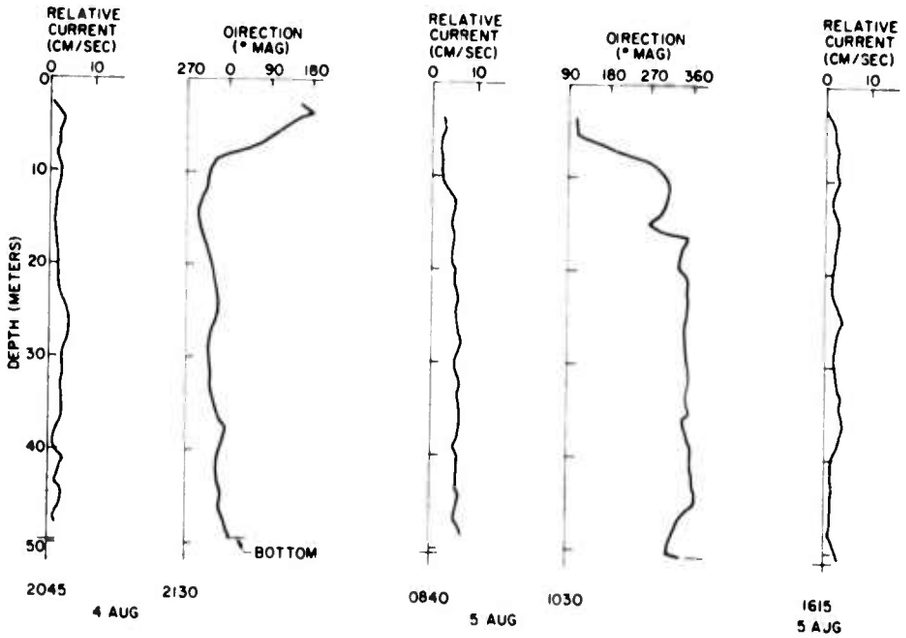

Figure 8. Current measurements from the ice floe on 4 and 5 August.

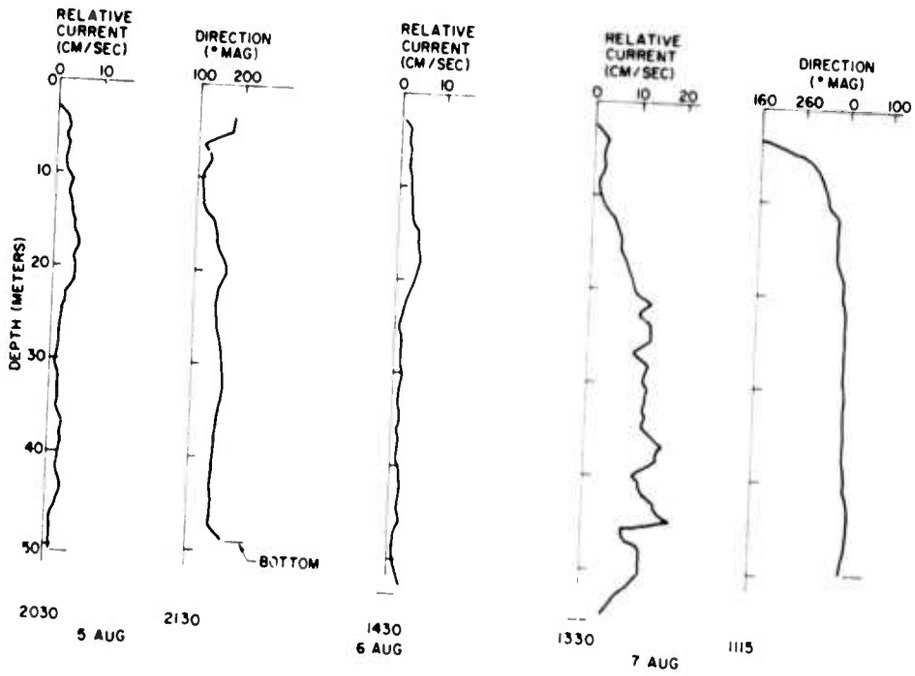

Figure 9. Current measurements from the ice floe on 5-7 August.

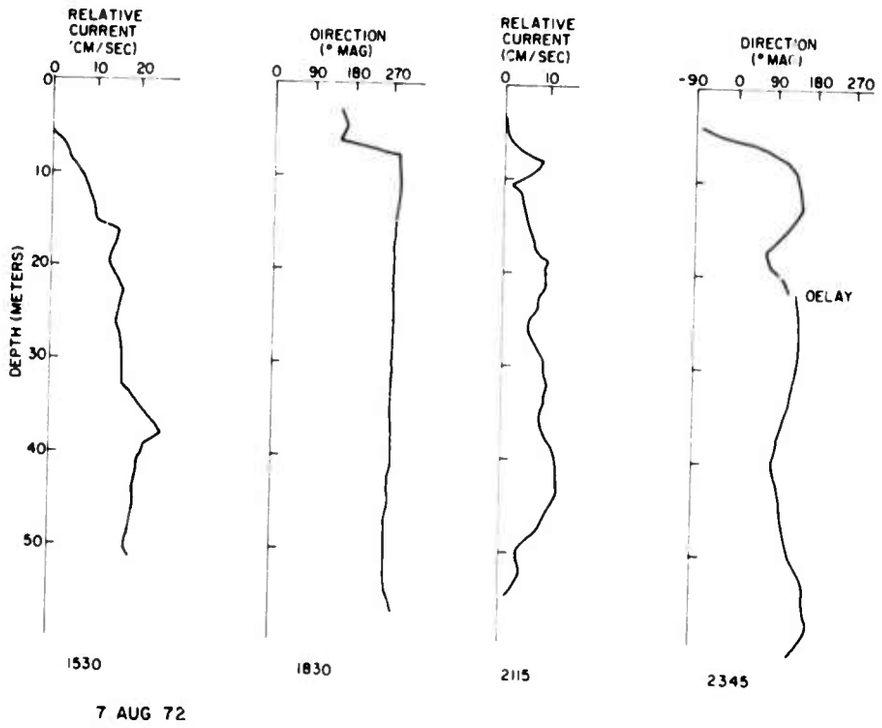

Figure 10. Current measurements from the ice floe on 7 August.

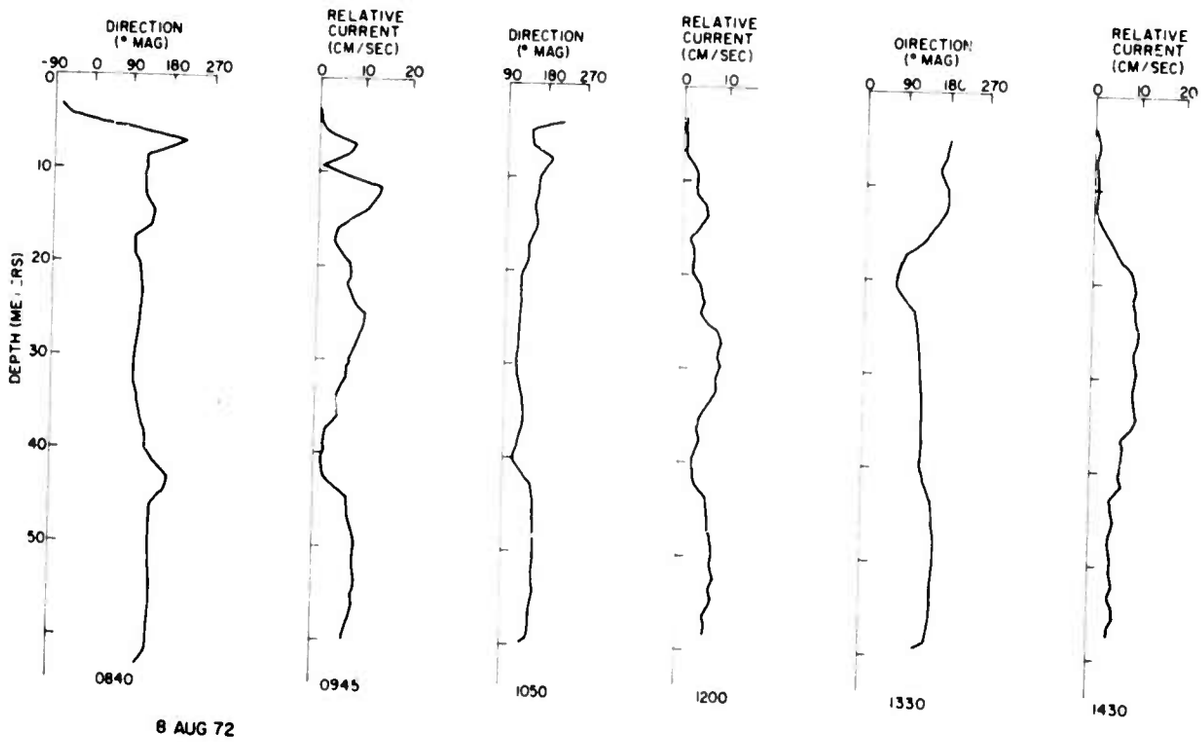

Figure 11. Current measurements from the ice floe on 8 August.

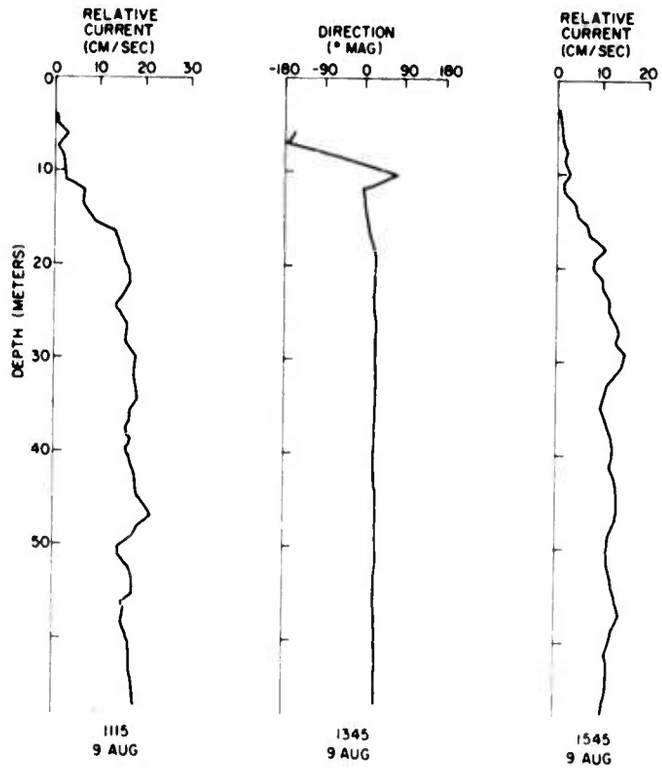

Figure 12. Current measurements from the ice floe on 9 August.

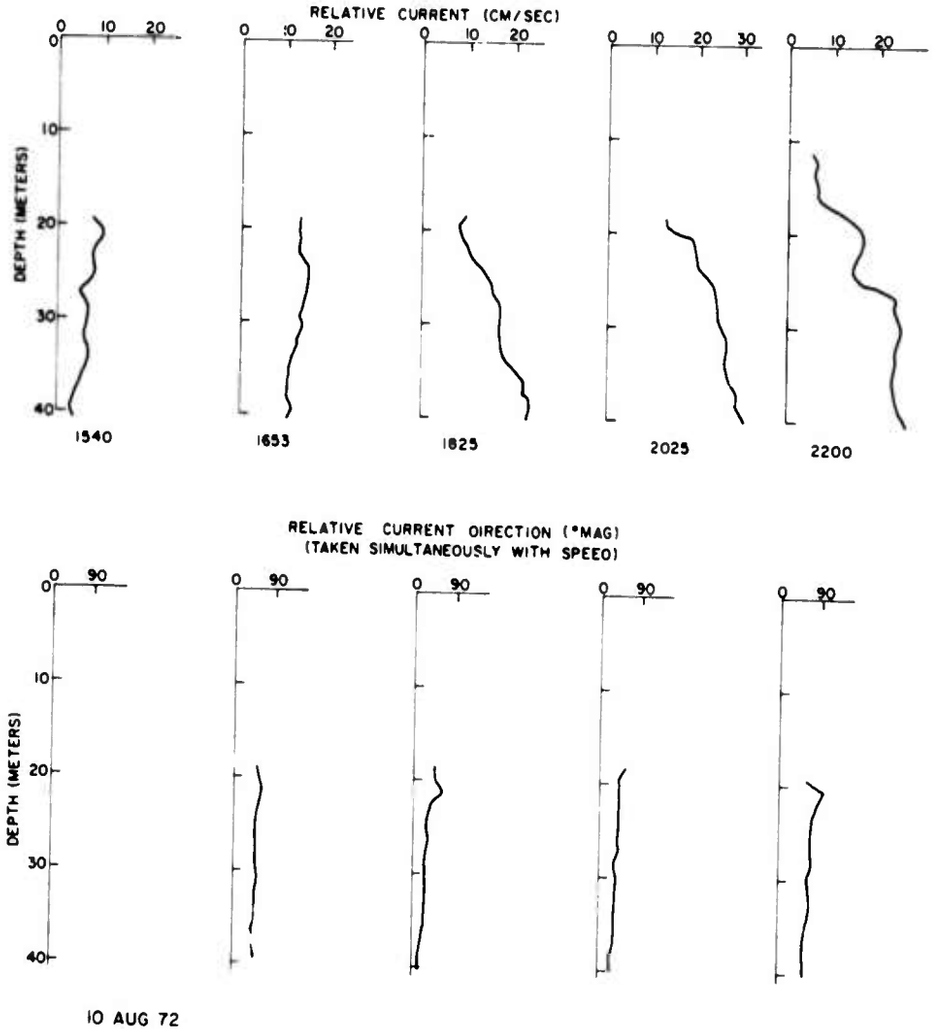

Figure 13. Current measurements from the ice floe on 10 August.

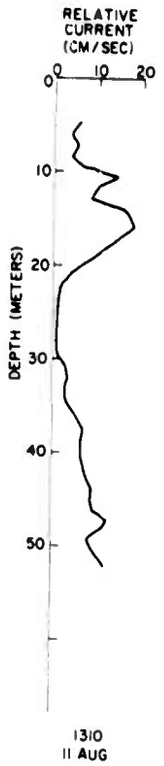

Figure 14. Current measurements from the ice floe on 11 August.

Weather Measurements

Weather observations and readings of several instruments were taken hourly about 16 hours each day for the period of the ice floe occupation, 2-12 August. Graphs for the 10-day period are plotted in Figures 15 and 16.

The wind speed was measured with a three-cup anemometer mounted on a 12-ft pole. A magnetic pick-off sent electrical pulses to a counter at the foot of the pole. Wind speeds were low except for winds of 20-30 mph on 6 August and 15-20 mph on 8 August.

Wind direction was estimated by facing the wind and noting the direction on the compass. Winds were from the east at first, changing to westerly on 5 August and continuing westerly or southwesterly until the floe was abandoned on 12 August.

The barometric pressure was recorded by an aircraft altimeter with a barometric correction. The correction control was varied to bring the altitude to zero and the barometric pressure was then obtained by reading the control setting. These data are plotted in Figure 16.

Air temperature was measured with a thermocouple meter sheltered from the sun. The temperature usually dropped to near freezing at night. On sunny days it rose as high as 52°F and during rainy days varied between 40°F and 45°F. Each temperature measurement, converted to degrees Celsius, is plotted in Figure 16.

The effect of the wind on the floe can be observed by comparing the floe orientation and wind characteristics in Figure 15 with the floe drift track in Figure 6. The high winds of 6 and 7 August from 300° true north apparently caused the floe to move with the wind toward 120°. A lull in the wind early on 8 August corresponds with the slow drift of the floe on that date. On 9 August the floe apparently entered the coastal current and was carried northeastward with steadily increasing speed despite the lull in the wind for the next two days.

This correlation between floe drift and wind or current suggested the possibility of predicting the drift track of the floe from the influence of the wind, which was measured, and the current, which had to be estimated. The transfer of momentum from wind to floe and from current to floe also had to be estimated. A simple current pattern was chosen, namely, 0.45 kn at 195° true north except near the coast where it was assumed to be 1.60 kn at 070°. (It was assumed that the floe was in the first current through 7 August, then in the other current for the remainder of the drift.) The assumption was made that the drift velocity $\vec{D}$ is related to the current $\vec{C}$ and the wind $\vec{W}$ by the vector equation

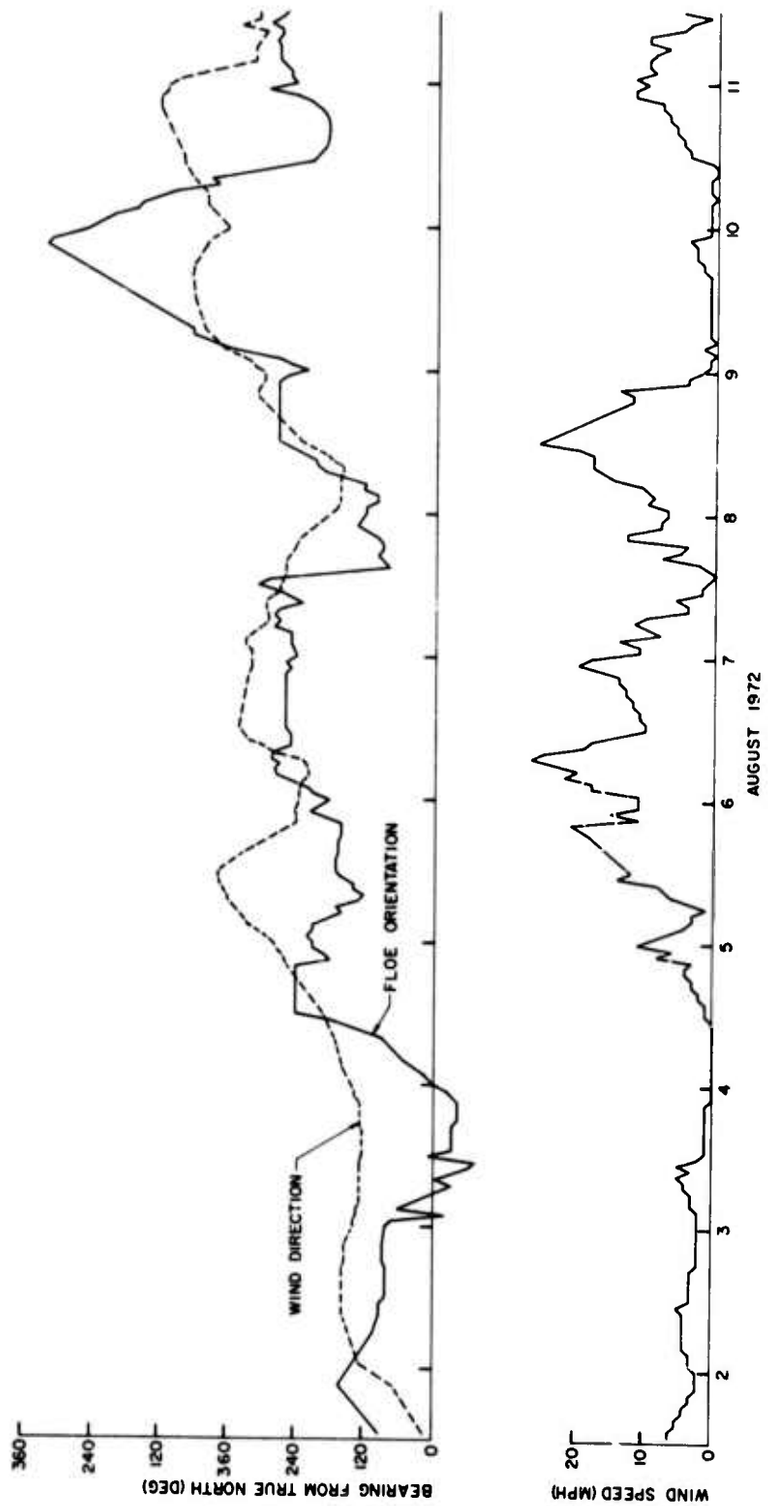

Figure 15. Record of ice floe orientation and the wind.

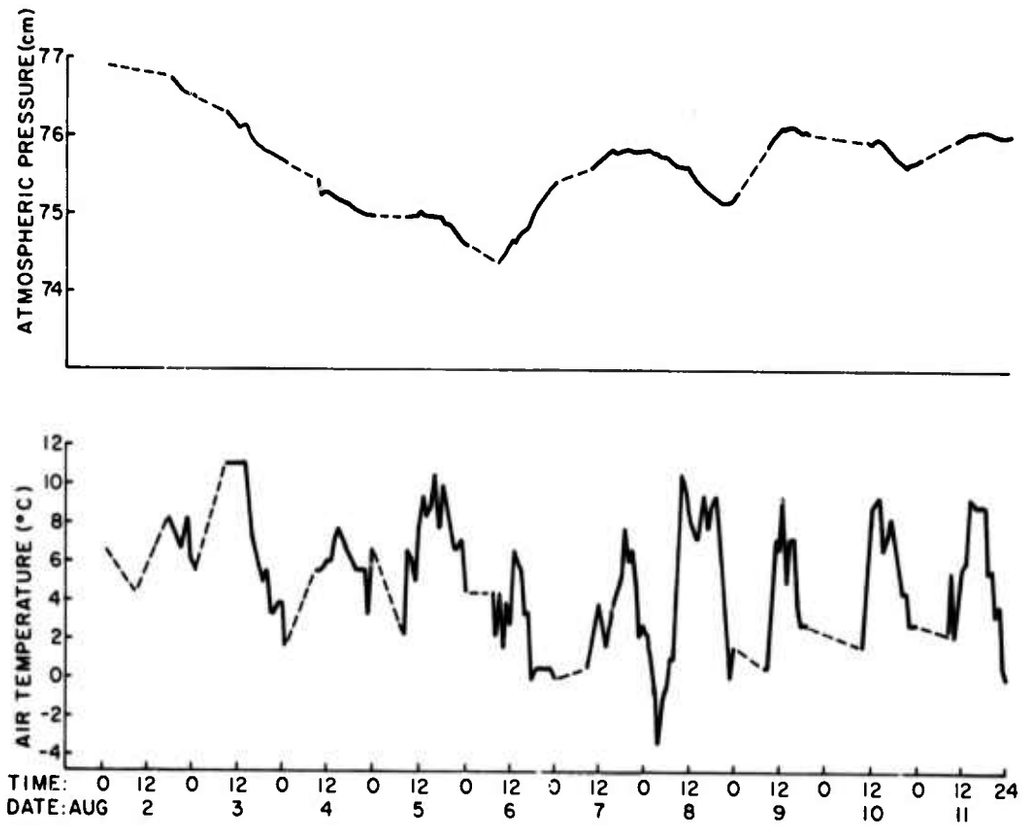

Figure 16. Record of pressure and air temperature at the ice floe camp.

$\vec{D} = a\vec{C} + b\vec{W}$. The movement of the floe was calculated for various values of a and b and compared to the measured movement. The best fit to the actual path was obtained with a = 1.0 and b = 0.1 (see Figures 6 and 17). The agreement is remarkably good and suggests, but does not prove, that the assumptions as to the current and the a and b constants are approximately correct. Predictions based on this calculation would fail, of course, if a land obstruction were to restrict the movement caused by the wind and cause the floes to pack together.

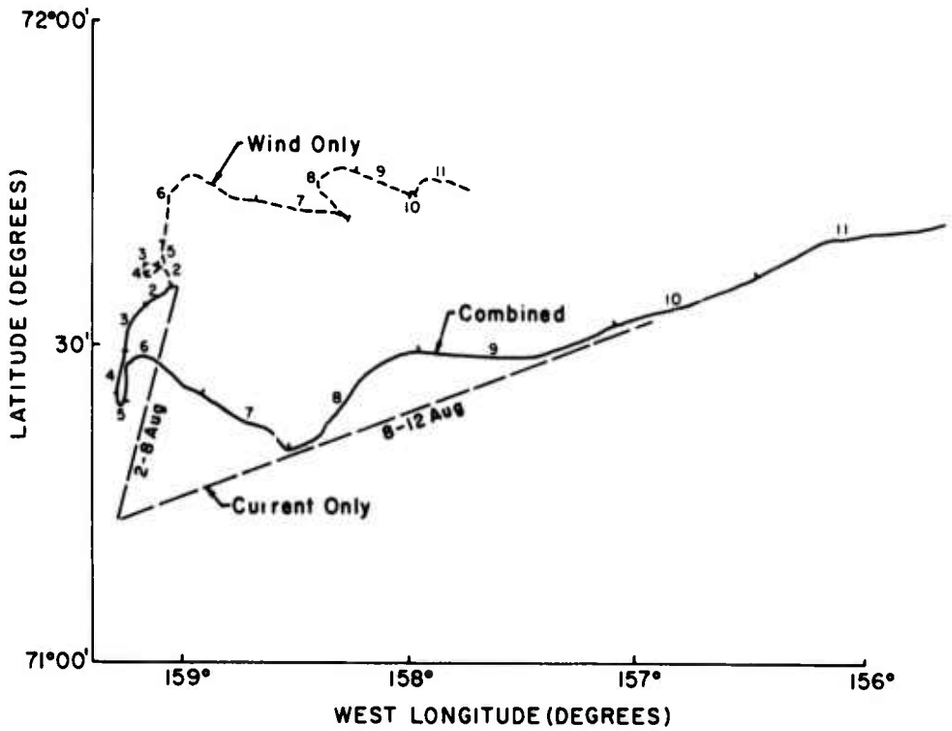

Figure 17. Predicted path of ice floe based on wind and current.

V. OCEANOGRAPHIC STUDIES

The oceanographic study of the area can be separated into two parts: (1) the pattern of the summer intrusion of warm Pacific water through the Bering Strait into the Chukchi Sea and (2) the thermal fine structure produced as this intrusion interacts with the existing cold and ice-covered water. The cruises during the first and last weeks of the project were for studying the intrusion while the main purpose of the ice camp was to study the fine structure.

Temperature measurements were made from a helicopter off the Alaskan coast in April to determine the spring conditions. Some Bering Strait temperature data were obtained from the Arctic Submarine Laboratory for comparison with the intrusion temperatures.

Most of the temperature and salinity profiling equipment was the same equipment that had been used the previous summer (Ref. 1). A new unit was developed, however, to operate automatically at prescribed time intervals. This equipment (see Figure 18) lowered a temperature-conductivity-depth probe to the bottom at regular intervals and recorded the data on paper tape. It was used mainly for overnight operations, but should be able to perform for long periods with improvements in tape storage and the battery pack. A detailed description of the automatic profiler appears in the appendix.

Figure 18. Automatic profiler.

Spring Measurements Off Barrow and at T-3

Measurements were made along the Barrow line on 29 April 1972 to determine spring conditions. A helicopter (Bell 205A-1) was rented from a firm in Anchorage and provided with a temperature-depth profiler and a small hand winch for taking Nansen samples. The procedure was for the helicopter to land on the ice and remain with rotor turning while the probe was carried to the ice edge and lowered to the bottom or to the full cable length (60 meters). The recording instrumentation remained aboard the helicopter.

The first stop was made at the edge of the shore-fast ice about a mile from shore. Stops were planned at 10-mile intervals but there was so much open water and thin ice that the second station was at 20 miles. Succeeding stations were spaced every 10 miles out to 70 miles.

A second series of four measurements at 20-mile intervals was taken at the edge of the shore-fast ice along the coast toward Wainwright. The last station of this series was midway between Wainwright and Icy Cape.

Nansen samples and reversing thermometer readings were taken at three of the stations, two in the first series and one in the second. One thermometer failed but the other showed fair agreement with the thermistor used for profiling.

The temperature profiles are shown in Figures 19 and 20. In these profiles the temperature scale is greatly expanded to bring out the fine structure in the nearly isothermal water. Reversing thermometer readings are shown as dots next to the profile and salinities are written near the dots.

Salinities were about 33‰ 60 miles off shore. The high salinity value at 5 m in the first profile would indicate a density inversion and may be in error.

The water temperature throughout the area was only slightly above the freezing point for water of this salinity. Some layering appears in the profiles taken at Barrow and 20 miles down the coast, but the measurements show that there was no appreciable amount of warm water entering the area at that time. The considerable amount of open water off Barrow was not related to the presence of a warm intrusion, since layers only 0.1°C warmer than the main body of water hardly could be considered significant.

A series of measurements at Fletcher's Ice Island (T-3) was taken in May. One of these has been plotted and included here for comparison (see Figure 21). The temperature remained near the freezing point to a depth of 50 m, below which both temperature and salinity increased.

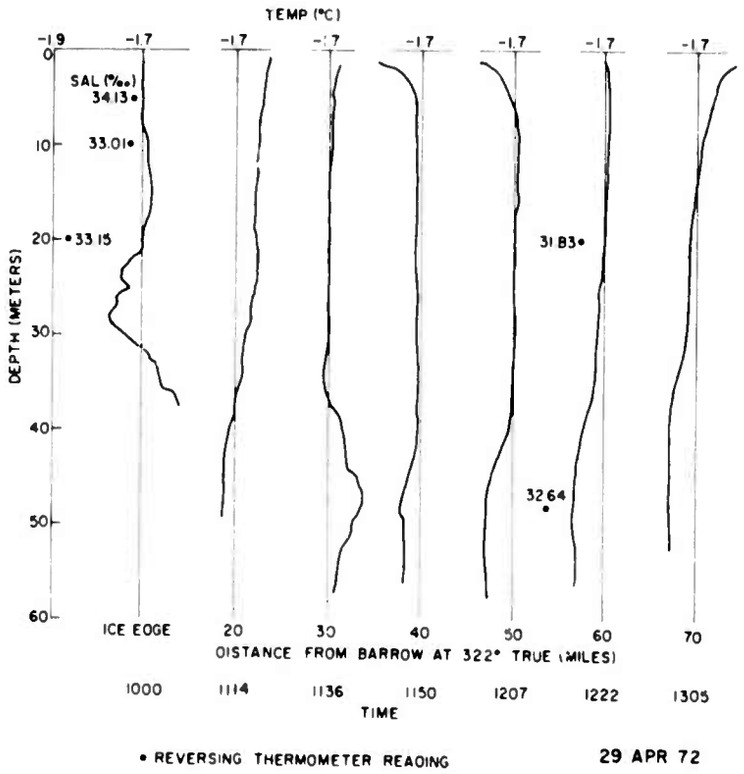

Figure 19. Oceanographic measurements along a line north of Barrow.

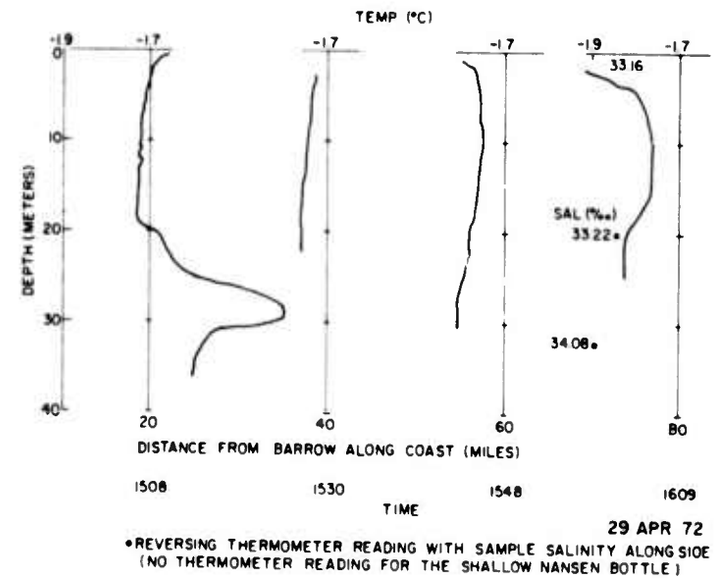

Figure 20. Oceanographic measurements along the coast southwest of Barrow.

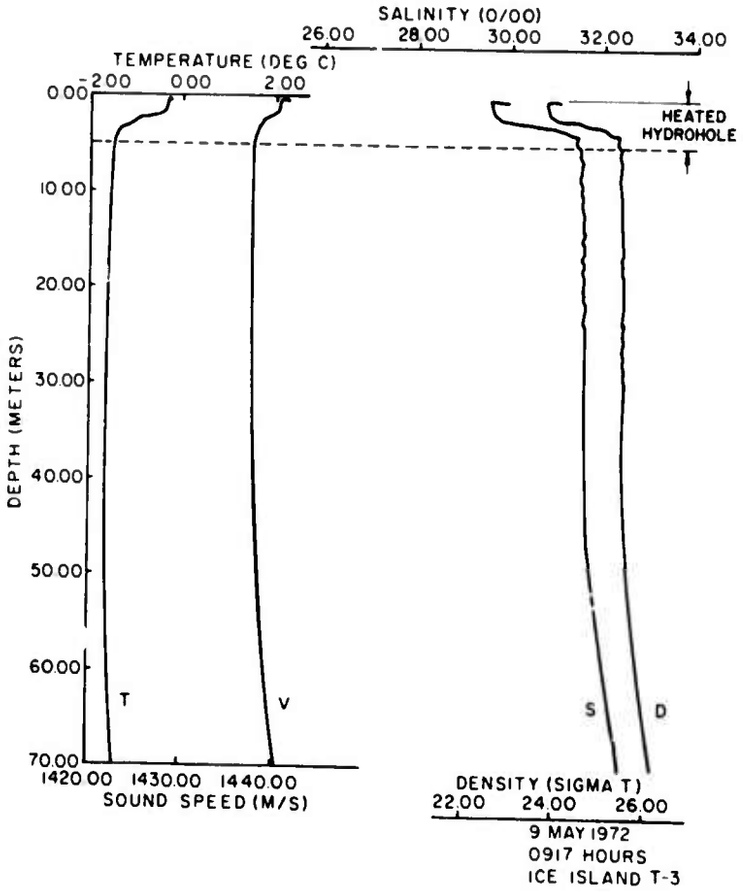

Figure 21. Profiles at T-3 in May 1972.

Chukchi Sea Intrusion

Two one-week cruises were planned to investigate temperature and salinity conditions along the marginal ice zone (MIZ) across the Chukchi Sea. The first started at Barrow on 20 July (see Figure 22) and included lines across the MIZ at Barrow, Wainwright and Icy Cape. After a westward cruise nearly to Herald Island and back, a final crossing of the MIZ was made at Wainwright. The second cruise started on 13 August and included lines at Barrow and Wainwright. The westward cruise was then made further north than before in order to remain close to the receding ice edge. At about 73°N 169°W the temperature measuring equipment failed, and the study was terminated. Between these cruises a few short lines were run to observe conditions in the vicinity of Wainwright and Barrow.

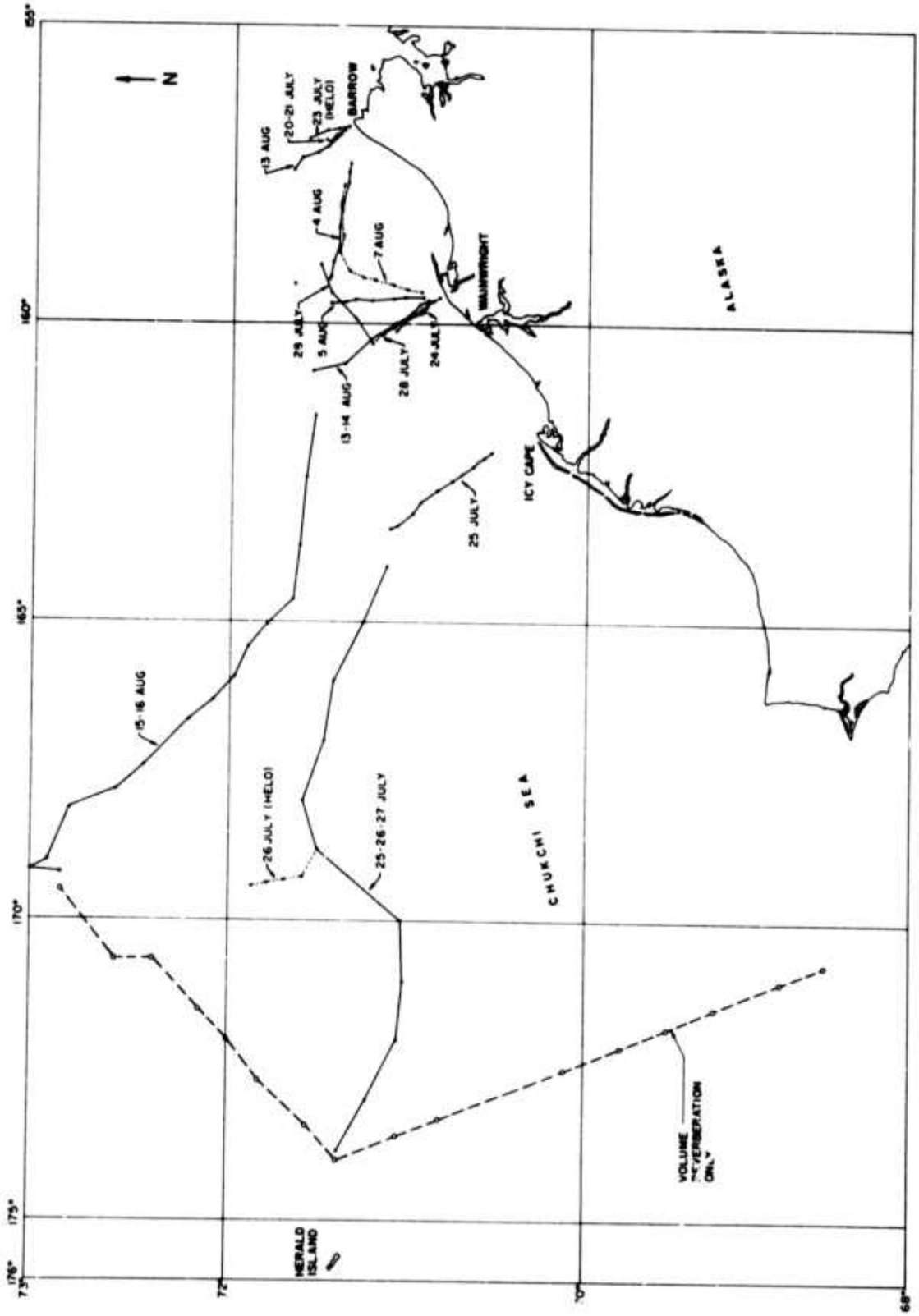

Figure 22. Oceanographic stations in the Chukchi Sea.

The temperature and salinity profiles for each of the stations shown in Figure 22 are presented in Ref. 2. These data have been used to construct sectional views of the temperature and salinity conditions at each line of stations across the MIZ.

Barrow Line, 20-21 July 1972

Representative profiles along the Barrow Line are presented in Figure 23. Sectional views of the temperature and salinity values along this line are presented in Figure 24. A slight warming and a surface layer of low salinity water can be noted near the coast. Two days later a series of stations from a helicopter gave similar results (see Figure 25).

Wainwright Line, 24 July 1972

Sample profiles along the Wainwright line are shown in Figure 26. Sectional views of temperature and salinity are shown in Figure 27. The intrusion is 10 m thick with a maximum temperature of 5°C and a salinity of about 29‰.

Icy Cape Line, 25 July 1972

The large surface layer shown for this region in Figures 28 and 29 increases in depth and temperature as one proceeds southwest toward the Bering Strait. The maximum temperature is 8°C.

Westward Crossing, 25-27 July 1972

Representative temperature and salinity profiles for this crossing of the Chukchi Sea are shown in Figure 30. Sectional views are presented in Figure 31. It appears that the intrusion has split into two parts separated by an ice-covered region. The salinity of the intrusion is not much lower than that of the existing water. A series of temperature profiles from a helicopter on a line to the north (Figure 32) shows a tongue of 4°C water extending into the cold region. No salinity data were taken along this line because the lightweight profiler used in the helicopter did not include a conductivity cell.

Wainwright Line, 28 July 1972

At the end of the first cruise the Wainwright line was repeated to determine what changes were taking place. The sectional temperature diagram of Figure 33 shows that the intrusion is similar in size to that on 24 July (Figure 27) but is now well away from the coast. A continuation of the measurements to the northeast (Figure 34) shows a pool of considerably warmer water which is somewhat cut off from the rest of the intrusion by colder water to the southwest. The warmer water may, however, connect to the main body of the intrusion directly west of this pool.

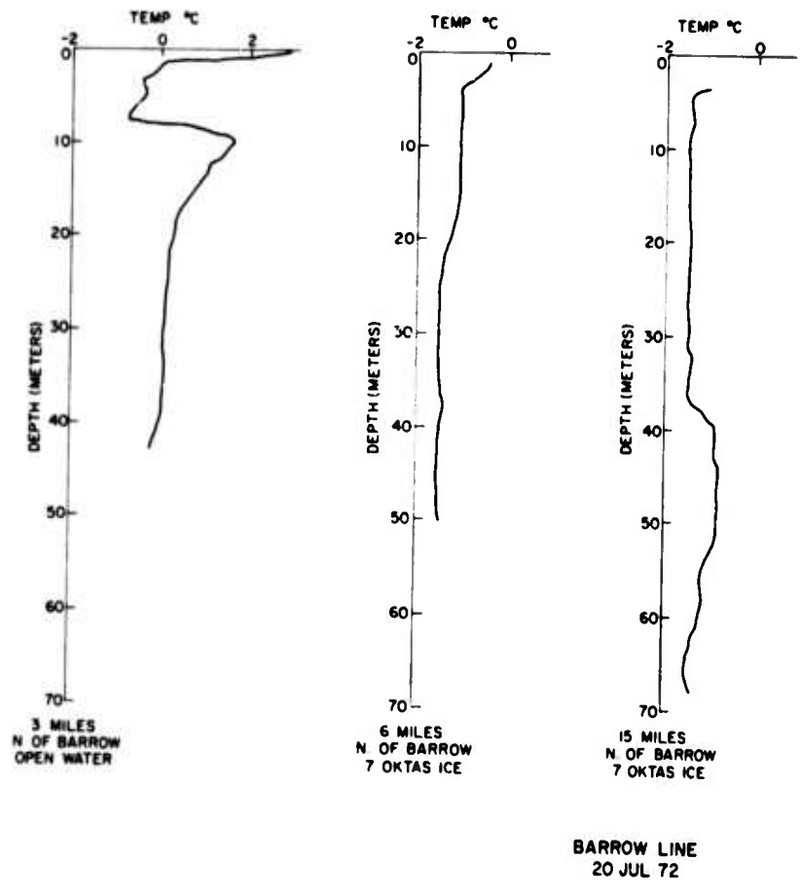

Figure 23. Temperature profiles along the Barrow line.

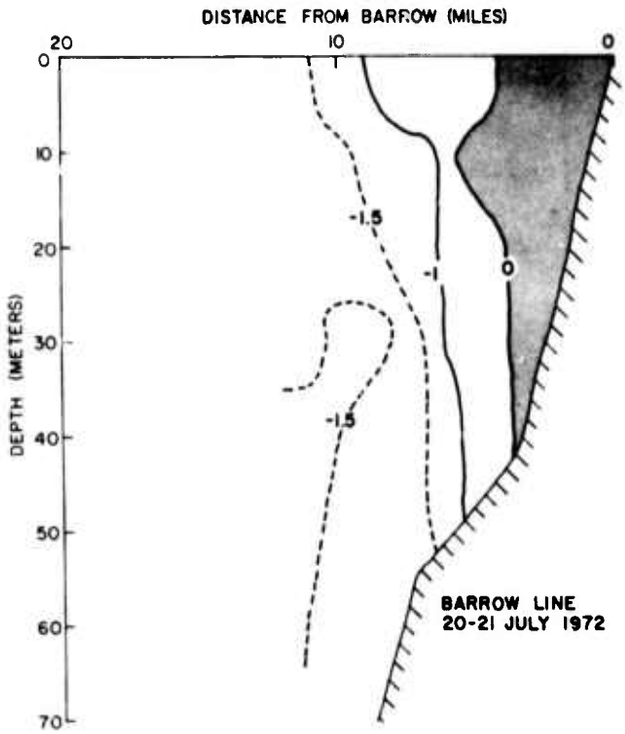

Figure 24. Isotherms and isohalines for a section along the Barrow line.

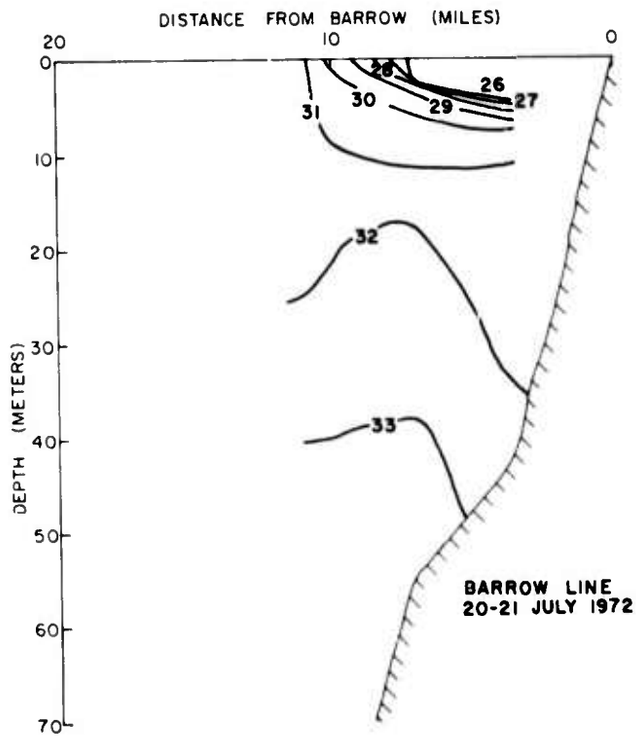

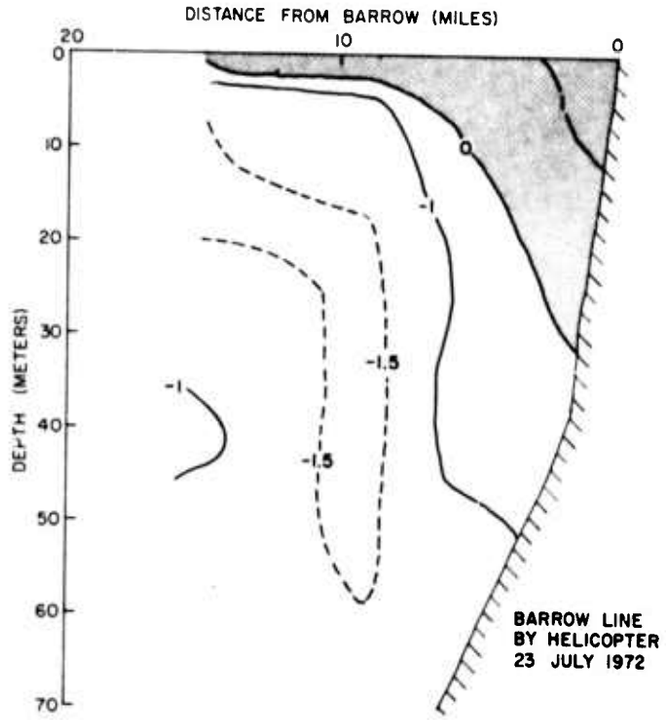

Figure 25. Isotherms for a section along the Barrow line.

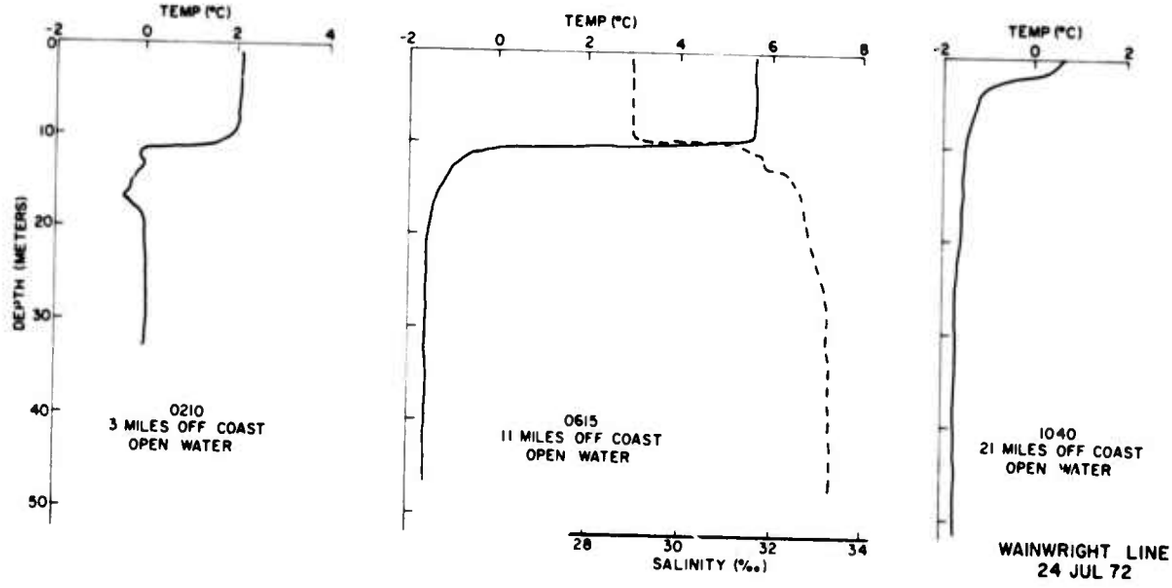

Figure 26. Temperature profiles along the Wainwright line.

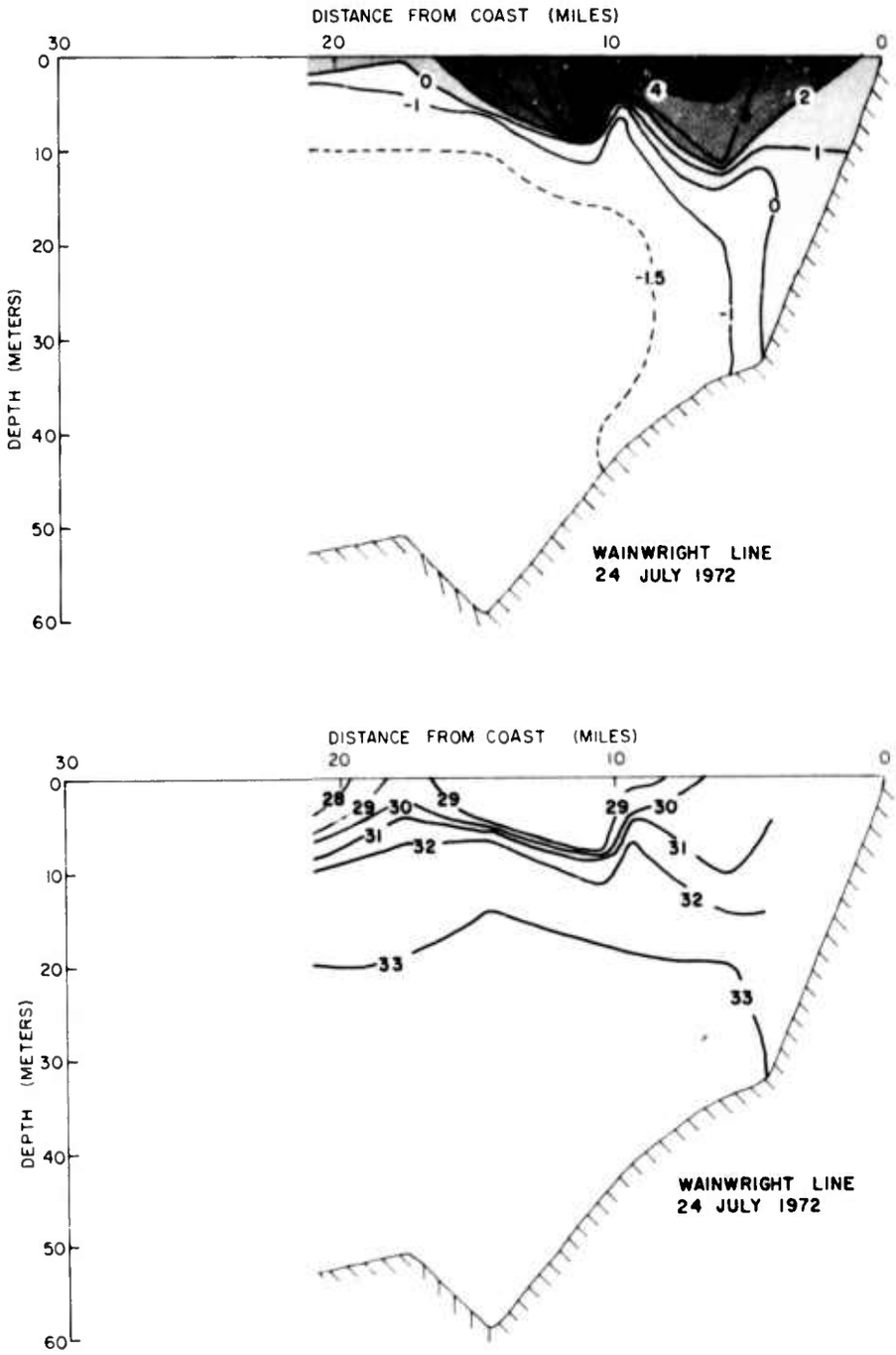

Figure 27. Isotherms and Isohalines for a section along the Wainwright line.

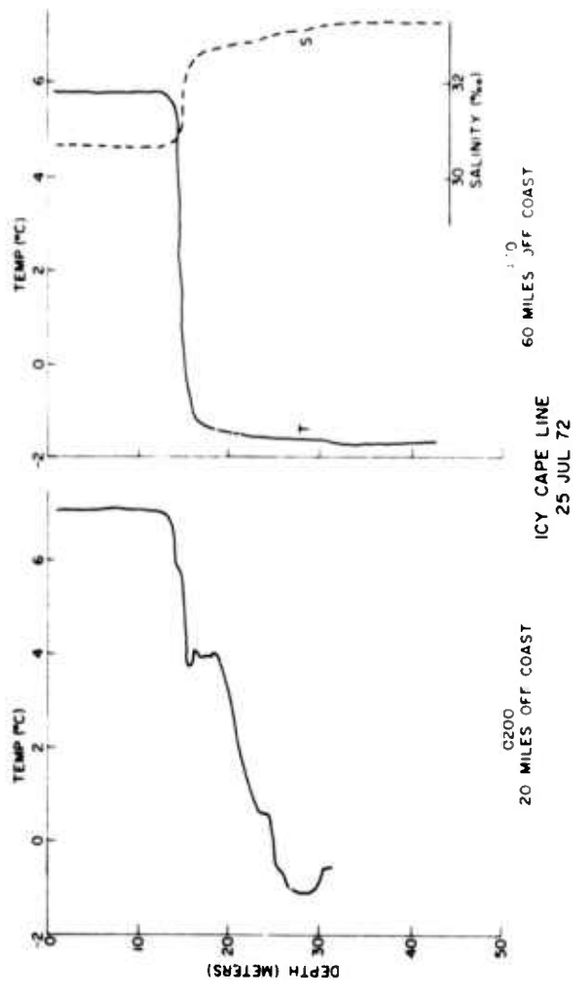

Figure 28. Temperature profiles along the Icy Cape line.

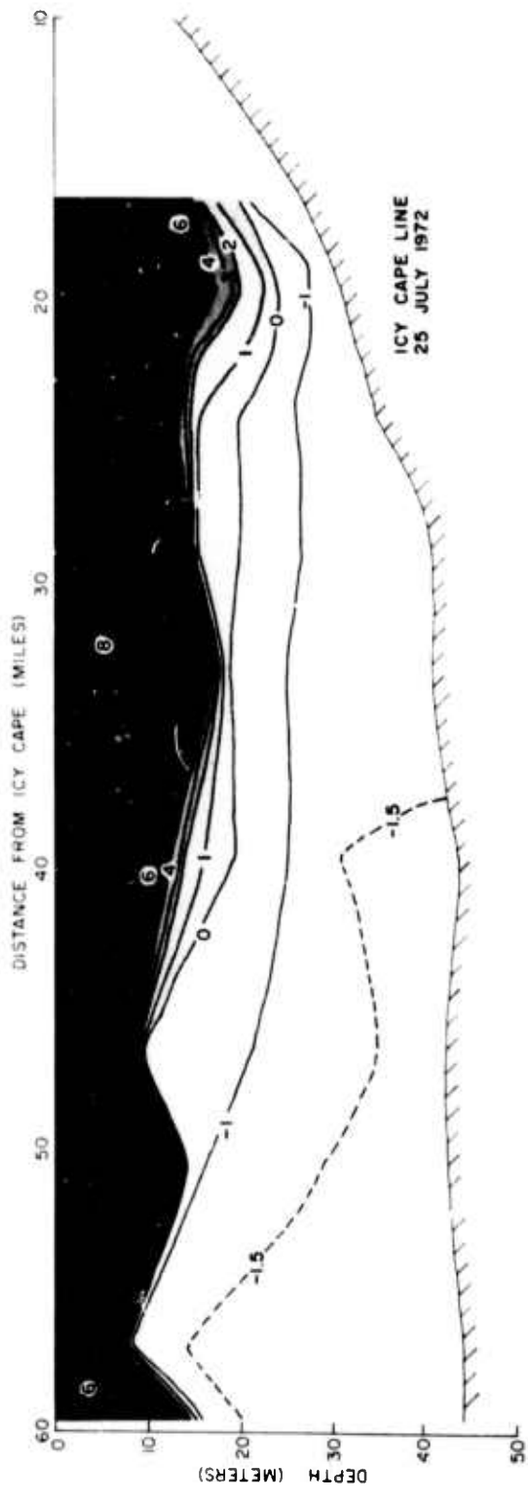

Figure 29. Isotherms for a section along the Icy Cape line.

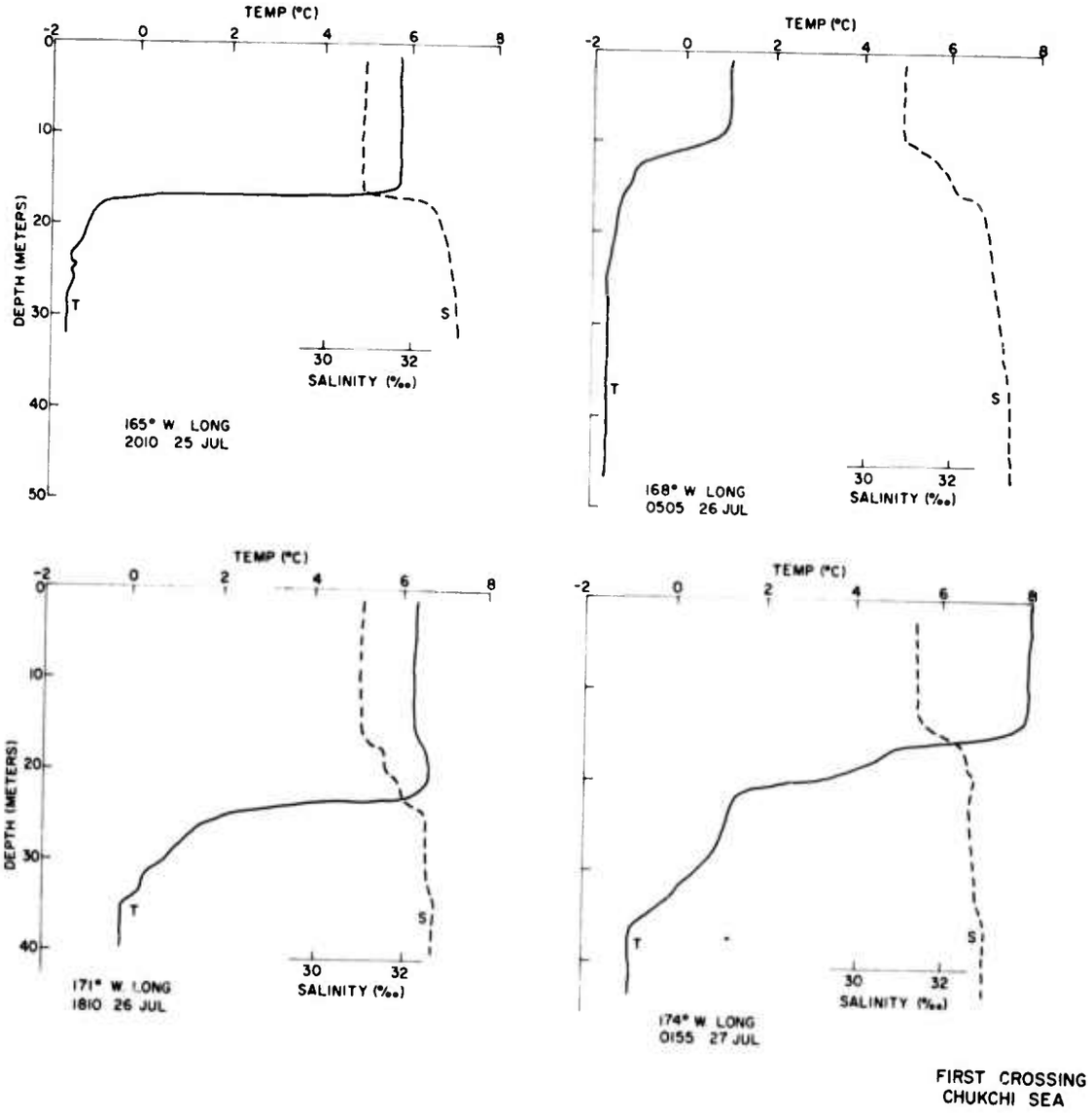

Figure 30. Temperature profiles for the cruise across the Chukchi Sea.

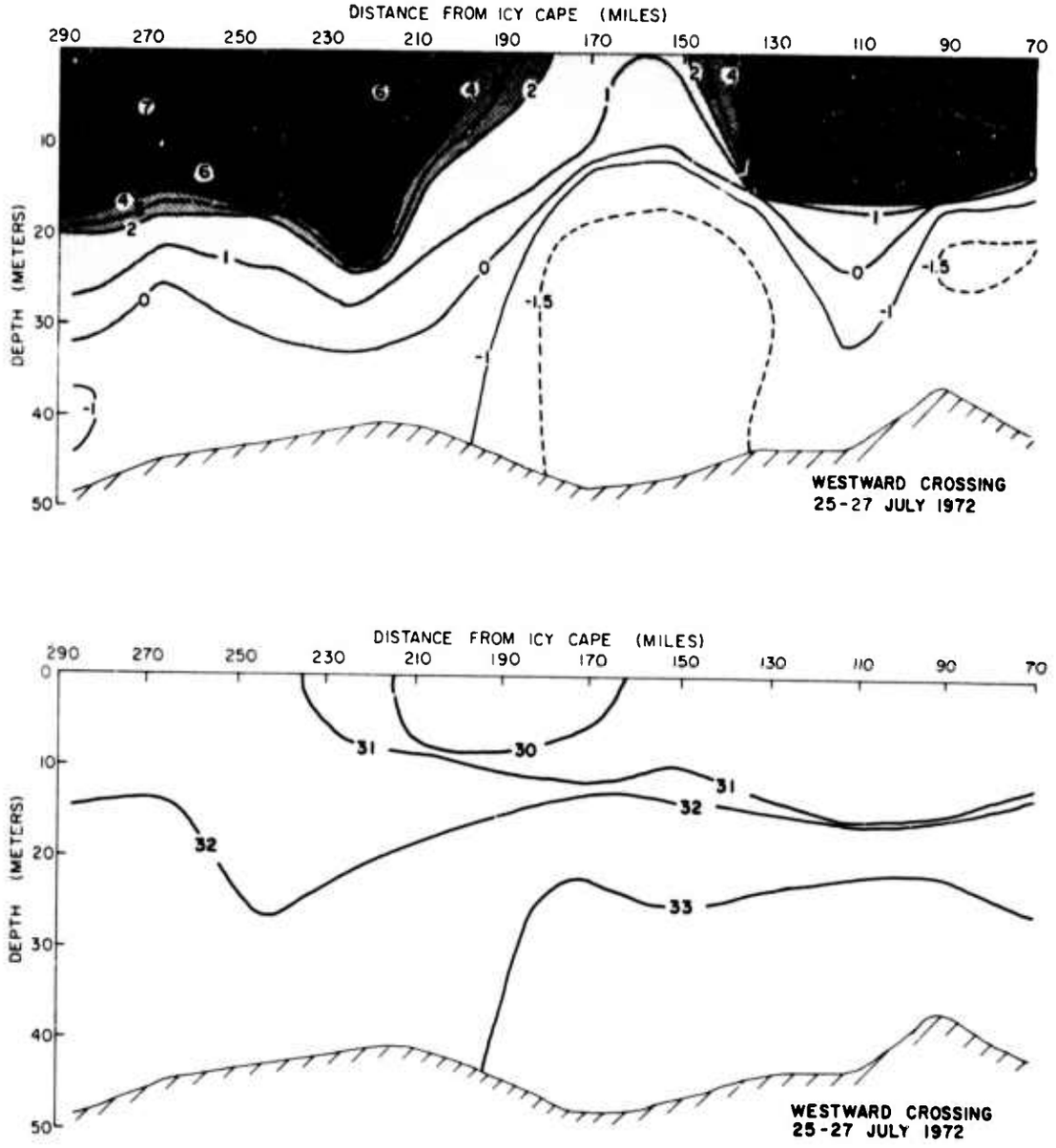

Figure 31. Isotherms and isohalines for an east-west section across the Chukchi Sea.

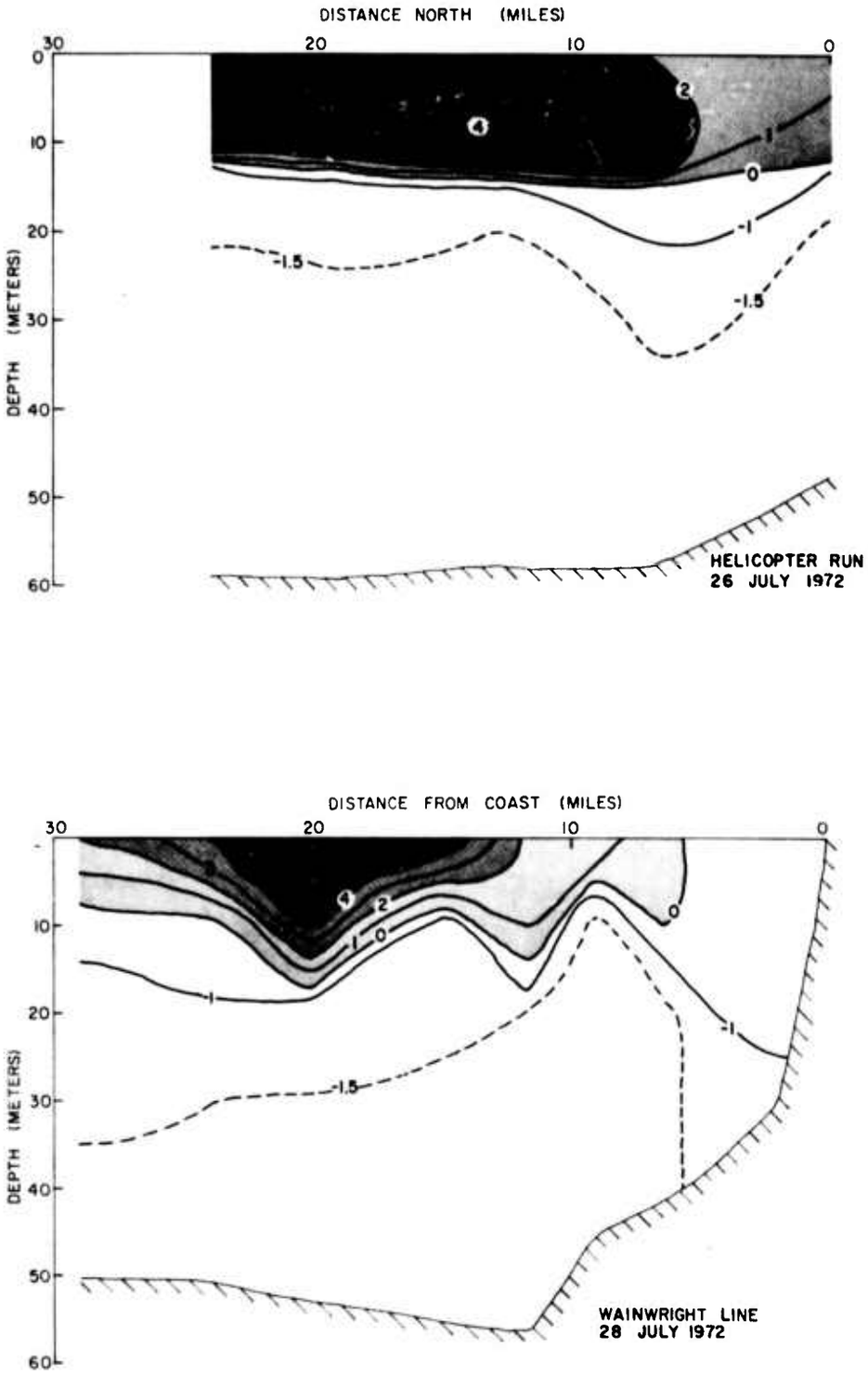

Figure 33. Isotherms for a section along the Wainwright line.

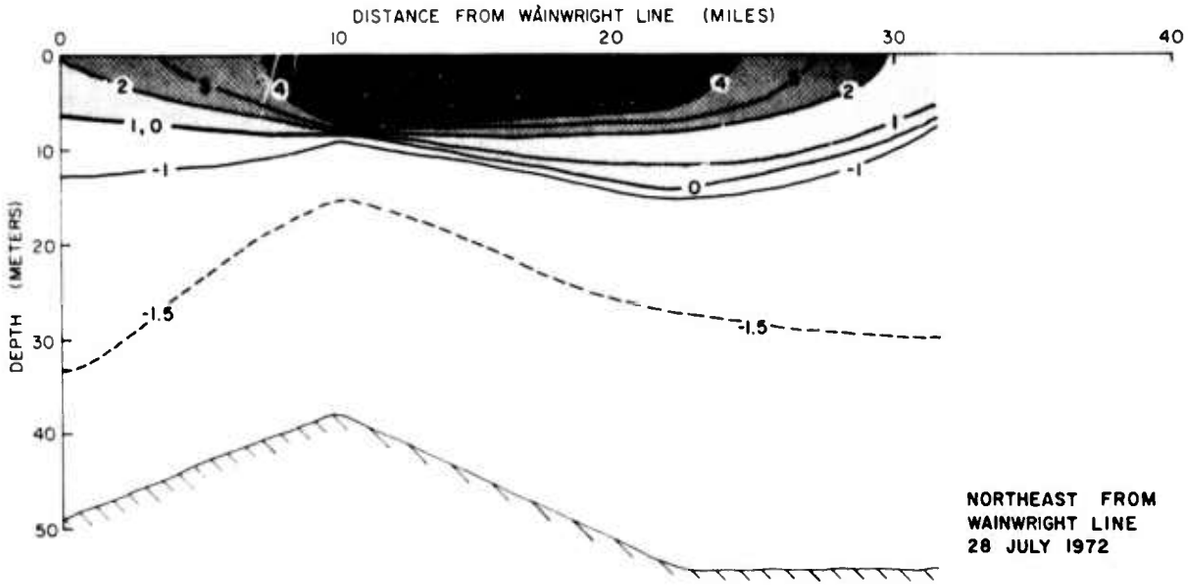

Figure 34. Isotherms for a section along a line northeasterly from the end of the Wainwright line.

Traverses, 4-7 August 1972

During the ice camp occupancy, the icebreaker was available for three traverses of the area between Wainwright and Barrow. The 4 August traverse in Figure 35 again shows a split in the intrusion, one part along the coast and one at 50 miles out. The 5 August traverse, Figure 36, which ends at about the center of the second Wainwright line (Figure 34), gives the impression that the intrusion has been forced to the coast. The third traverse from Wainwright northward then eastward toward Barrow, Figure 37, shows a concentration of the intrusion along the coast at Wainwright and very little 22 miles off Barrow.

Barrow Line, 13 August 1972

The second one-week cruise started after the ice camp was abandoned. The profiles of Figure 38 and the sections presented in Figure 39 show that the intrusion is still crowding the coast, with only remnants beyond 8 miles.

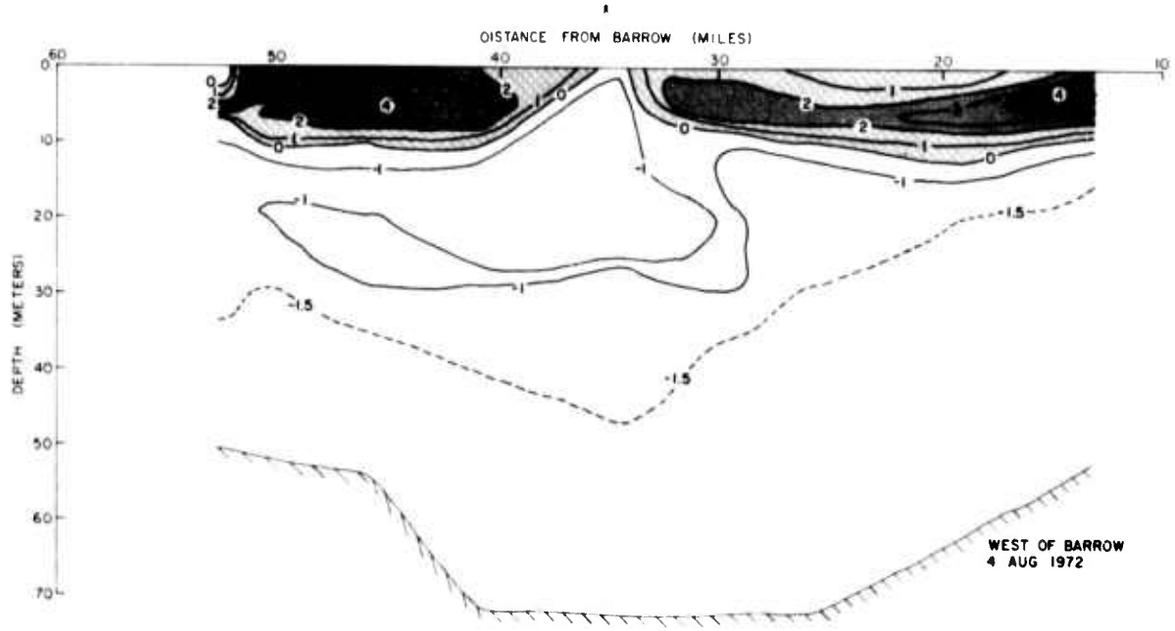

Figure 35. Isotherms for a section along a line west from Barrow.

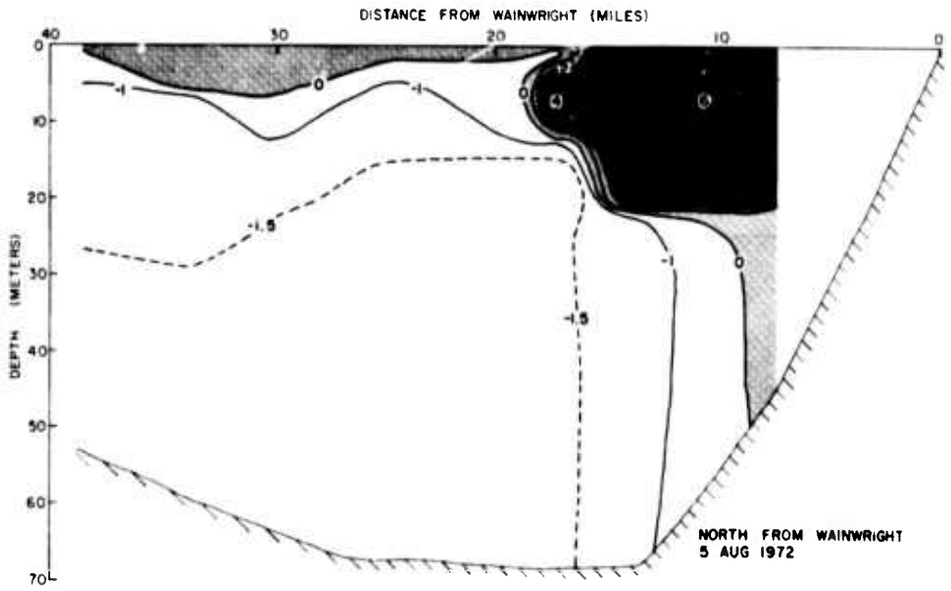

Figure 36. Isotherms for a section along a line north from Wainwright.

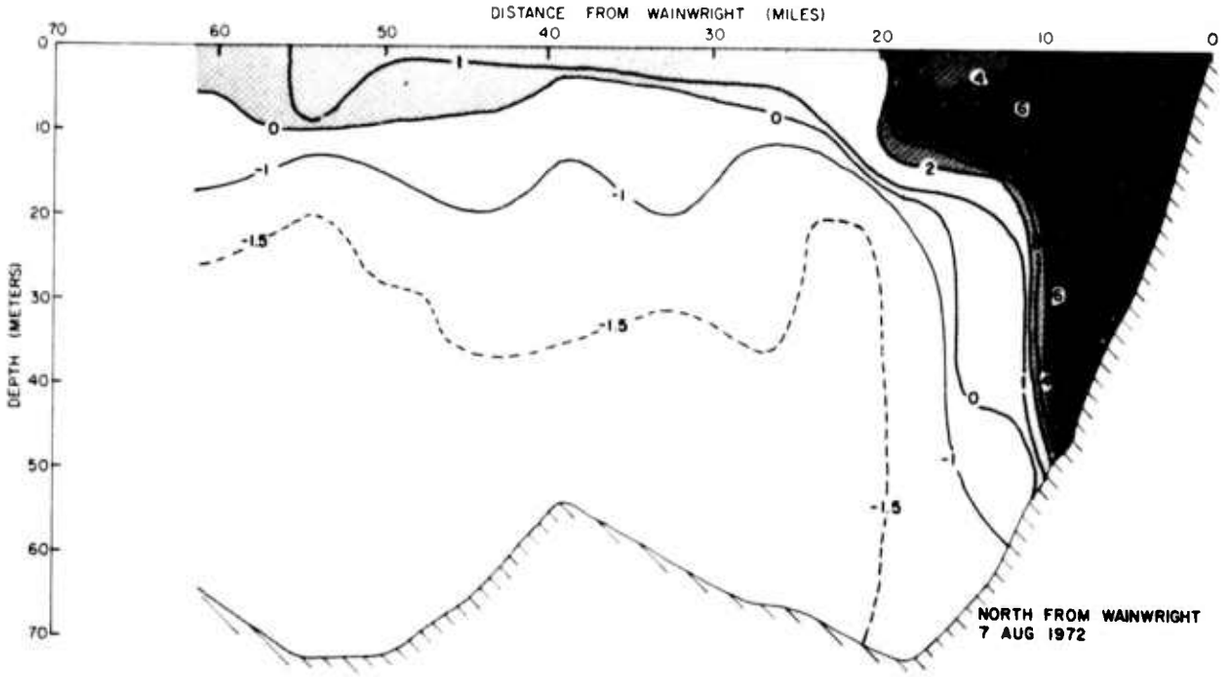

Figure 37. Isotherms for a section along a line northerly from Wainwright.

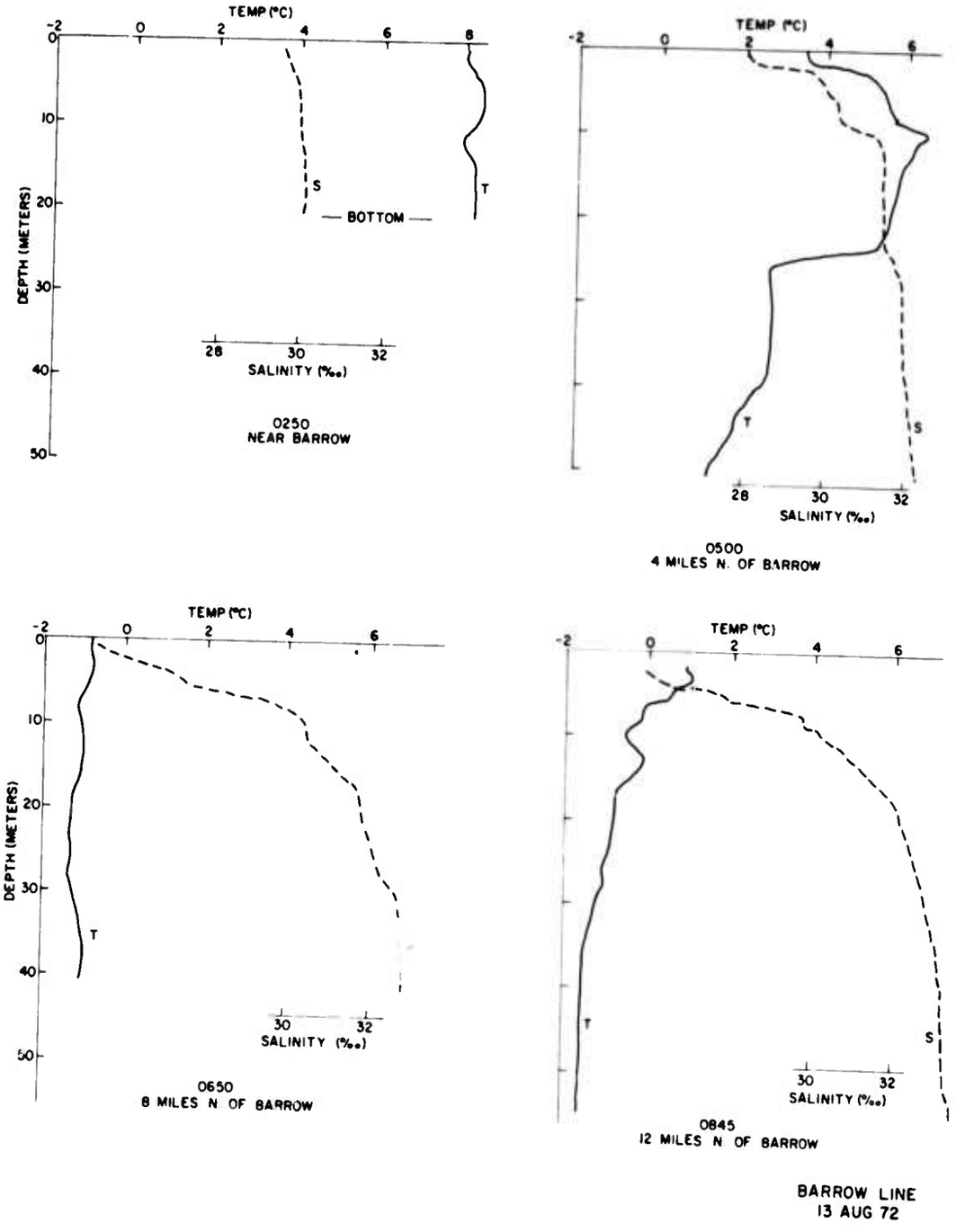

Figure 38. Temperature profiles along the Barrow line.

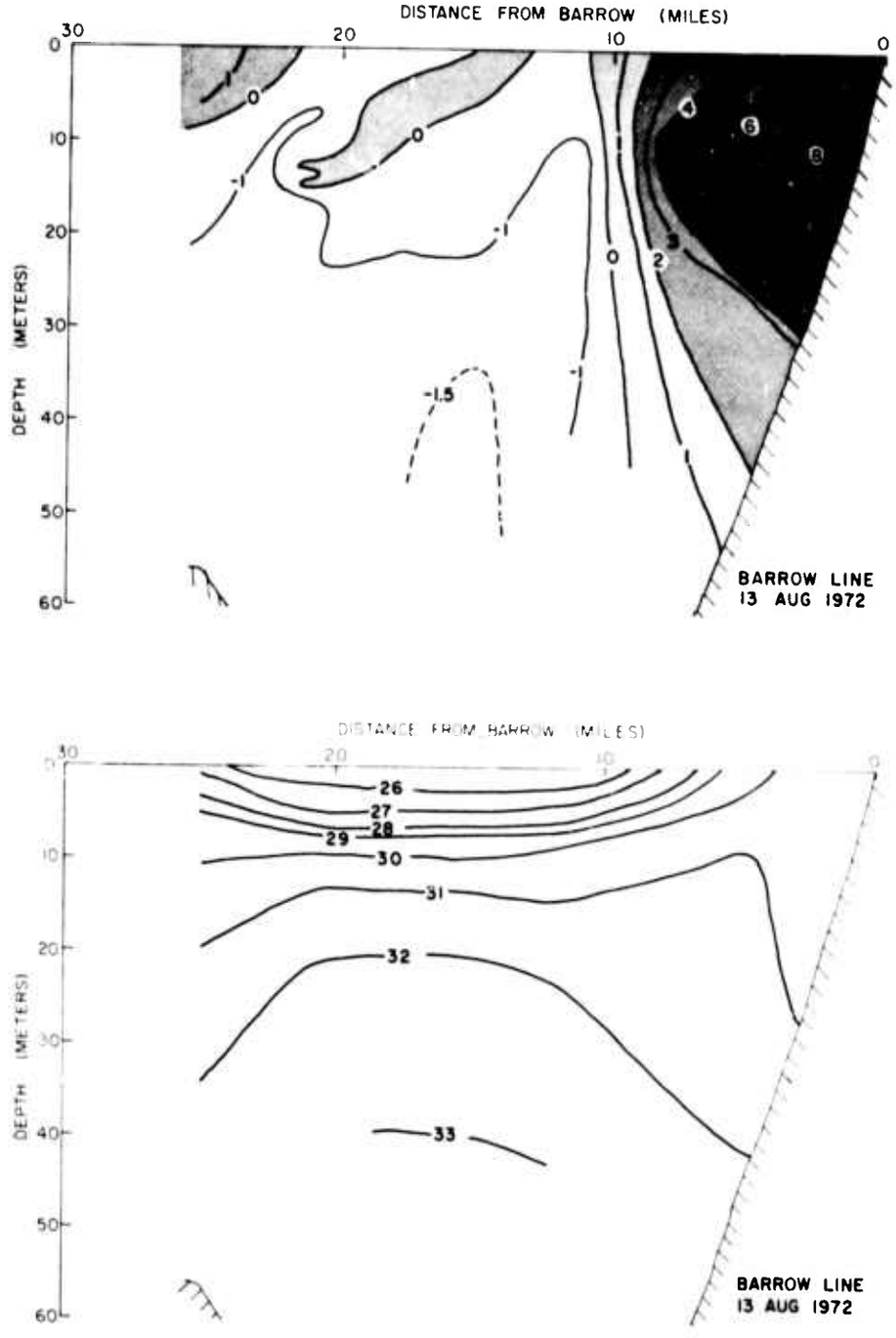

Figure 39. Isotherms and isohalines for a section along the Barrow line.

Wainwright Line, 14 August 1972

The highest temperature of the intrusion, over 8°C, is shown in the profiles taken near Wainwright on 14 August (see Figure 40). The extent of the warm, high-salinity surface layer can be seen in the sections in Figure 41. It appears that the surface water has moved toward the coast in the same manner as the manned ice floe.

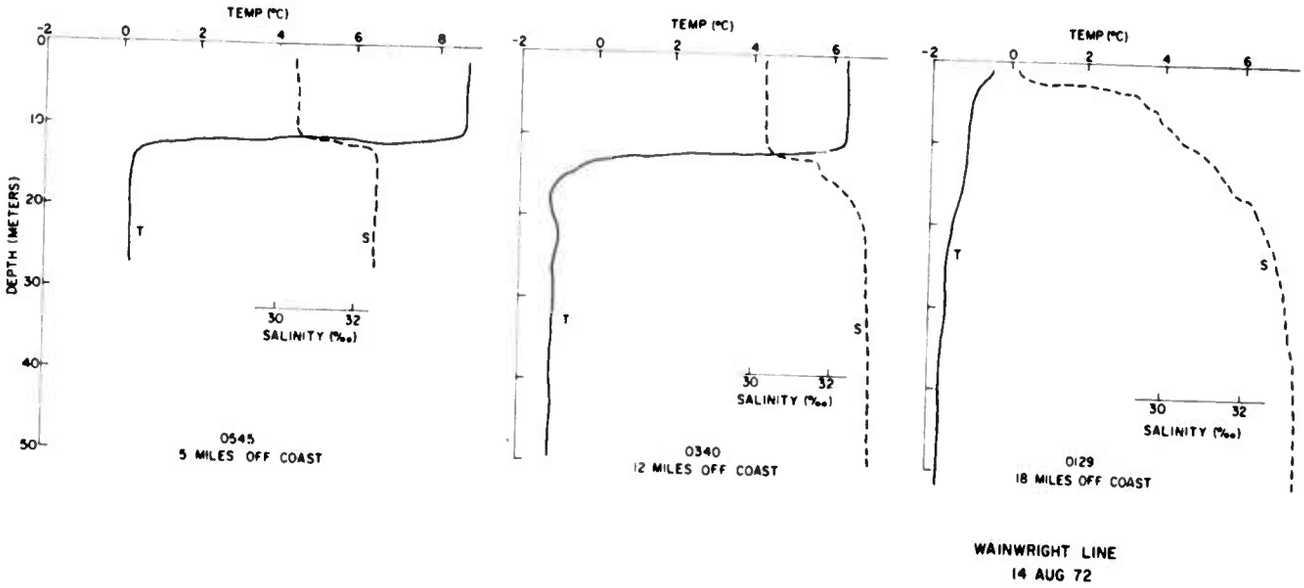

Figure 40. Temperature profiles along the Wainwright line.

Second Chukchi Crossing, 15-16 August 1972

The profiles of Figure 42 and the sections in Figure 43 show the outline of the intrusion farther north. Again, as in the first crossing, there appears to be an ice projection from the north that resists the intrusion.

The conditions during the first one-week cruise and the second cruise three weeks later can be compared by examining Figures 44 and 45 in which the maximum temperature of the intrusion has been plotted. Although the Chukchi Sea crossing was a single line of stations, an area about 20 miles wide has been shaded for illustration purposes. The first figure shows the intrusion spread all across the sea with a weak area in the center and a slight concentration along the coast. In the second figure the surface layer appears to have concentrated in a narrow region along the coast and colder water from the north has moved southwestward to replace it.

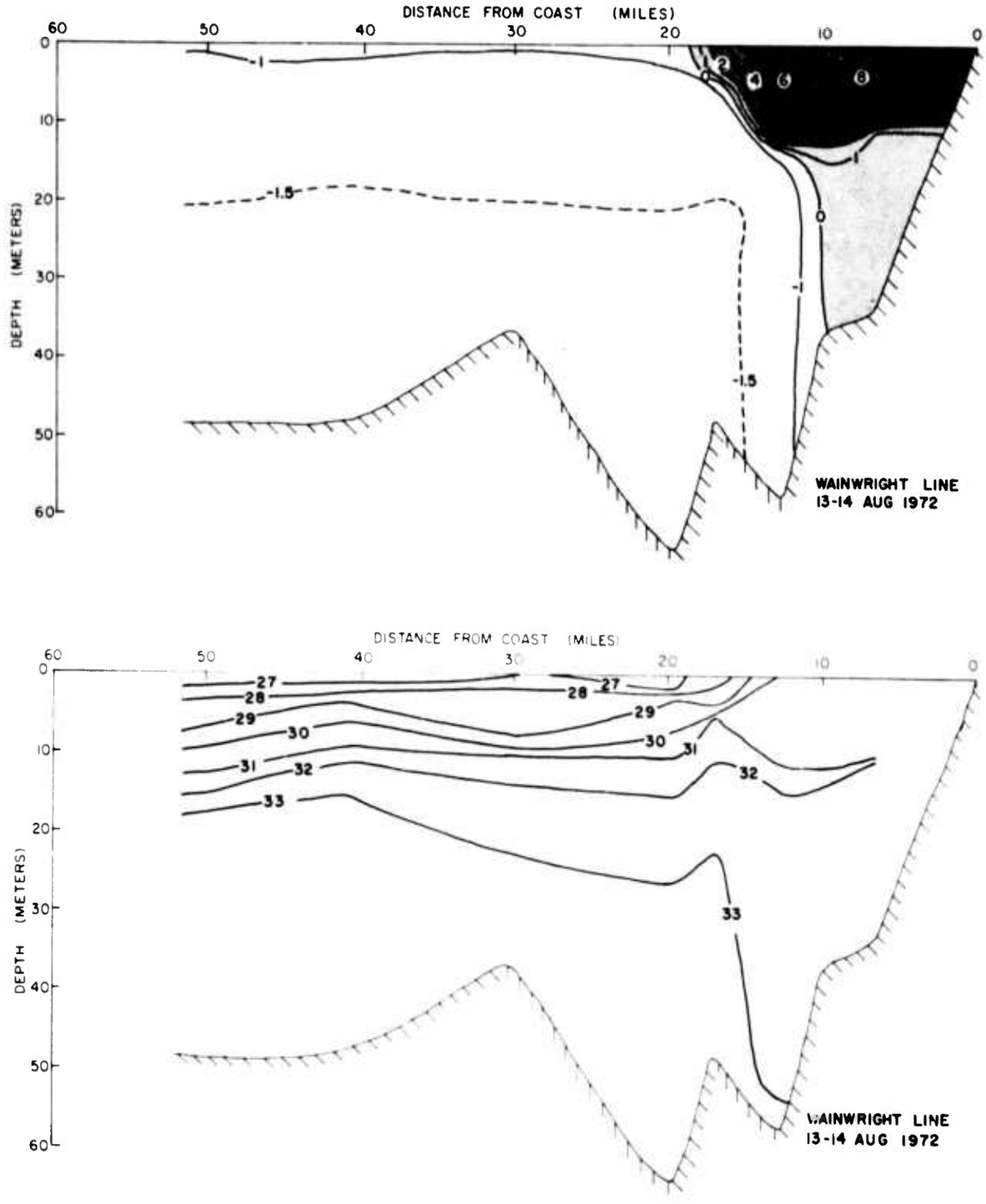

Figure 41. Isotherms and isohalines for a section along the Wainwright line.

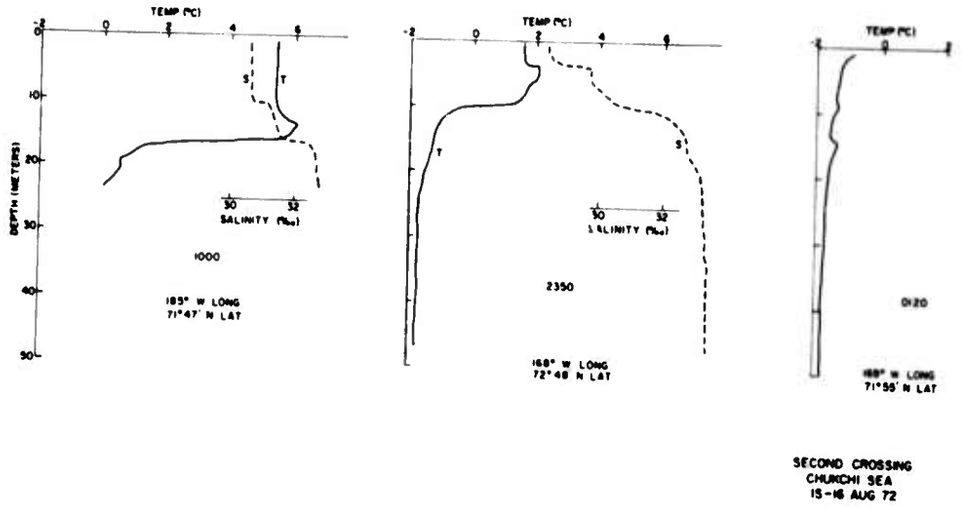

Figure 42. Temperature profiles for the second cruise across the Chukchi Sea.

A comparison with the previous summer can be made by comparing these plots with Figure 46, where the heaviest shading represents 4 to 5°C. In mid-August 1971 the intrusion was 3° lower in temperature but had a similar tendency to be concentrated along the coast.

The Arctic Submarine Laboratory provided some Bering Strait surface layer temperatures taken in shallow water near Wales, Alaska. The daily temperatures for the summers of 1971 and 1972 are plotted in Figure 47. This graph shows 6°C water arriving off Wales about 20 July 1972 while Figure 44 shows the 6°C water at Wainwright by 24 July. Such an advance would require a speed of over 3 kn, which is very unlikely. Perhaps the station at Wales is out of the main stream and the warm intrusion through the strait was several days earlier than the observed temperature increase off Wales. The temperature peaks at Wales were 1 or 2°C lower in 1971 than in 1972, which agrees with the lower temperature of the intrusion in the eastern Chukchi Sea in 1971.

The extensive surface layer produced by the warm intrusion presents an often impenetrable barrier to low angle acoustic propagation. For example, an increase in temperature of 8°C will cause sound rays less than 11° above the horizontal to be bent downward. Examples of the effect of the layer on sound transmission are given in Figure 48. In the upper sound ray plot the source is in the thermocline; in the lower plot the source is below the thermocline and the 9° ray is refracted downward.

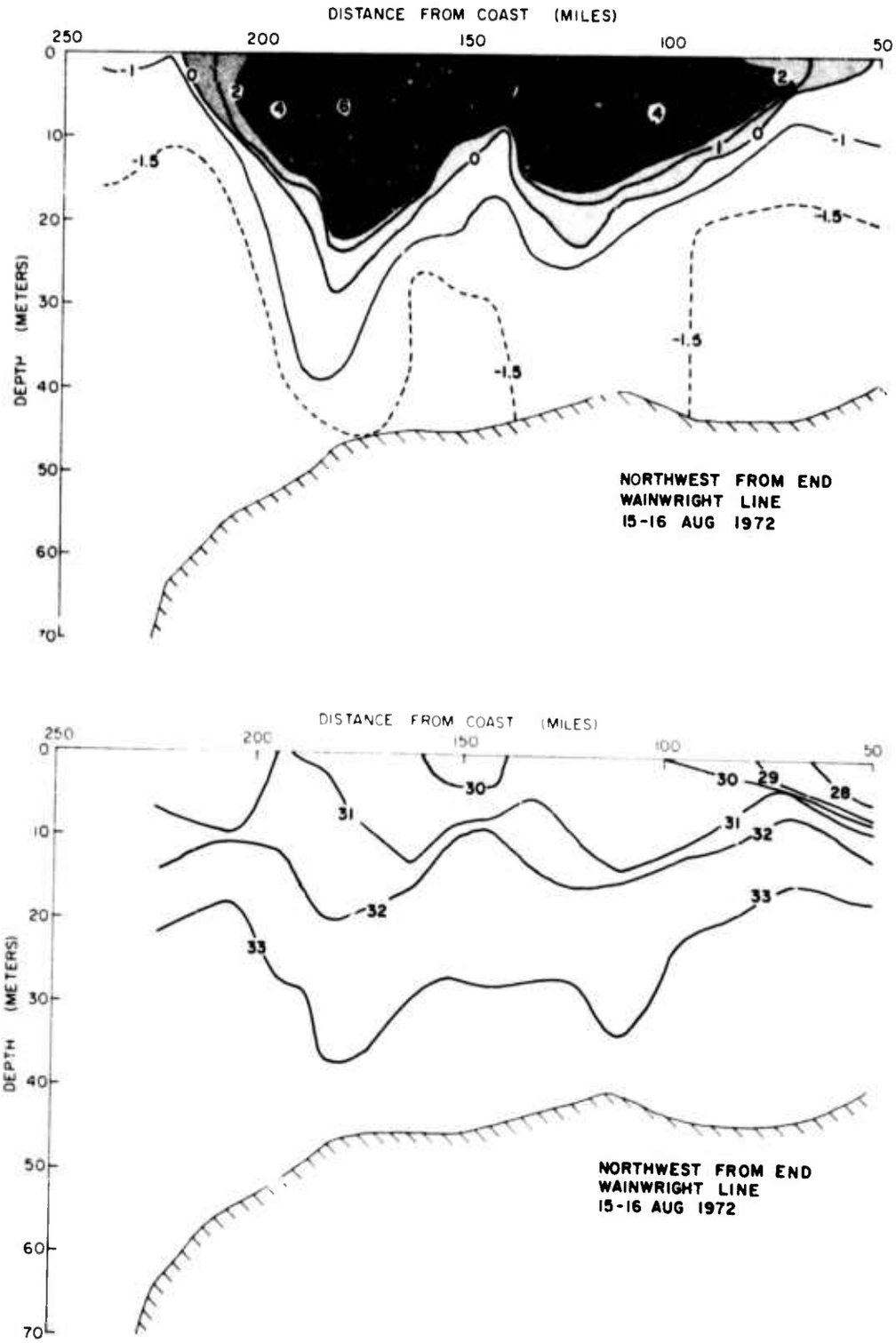

Figure 43. Isotherms and isohalines for a section along a line northwest from the end of the Wainwright line into the central Chukchi Sea.

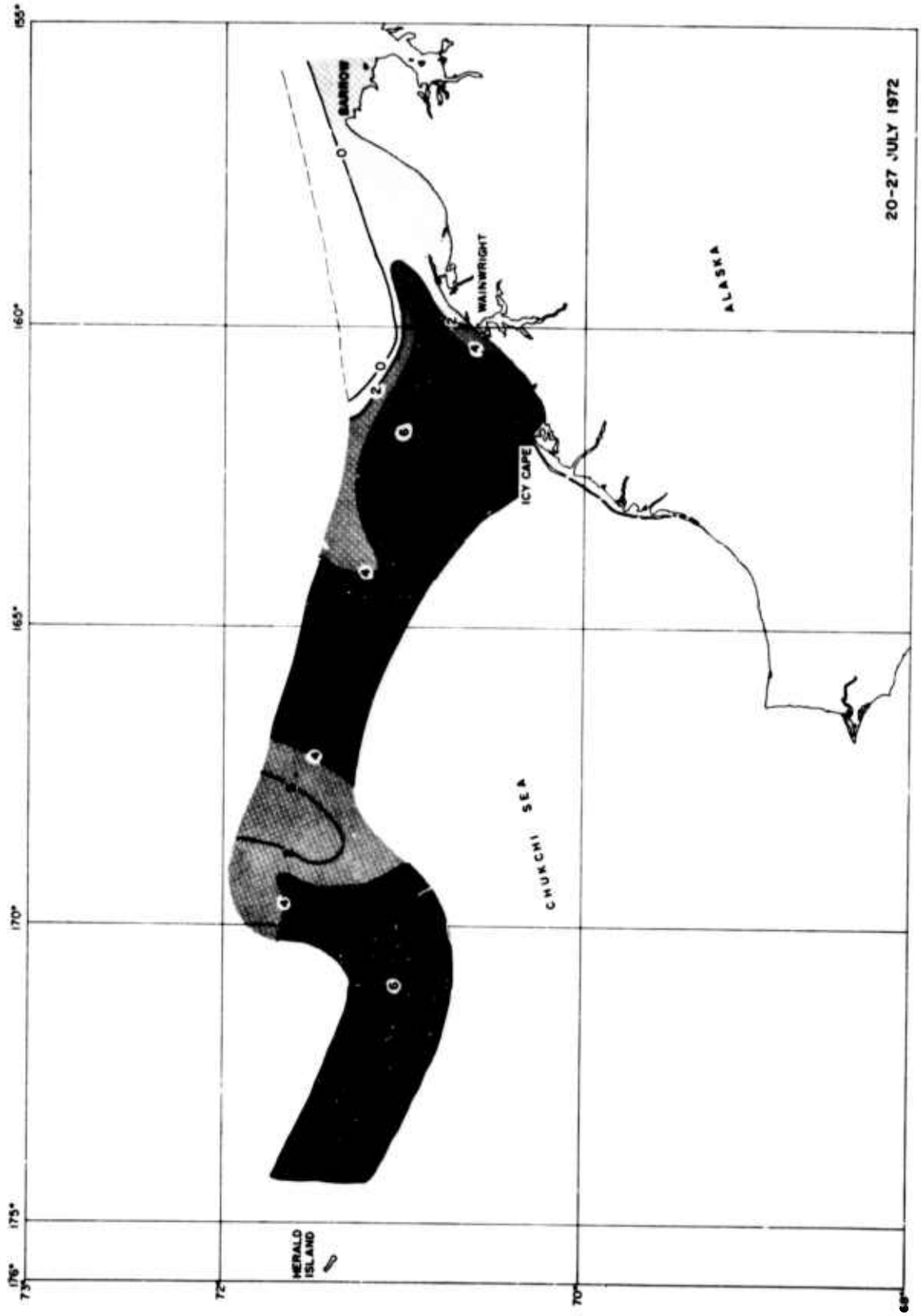

Figure 44. Isotherms of maximum temperature for the first crossing of the Chukchi Sea.

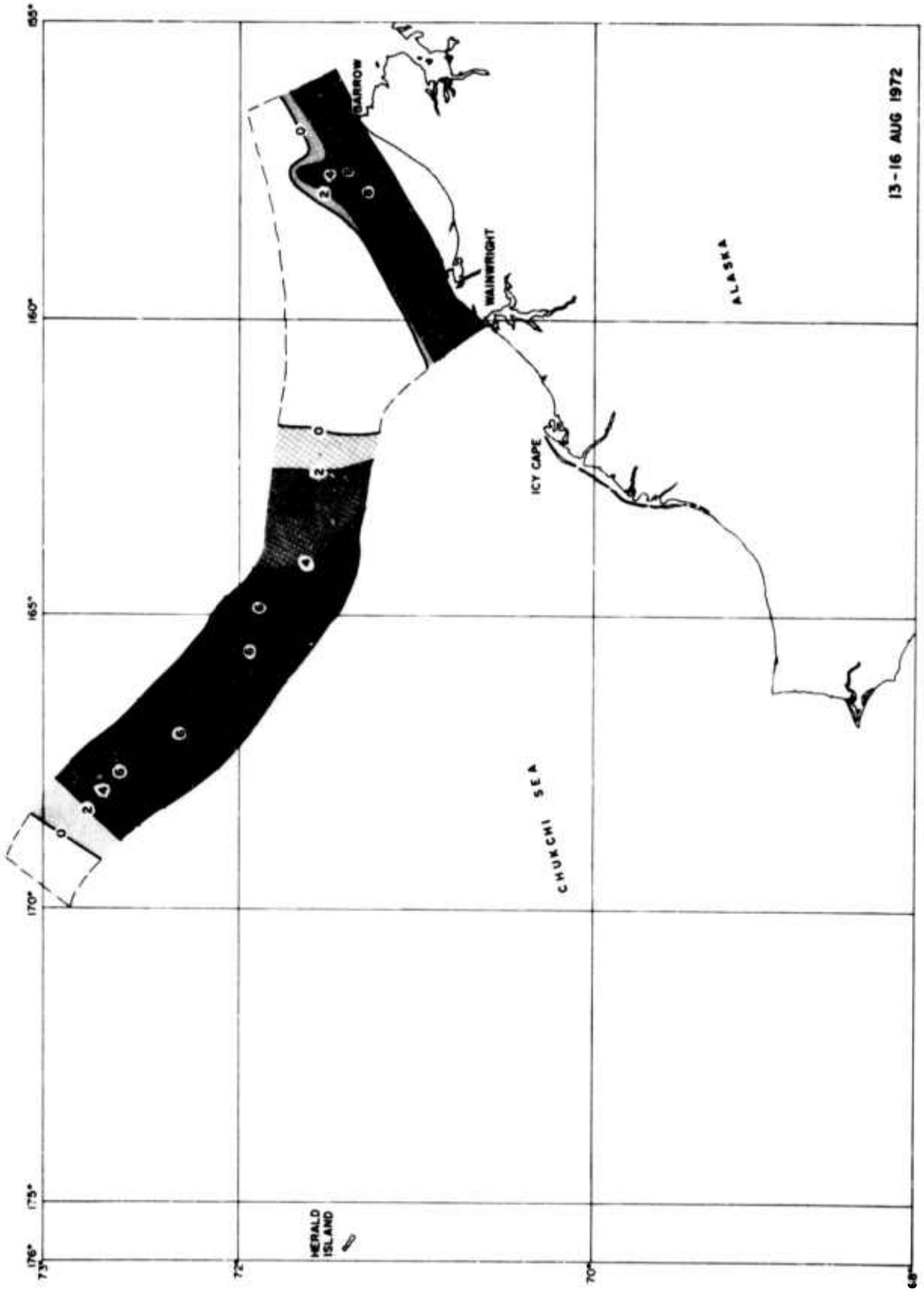

Figure 45. Isotherms of maximum temperature for the second cruise across the Chukchi Sea.

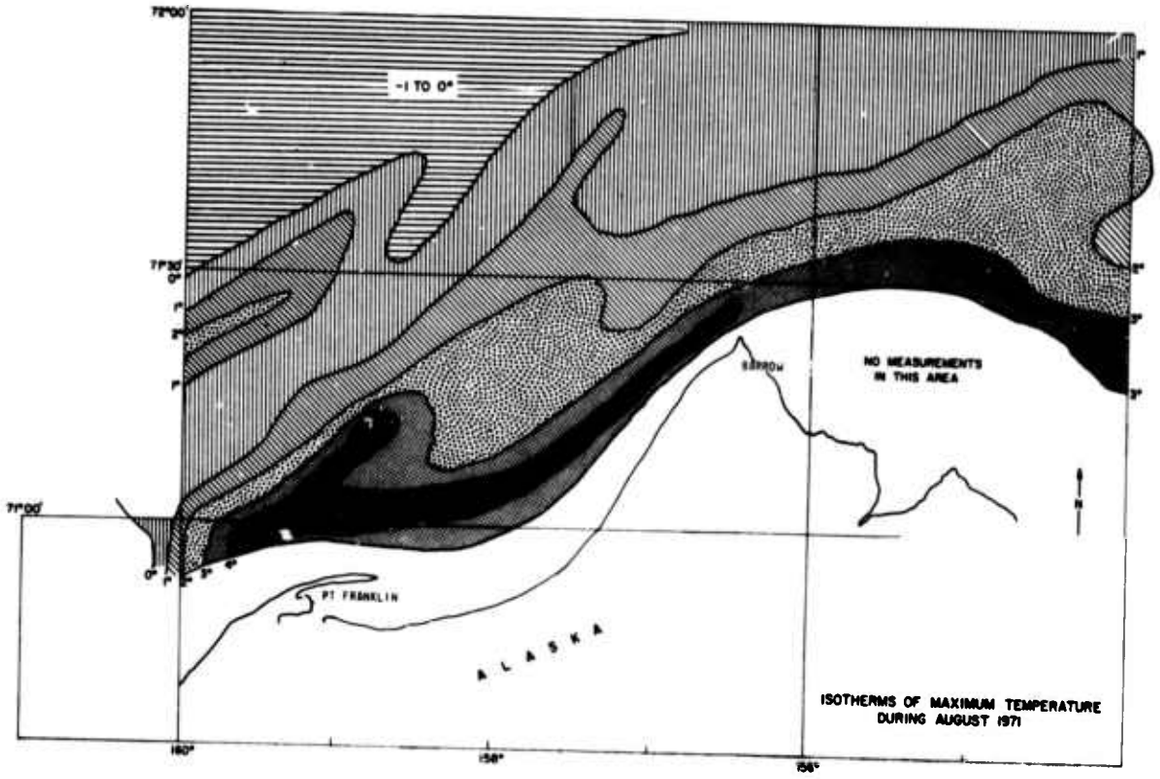

Figure 46. Isotherms of maximum temperature for August 1971.

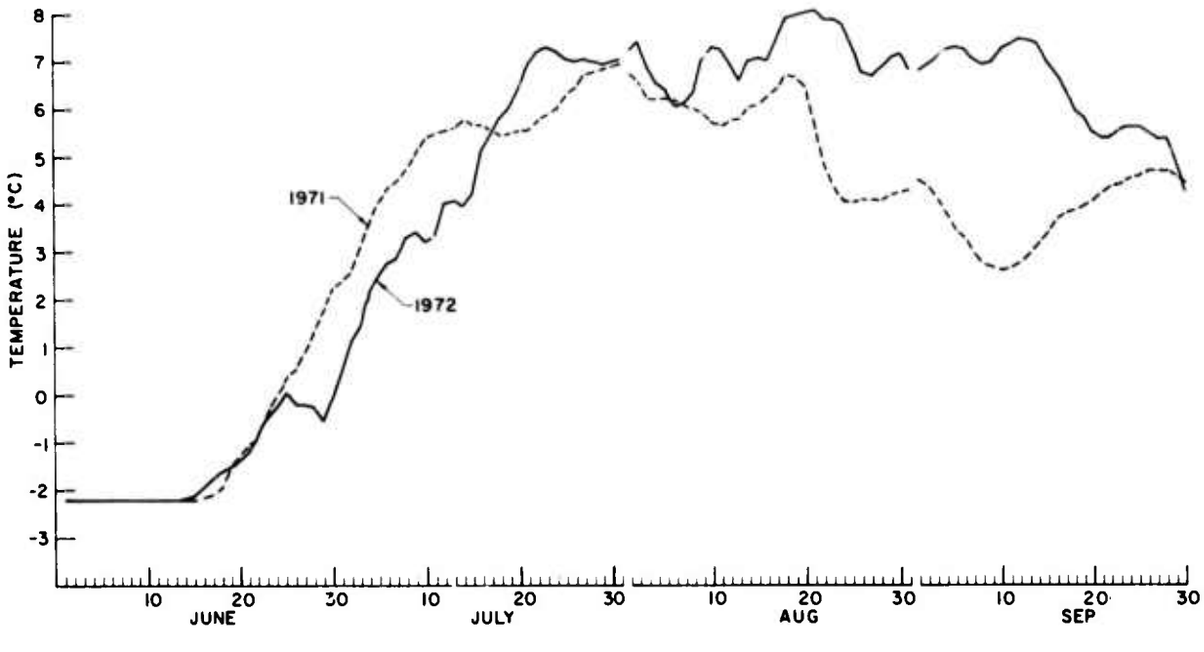

Figure 47. Bering Strait temperature as recorded near Wales by the Arctic Submarine Laboratory.

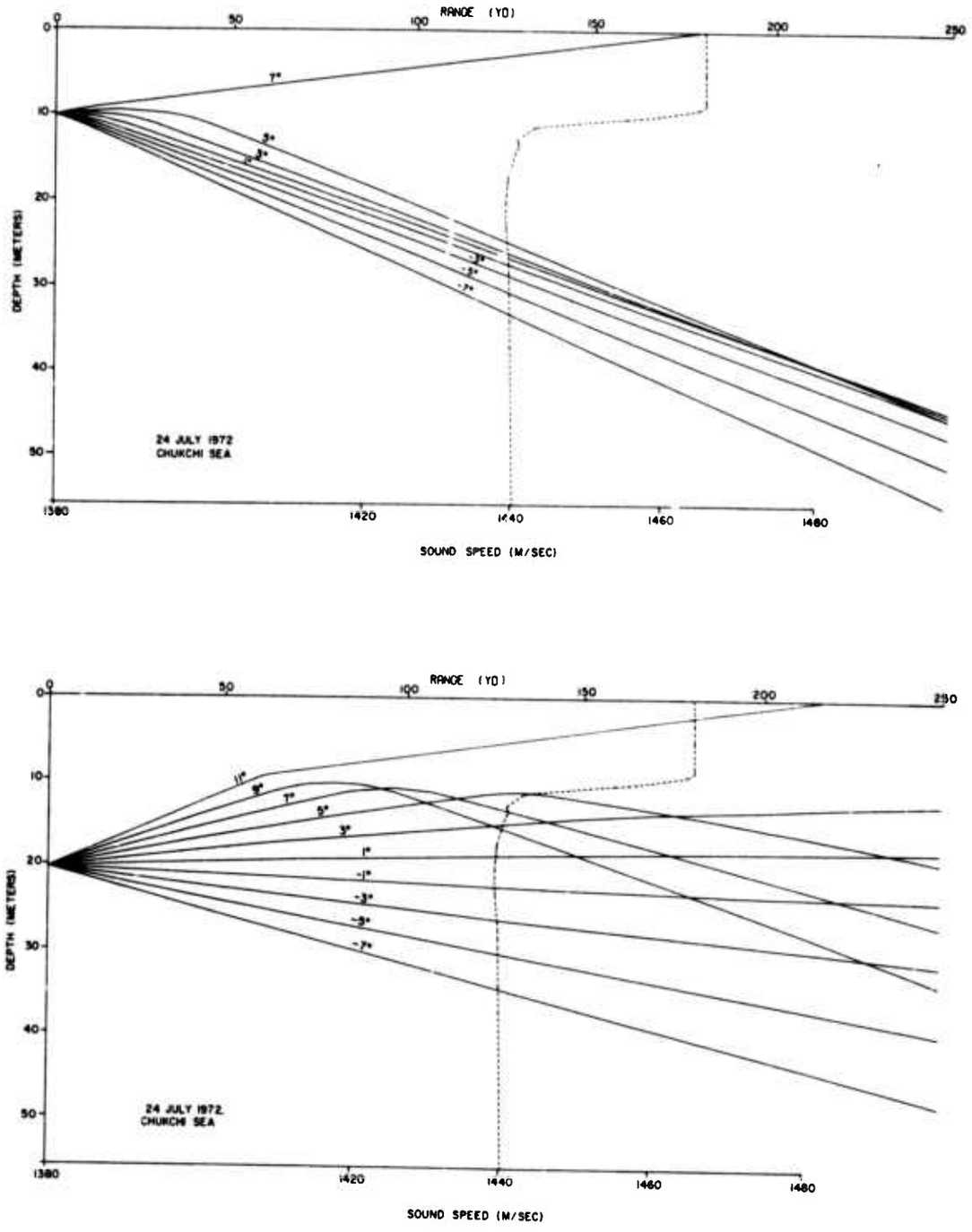

Figure 48. Sound ray diagrams showing the effect of the warm surface layer.

Thermal Microstructure

Measurements taken simultaneously at two stations the year before had shown that the thermal microstructure was distributed in layers of considerable horizontal extent. In order to obtain a better understanding of the size and movement of the layers, four stations were established on the floe at the corners of a 140-m square and provided with equipment for recording temperature profiles at regular intervals. Carefully calibrated thermistors ensured that the profiles at the four stations could be compared.

The profile data were transferred from paper tape to magnetic tape for processing by the CDC 6400 computer at the University of Washington. A special program was developed to read the tapes, calculate and plot the profiles, select and characterize all thermal layers, and punch a card for each layer. The profiles were then examined and compared to determine which layers were identifiable in profiles taken at other times or at other stations. Such layers were numbered and all cards for that layer were segregated.

To facilitate computations, a layer was defined as what might better be described as a "half layer" (Figure 49). For many closely spaced layers, the definition is a convenient one. A negative layer is shown in the figure; the next layer below it would be positive. Layers with temperature differences less than 0.03°C were ignored.

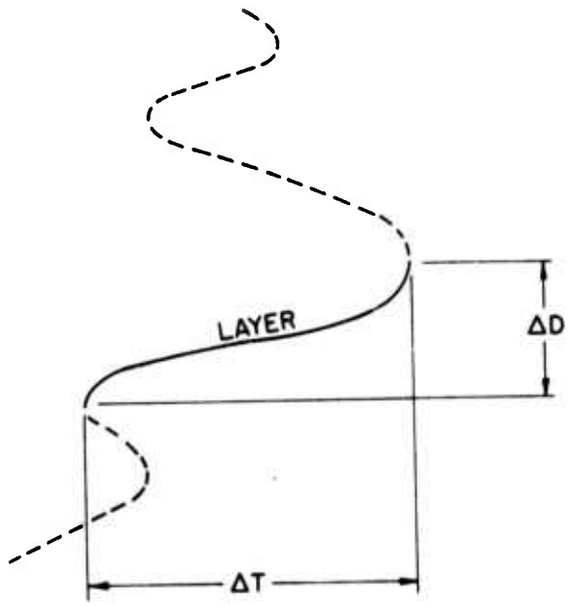

Figure 49. Authors' definition of a thermal layer.

The first measurements of the temperature profile at Camp 1 indicated a fairly smooth transition from 0°C at the surface to -1.75°C at 50 m. However, when the profiles were replotted at an expanded scale, microstructure with variations up to 0.2°C was observed to a depth of 40 m. The microstructure changed character hourly but persisted throughout the ice floe occupation.

The most complete series of hourly temperature profiles was made at Camp 1. Figure 50 is a plot of this series for the 8-day period. In the figure each successive profile is offset 0.5° from the previous one.

From 4 to 9 August an attempt was made to take hourly profiles at all four stations simultaneously. Because of equipment failure, however, usually only three stations were operating. These profiles are plotted for comparison in Figure 51.

On 8 and 9 August profiles were taken simultaneously at all four stations every 15 minutes for a 6-hour period except that equipment failure at Camp 3 caused loss of the 9 August afternoon data. These two series of profiles are plotted for comparison in Figures 52 and 53. The average temperature difference (ΔT) of all layers observed for the 6-hour period on each day was calculated. The distribution in temperature difference and the average depth interval (ΔD) of the layers are shown in Figure 54. The extreme variability of the layers is indicated by the large standard deviation, which tends to exceed the average.

The effect of a layer on sound transmission also depends on the sharpness of the layer, defined here as $\Delta T/\Delta D$. For 8 and 9 August the layer sharpness was:

	Sharpness (degrees/meter)	
	Positive Layers	Negative Layers
8 Aug	0.092	0.057
9 Aug	0.080	0.107

The thermal layers can usually be identified by their temperature, depth and shape on the temperature-depth profile. Many of the layers during the 8 and 9 August series were observed at two or more of the four stations. The average number of stations observing each layer was 2.22 for 8 August and 2.23 for 9 August--a remarkably close agreement considering the difference in current for those two days. A calculation of the number of stations that would observe a circular layer of radius R when all layer locations are considered resulted in the curve shown in Figure 55. The layer radius that would agree with an observation by an average of 2.23 stations is 255 m. This value is one estimate of the size of the layers.

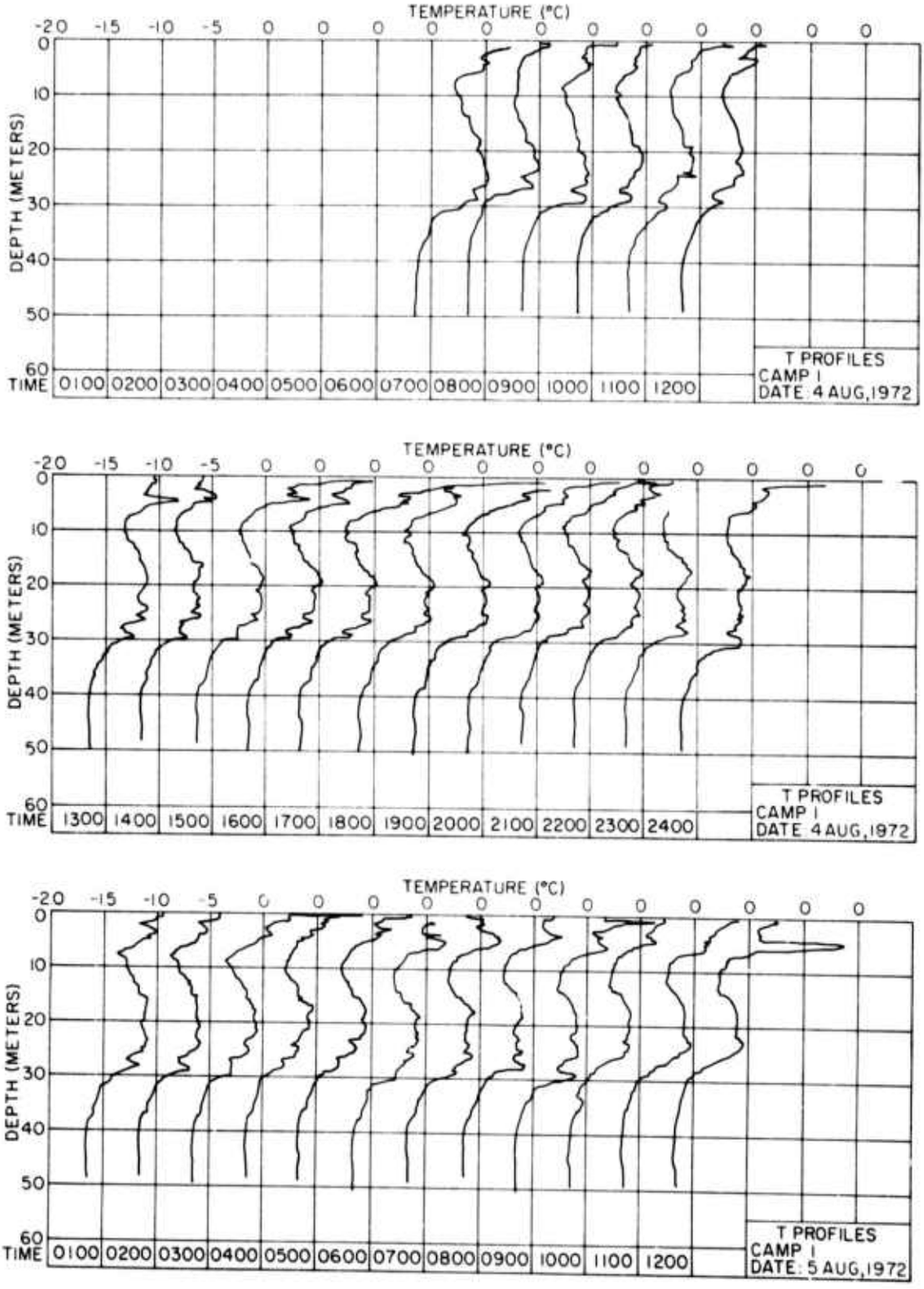

Figure 50. Hourly temperature profiles at Camp 1.

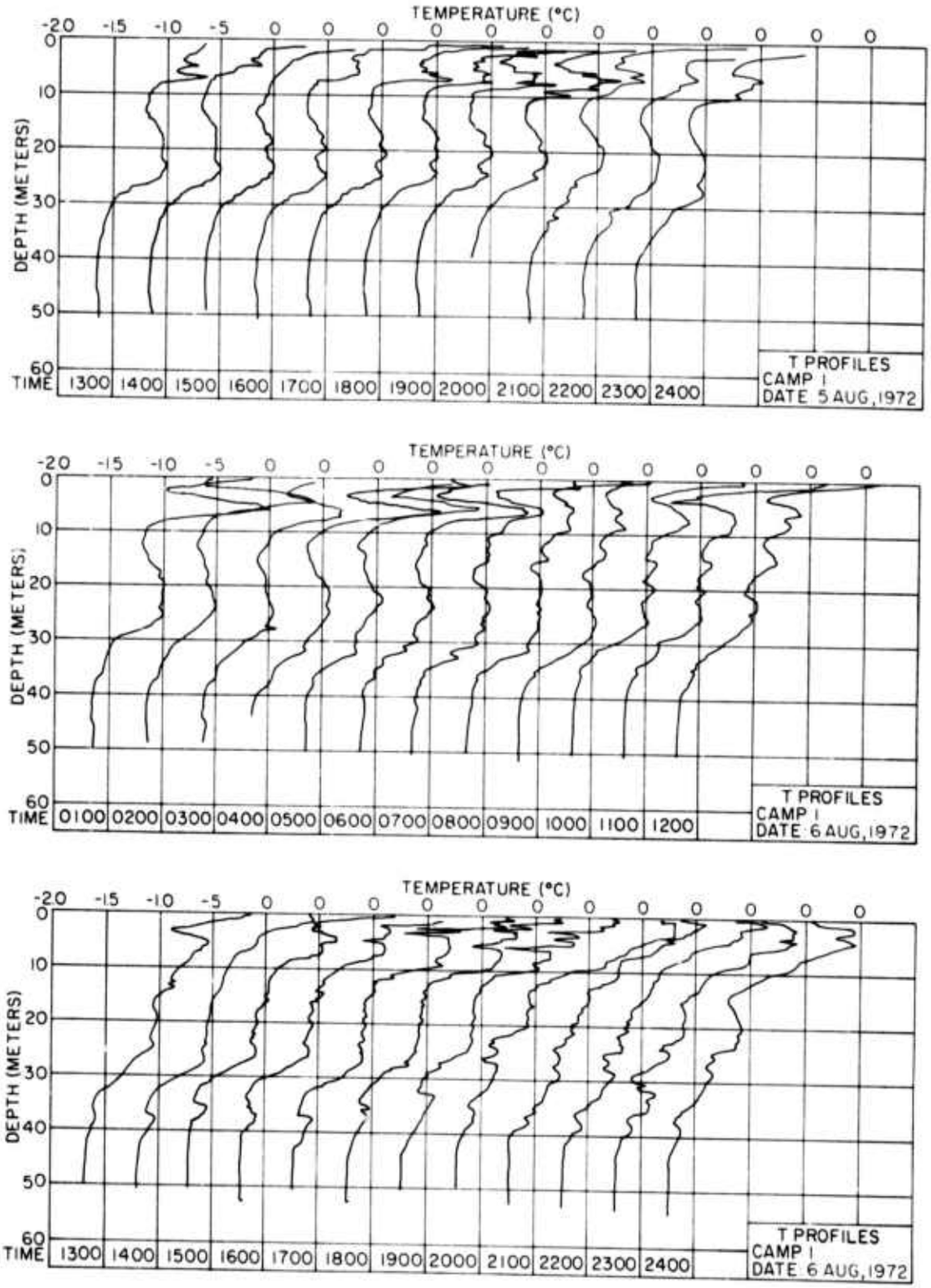

Figure 50. Hourly temperature profiles at Camp 1, cont.

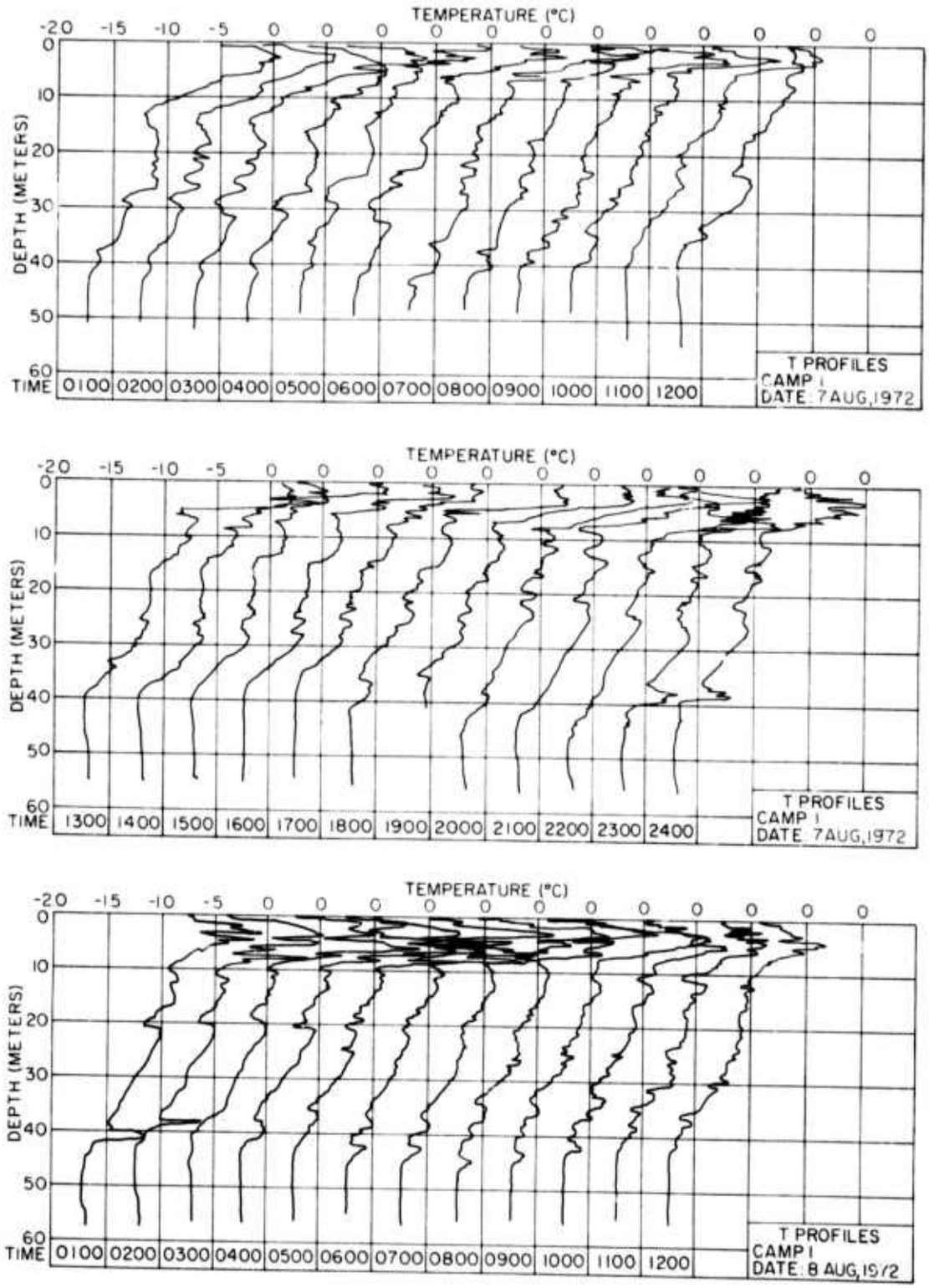

Figure 50. Hourly temperature profiles at Camp I, cont.

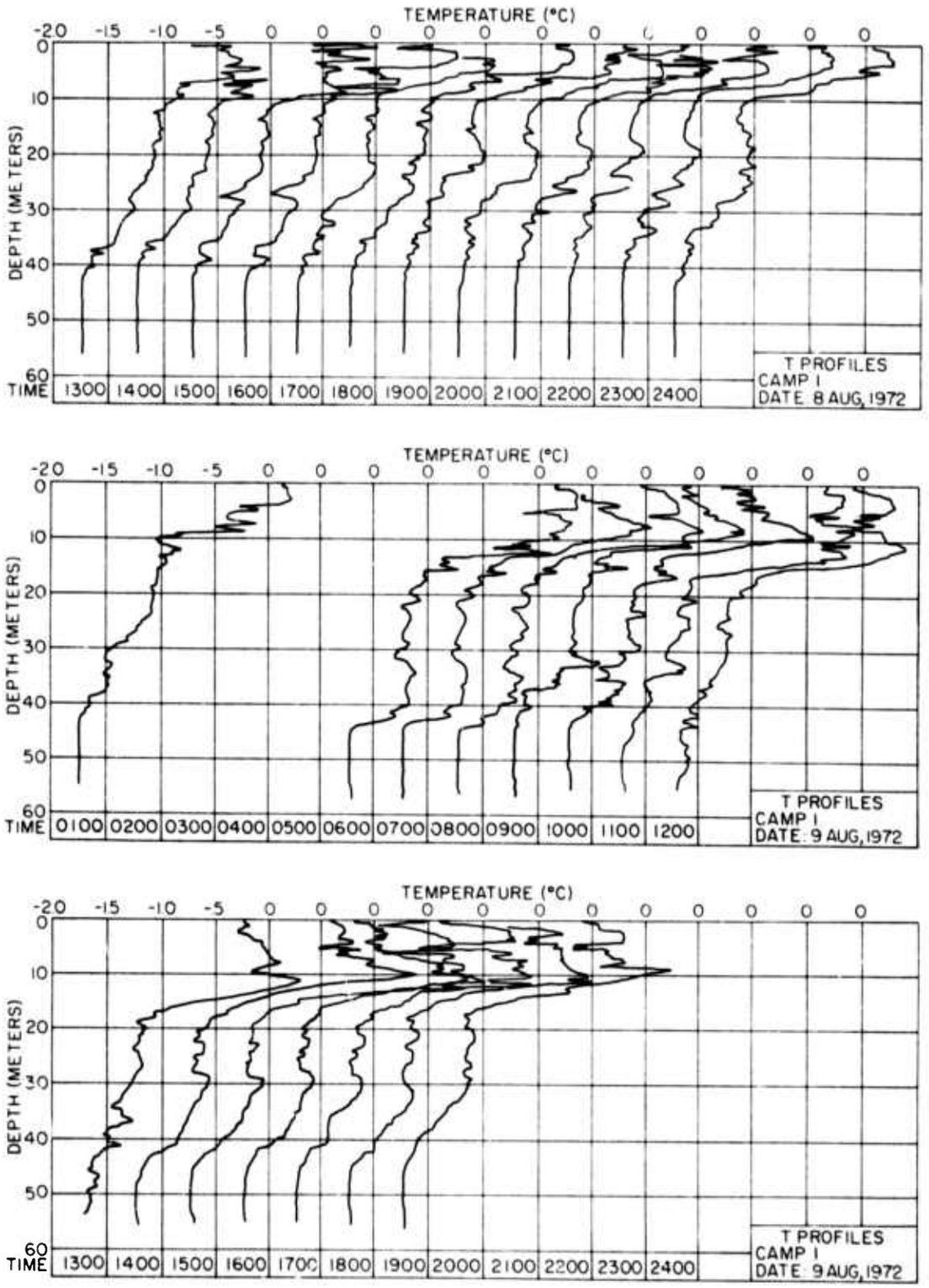

Figure 50. Hourly temperature profiles at Camp 1, cont.

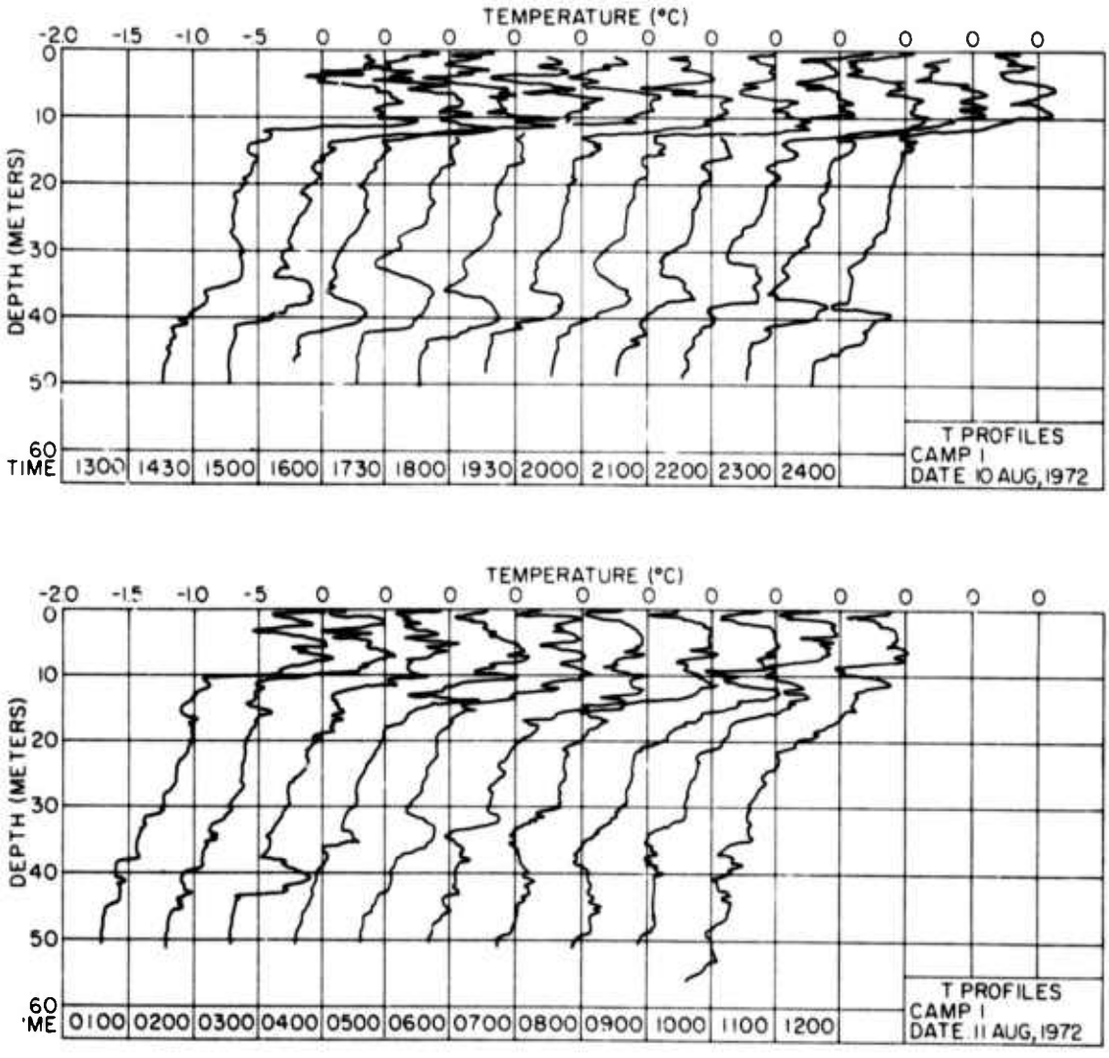

Figure 50. Hourly temperature profiles at Camp 1, cont.

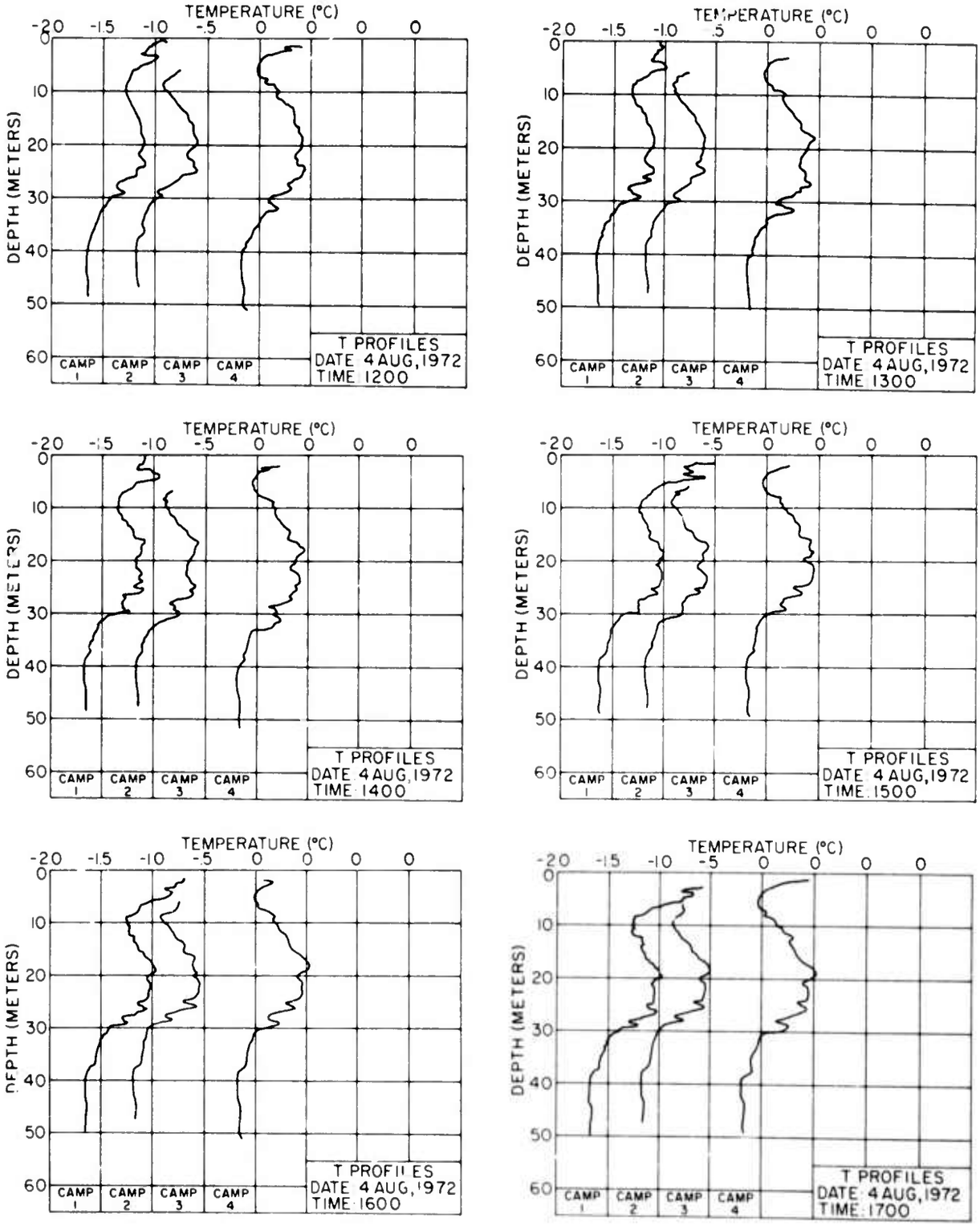

Figure 51. Simultaneous temperature profiles at four stations.

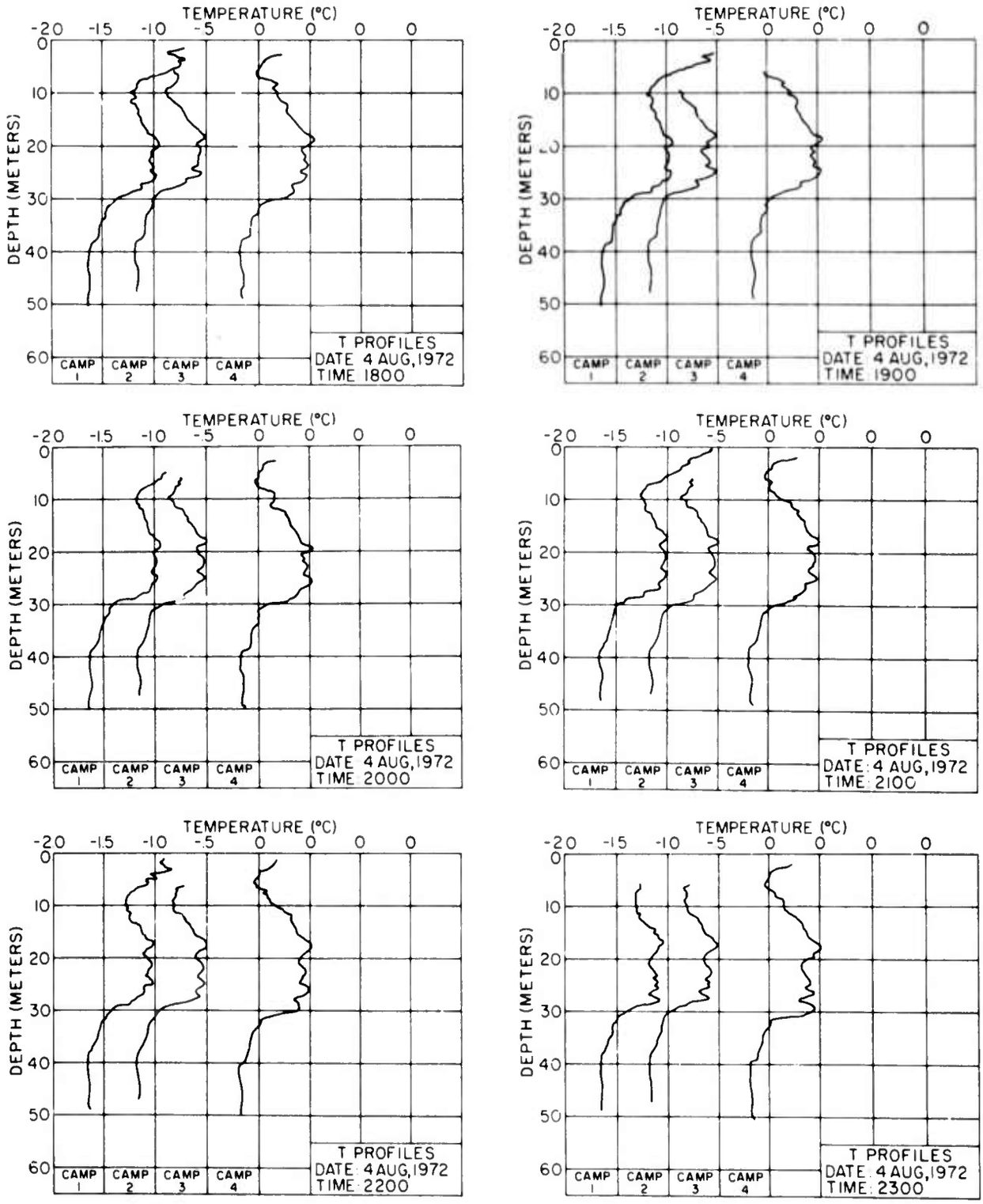

Figure 51. Simultaneous temperature profiles at four stations, cont.

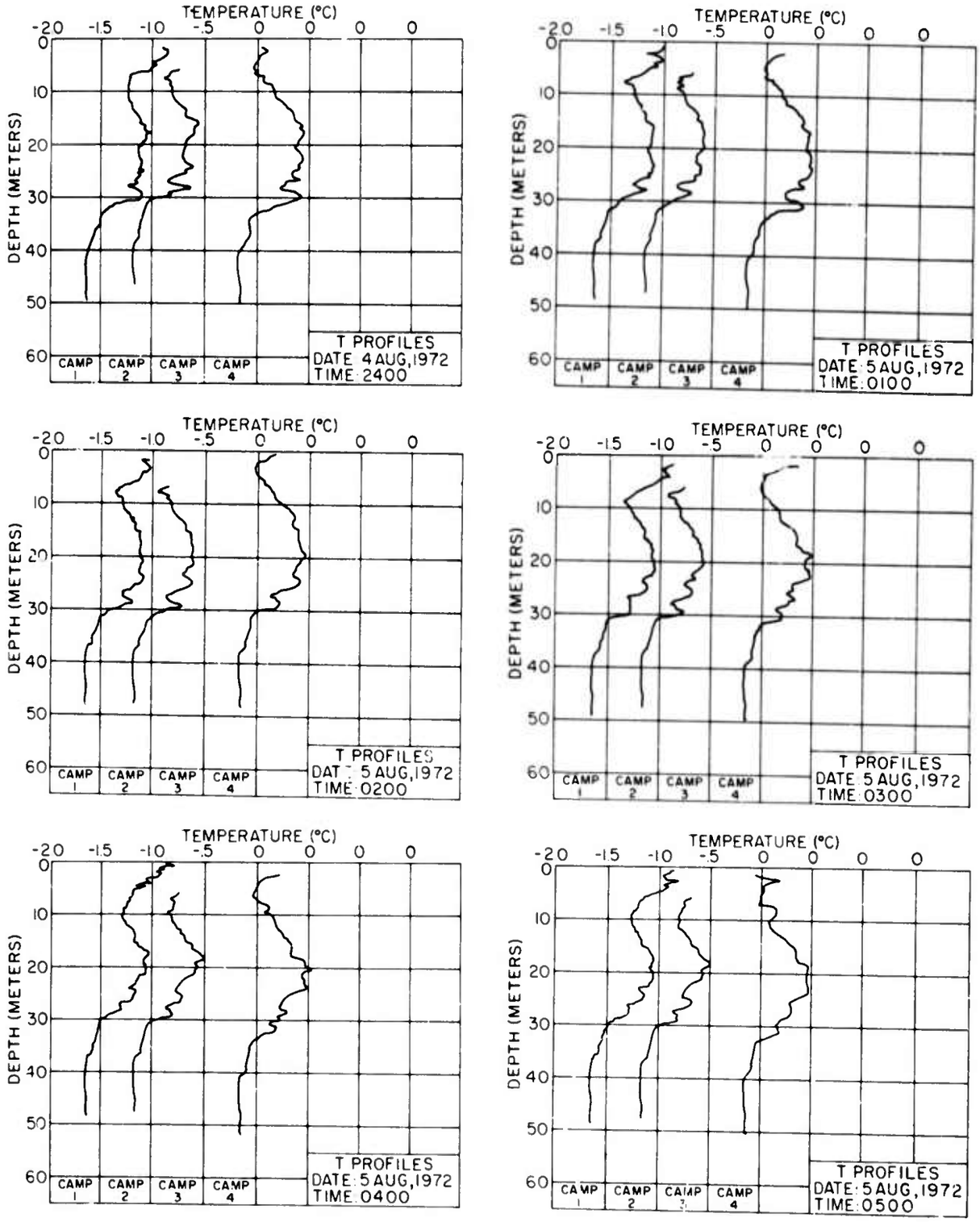

Figure 51. Simultaneous temperature profiles at four stations, cont.

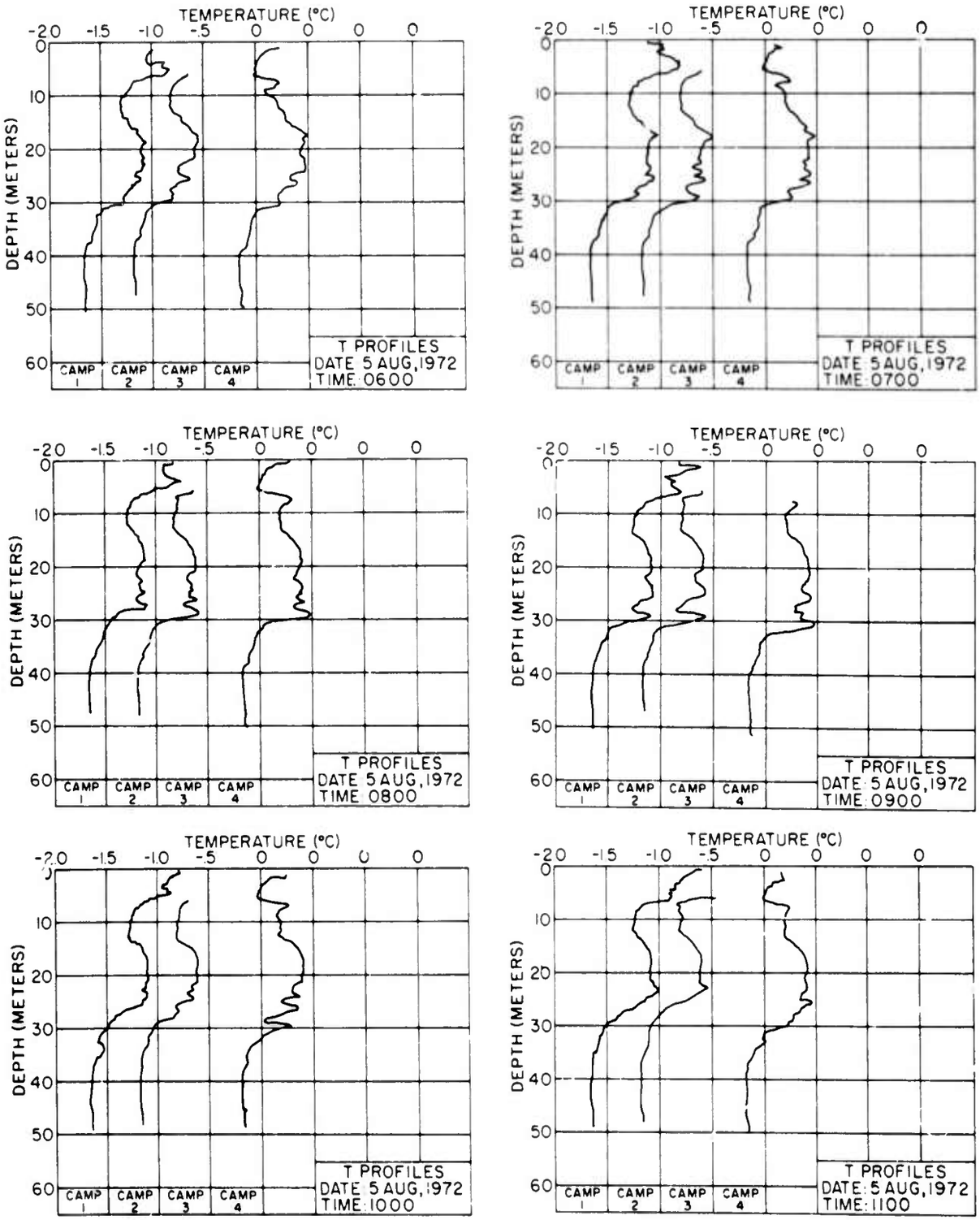

Figure 51. Simultaneous temperature profiles at four stations, cont.

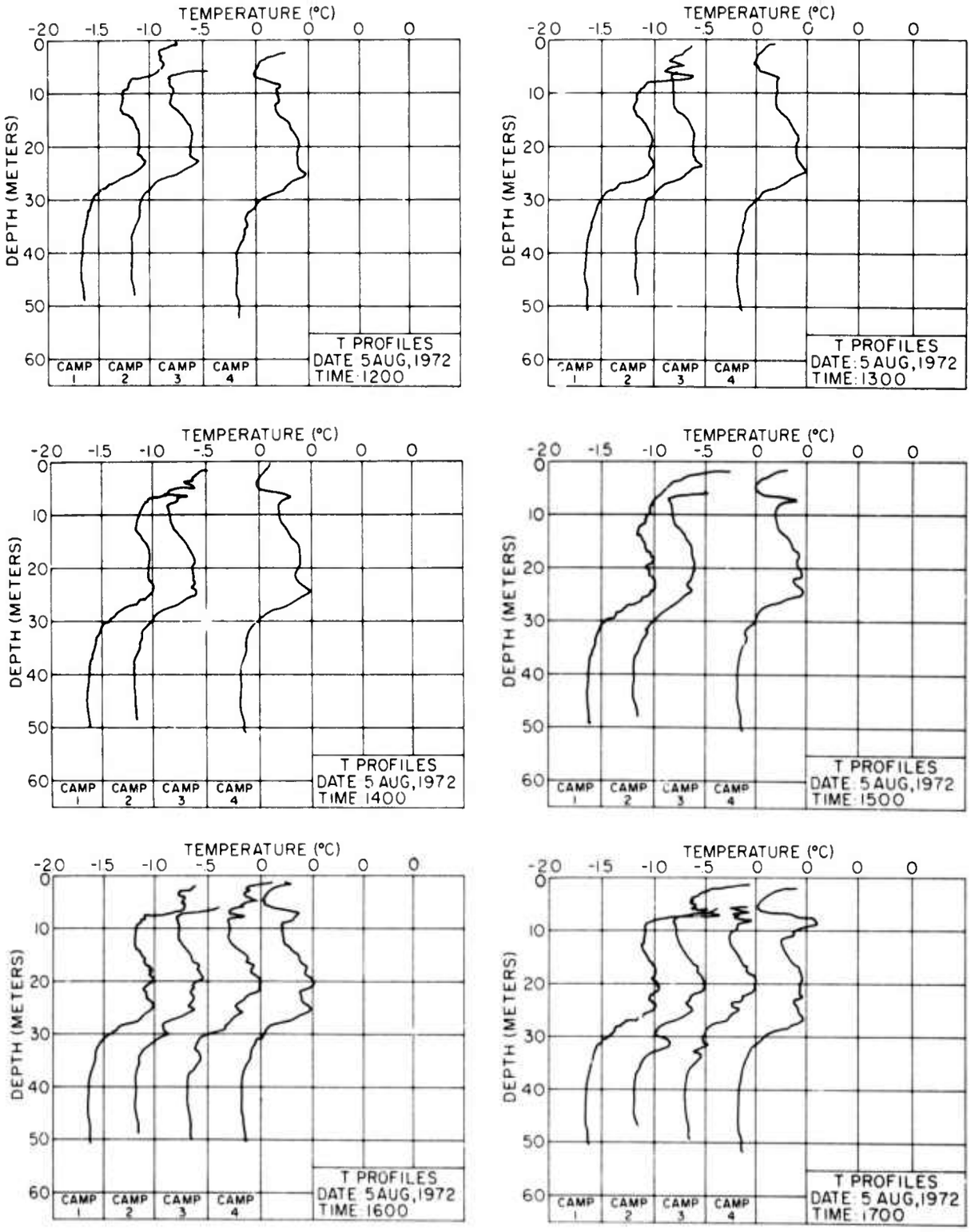

Figure 51. Simultaneous temperature profiles at four stations, cont.

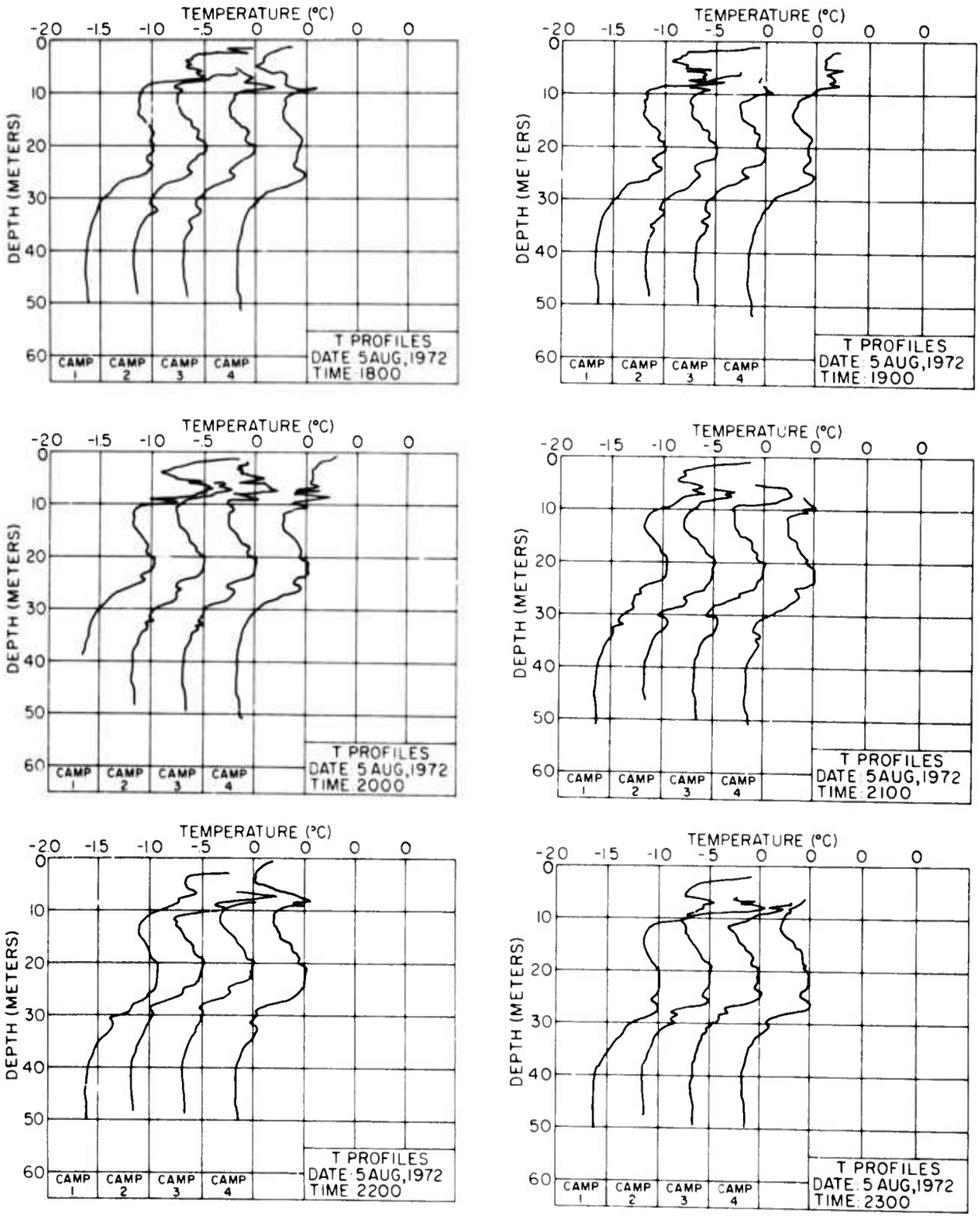

Figure 51. Simultaneous temperature profiles at four stations, cont.

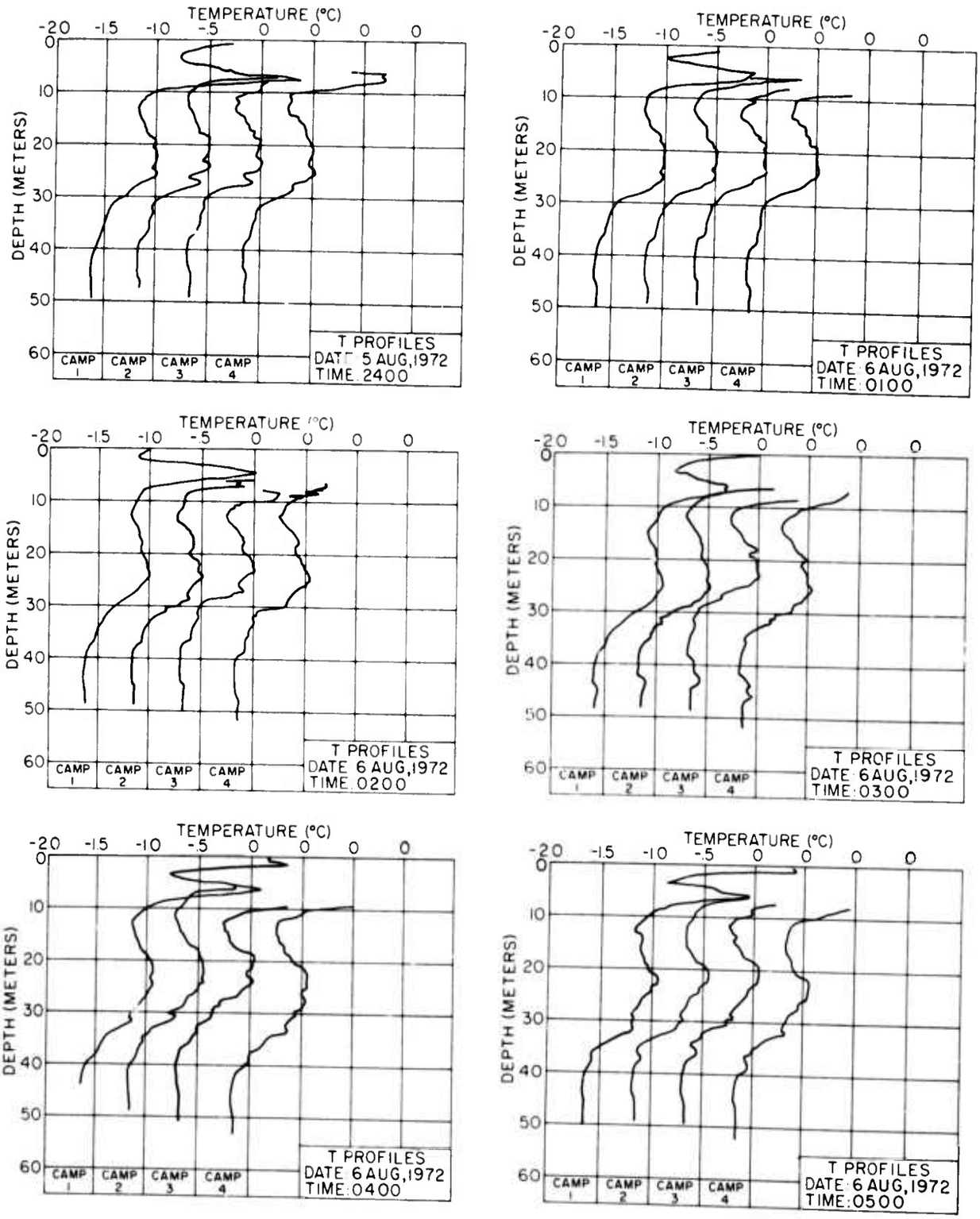

Figure 51. Simultaneous temperature profiles at four stations, cont.

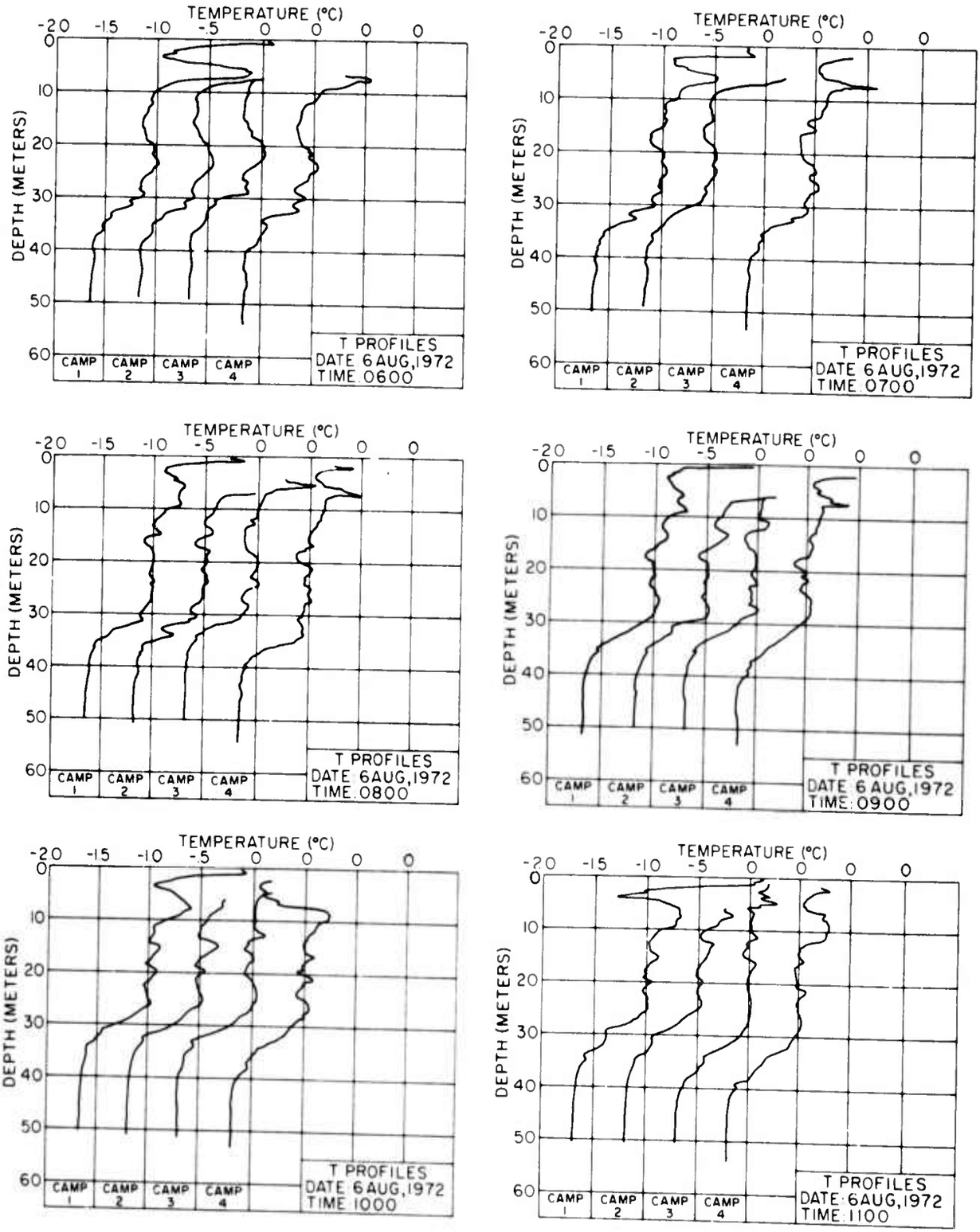

Figure 51. Simultaneous temperature profiles at four stations, cont.

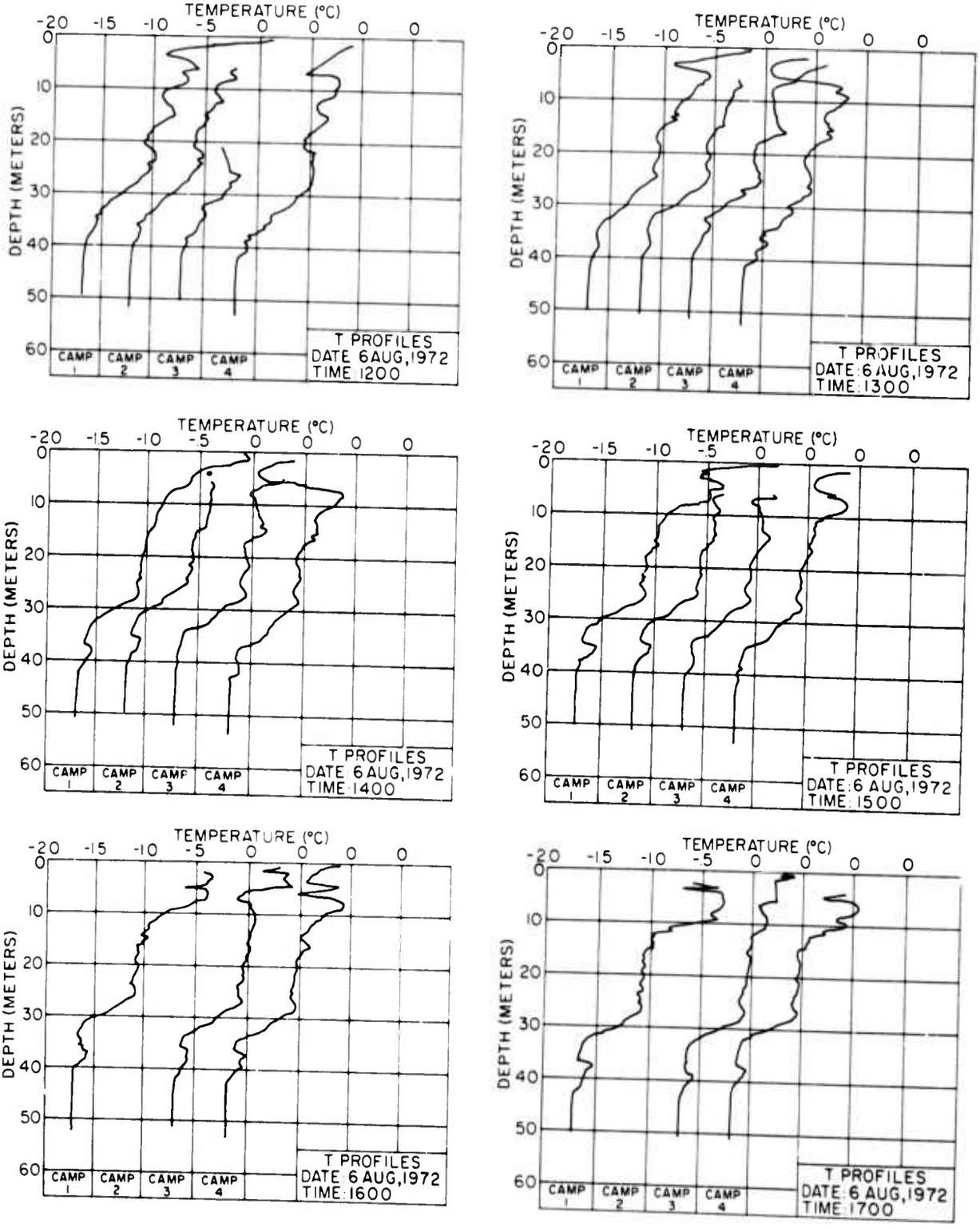

Figure 51. Simultaneous temperature profiles at four stations, cont.

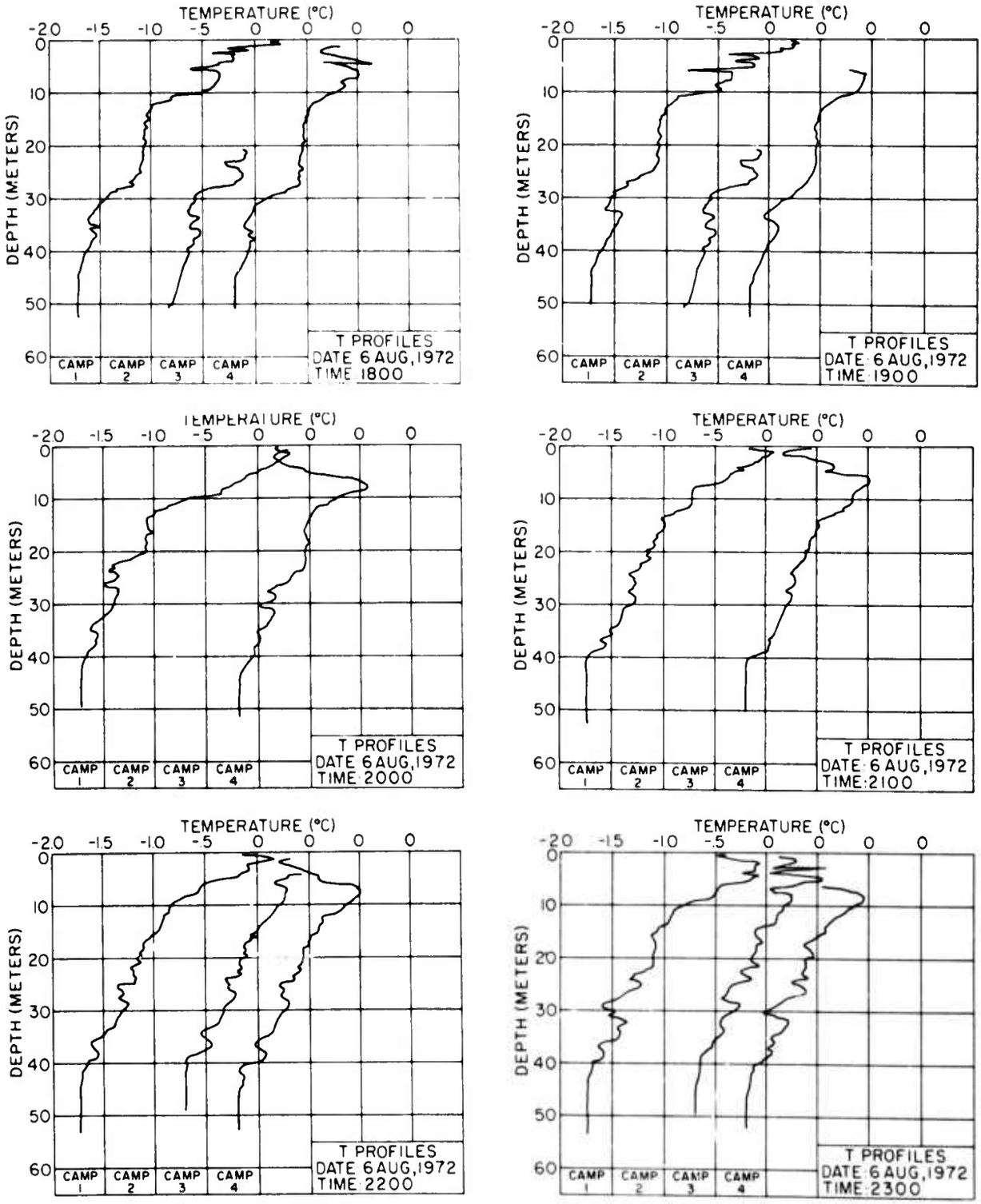

Figure 51. Simultaneous temperature profiles at four stations, cont.

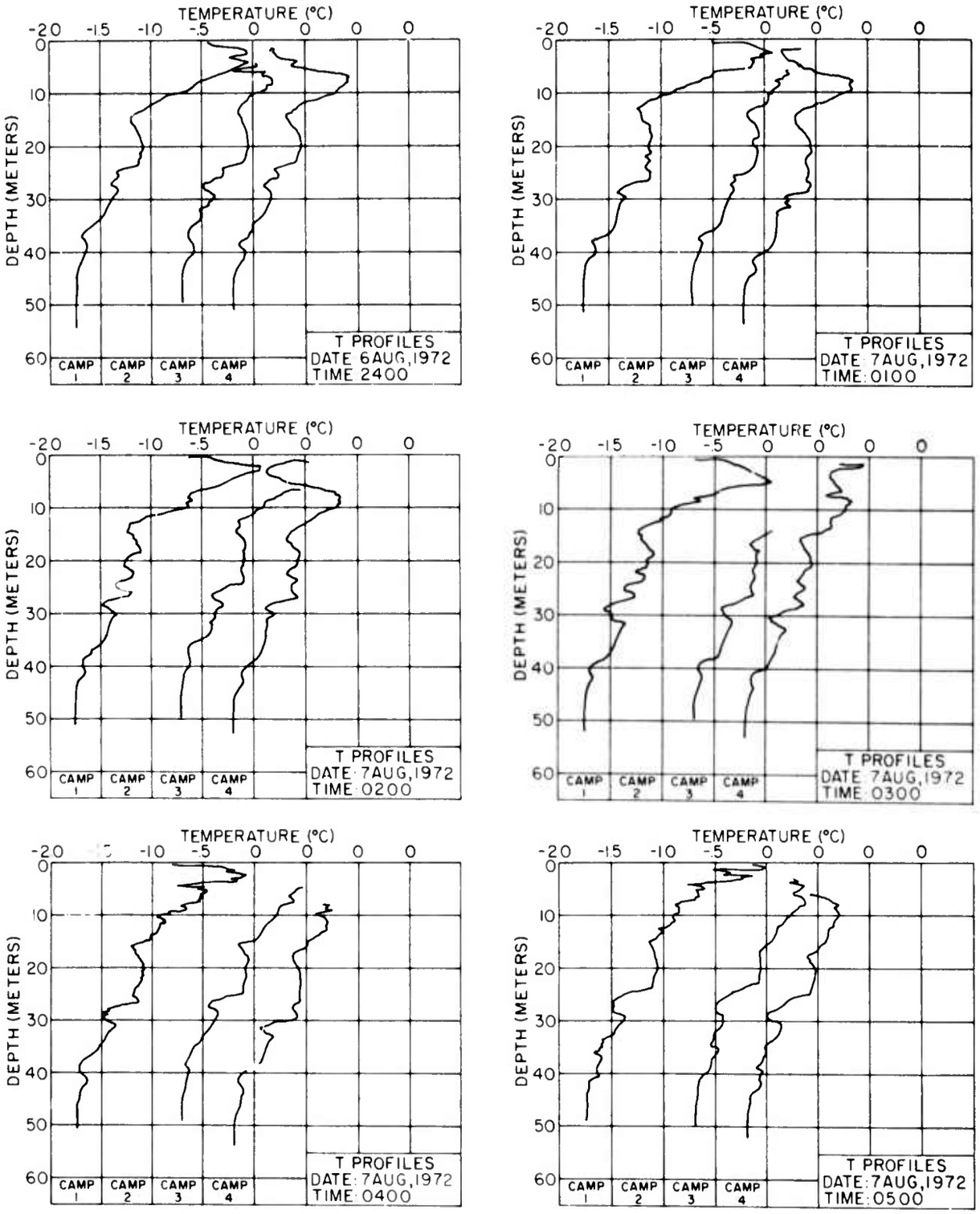

Figure 51. Simultaneous temperature profiles at four stations, cont.

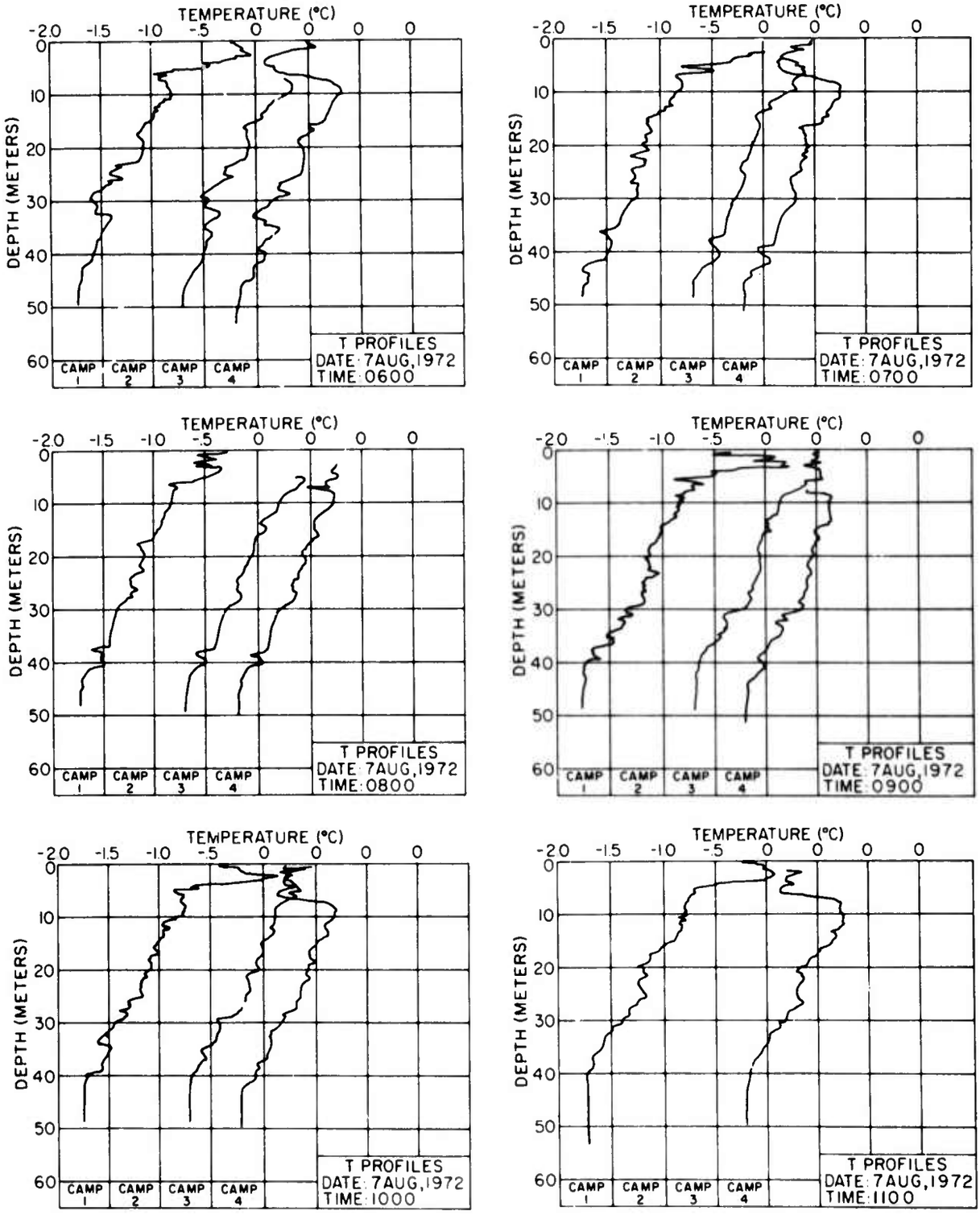

Figure 51. Simultaneous temperature profiles at four stations, cont.

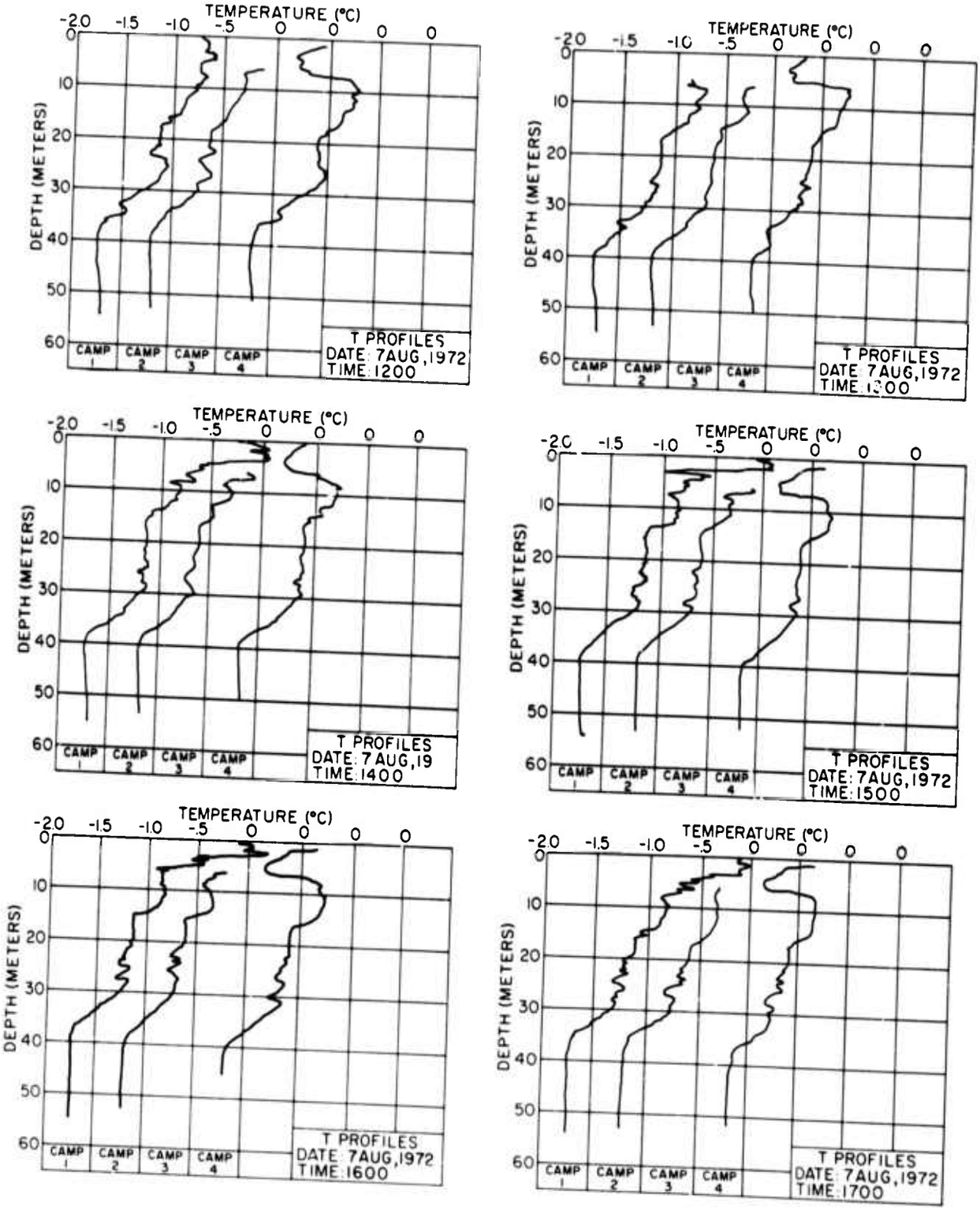

Figure 51. Simultaneous temperature profiles at four stations, cont.

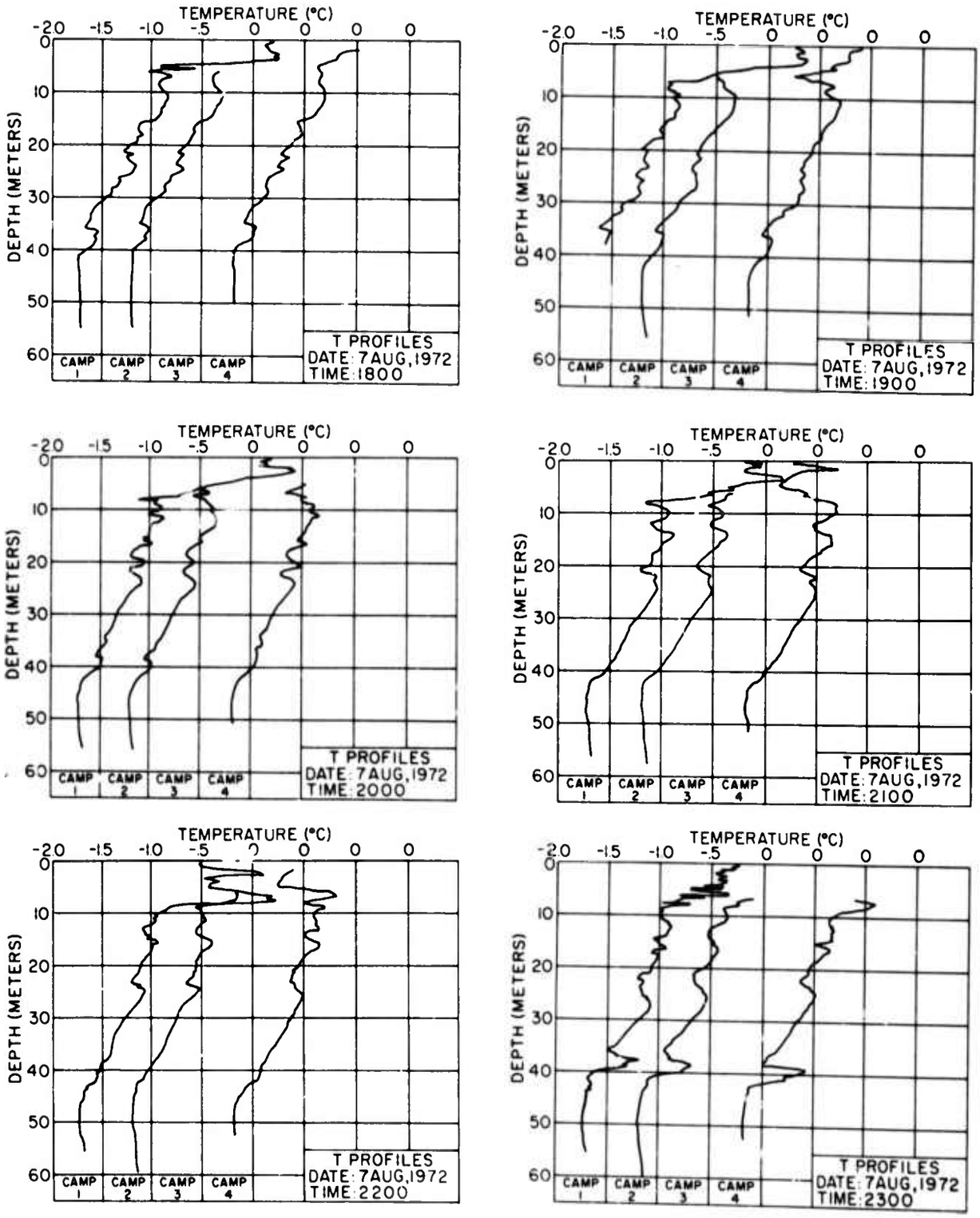

Figure 51. Simultaneous temperature profiles at four stations, cont.

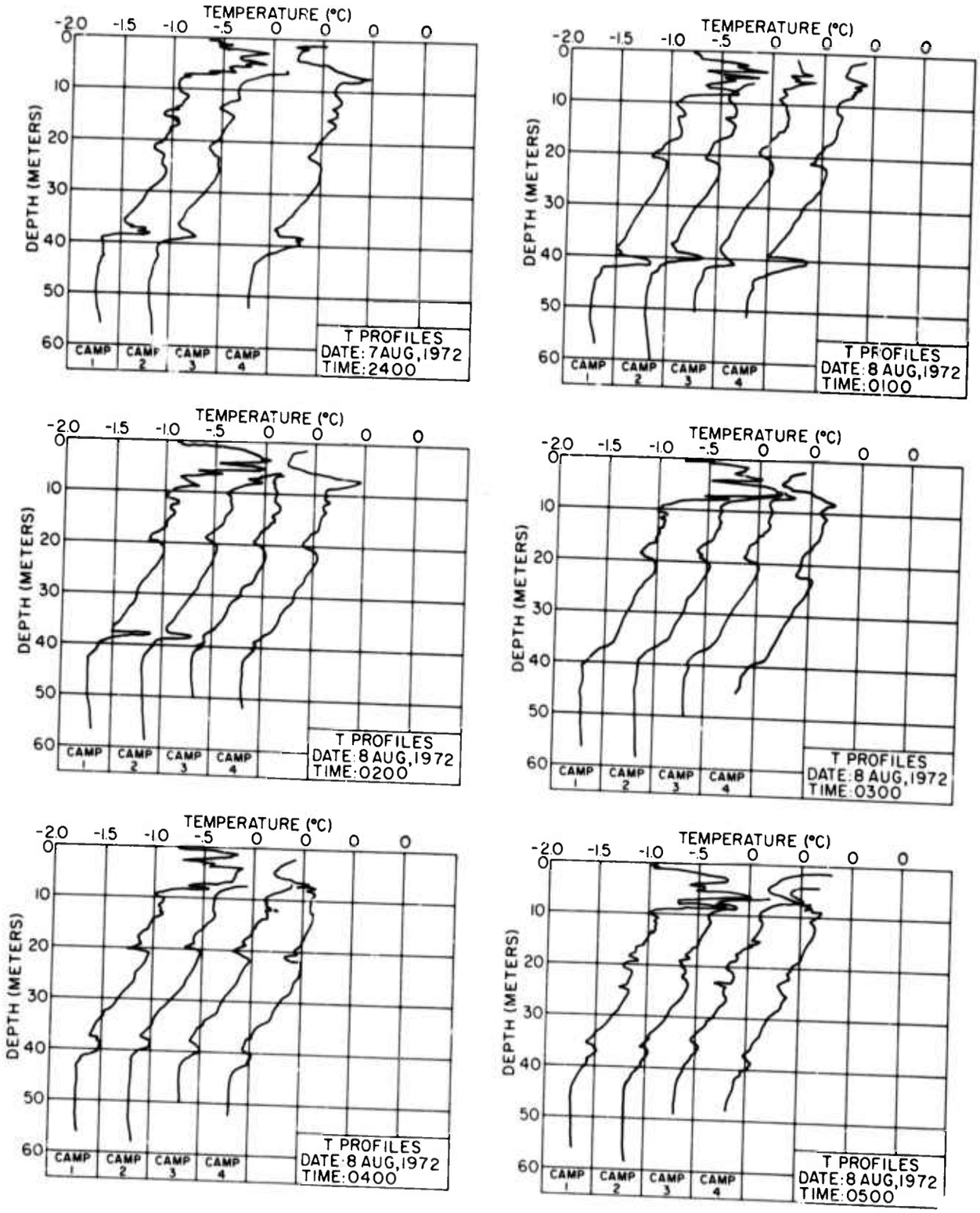

Figure 51. Simultaneous temperature profiles at four stations, cont.

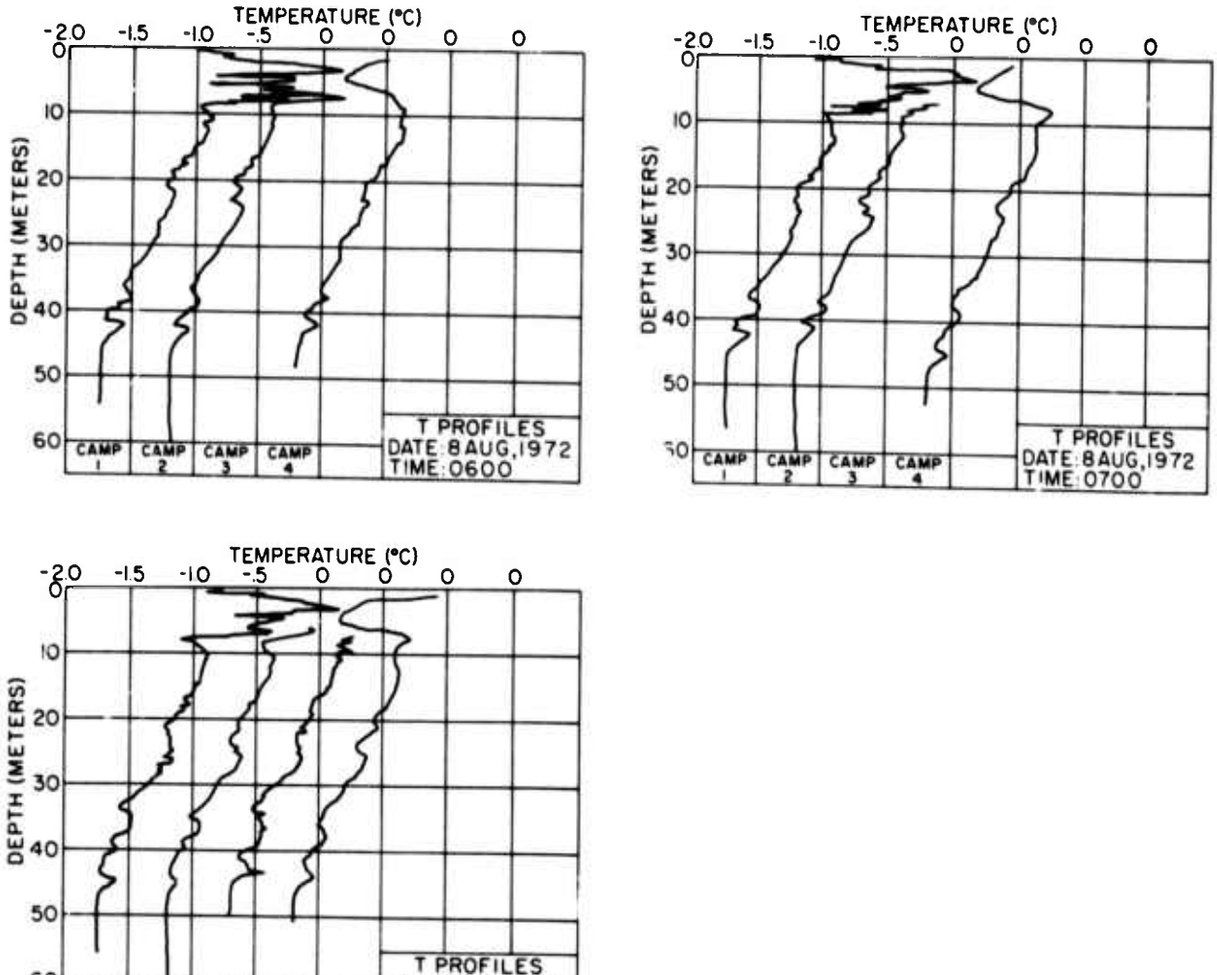

Figure 51. Simultaneous temperature profiles at four stations, cont.

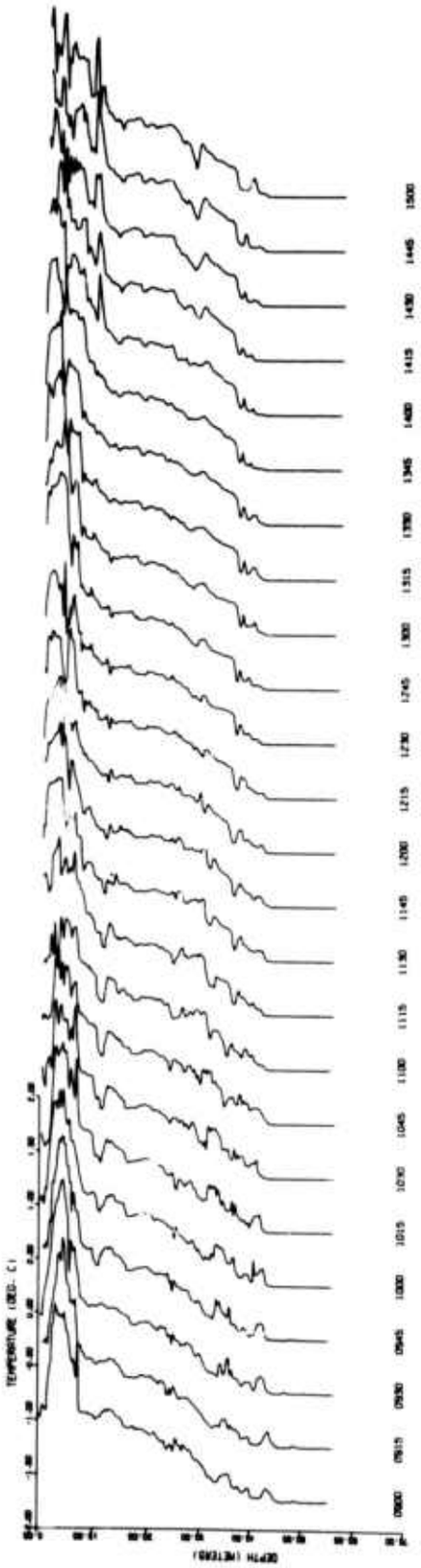

Camp 1

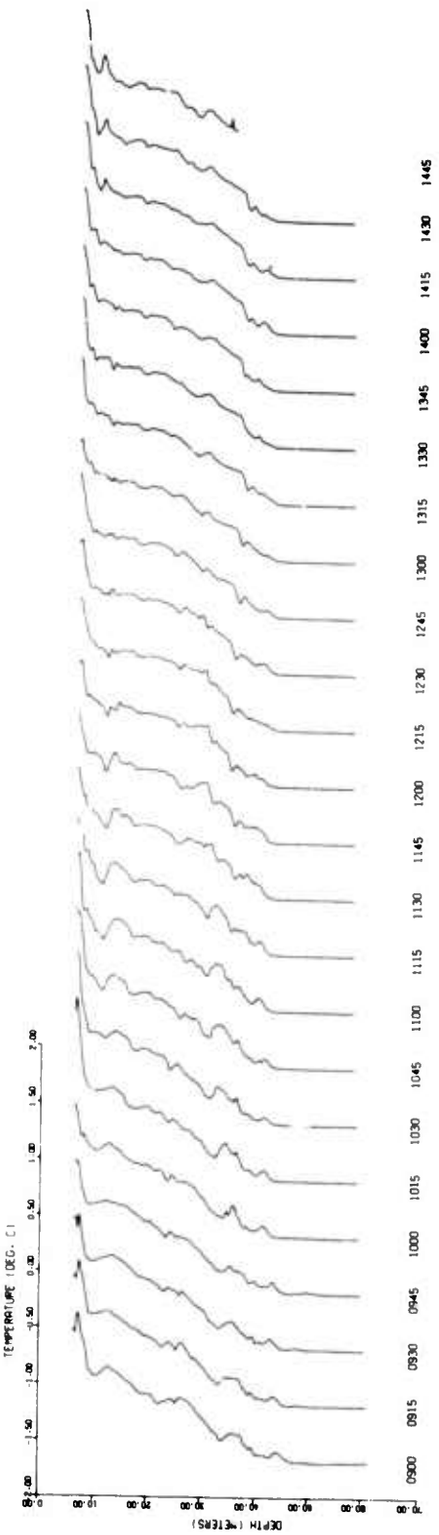

Camp 2

Figure 52. Temperature profiles for Camps 1-4, 8 August 1972.

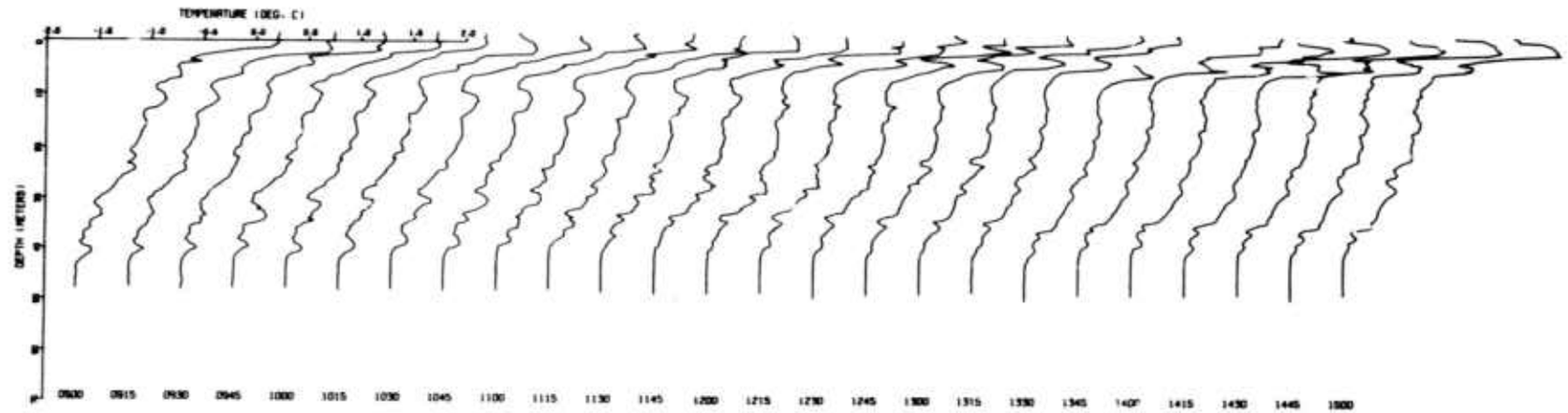

Camp 3

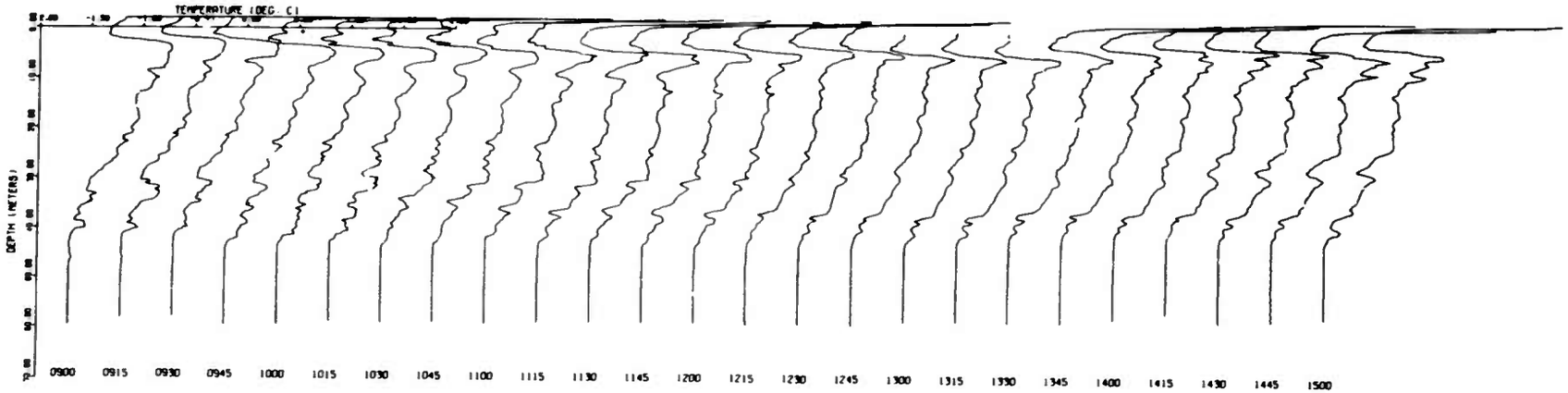

Camp 4

Figure 52. Temperature profiles for Camps 1-4, 8 August 1972, cont.
(inaccuracies in the pressure transducer account for the error in depth at the surface)

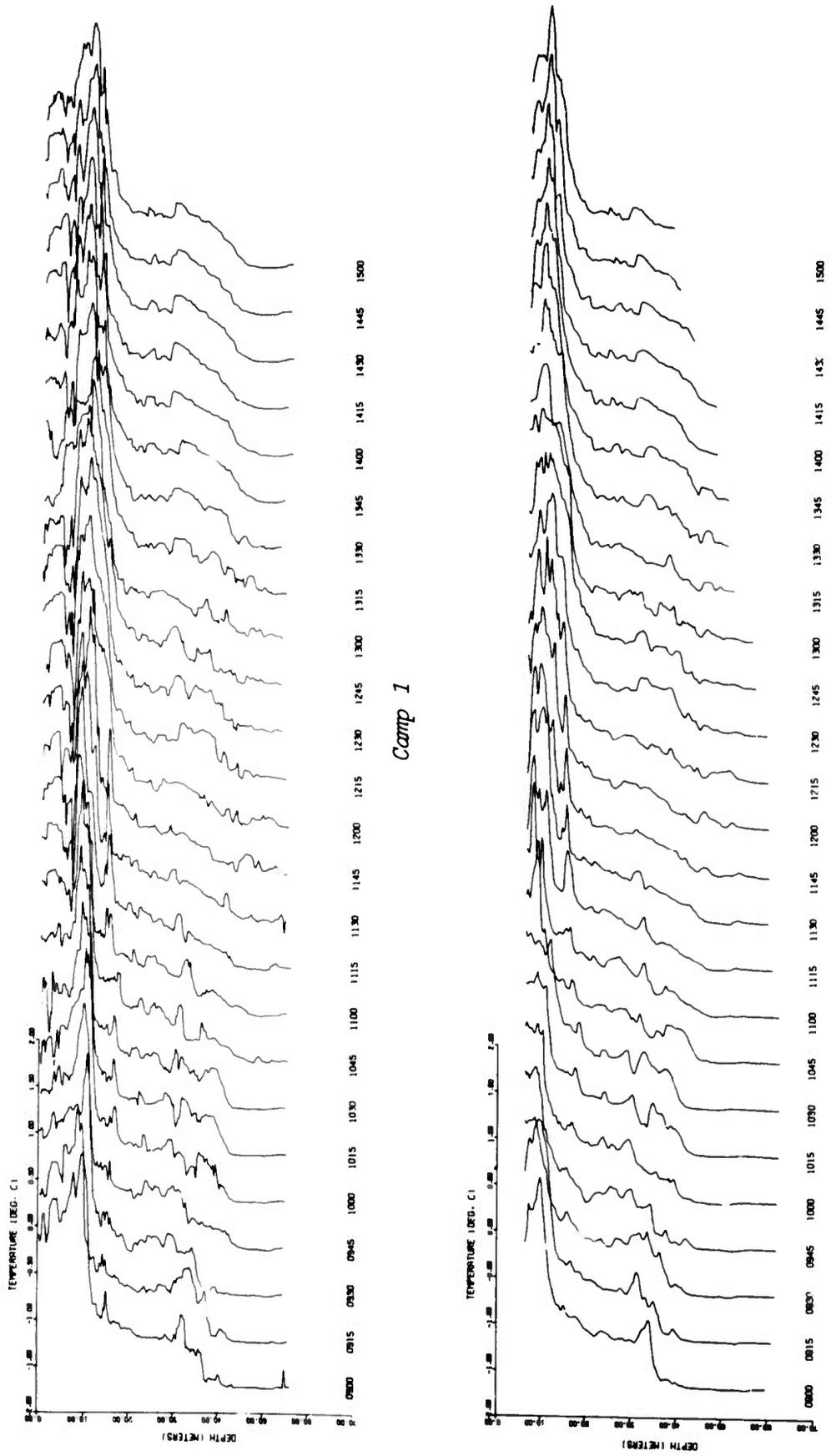

Figure 53. Temperature profiles for Camps 1-4, 9 August 1972.

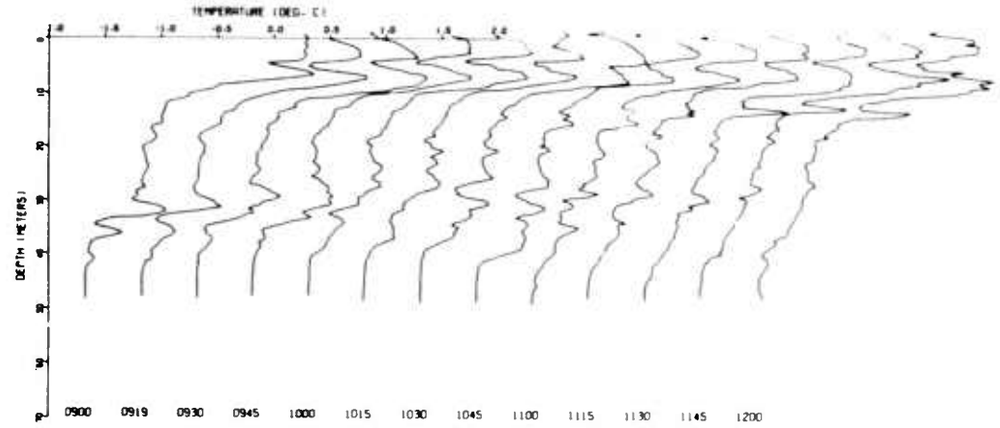

Camp 3

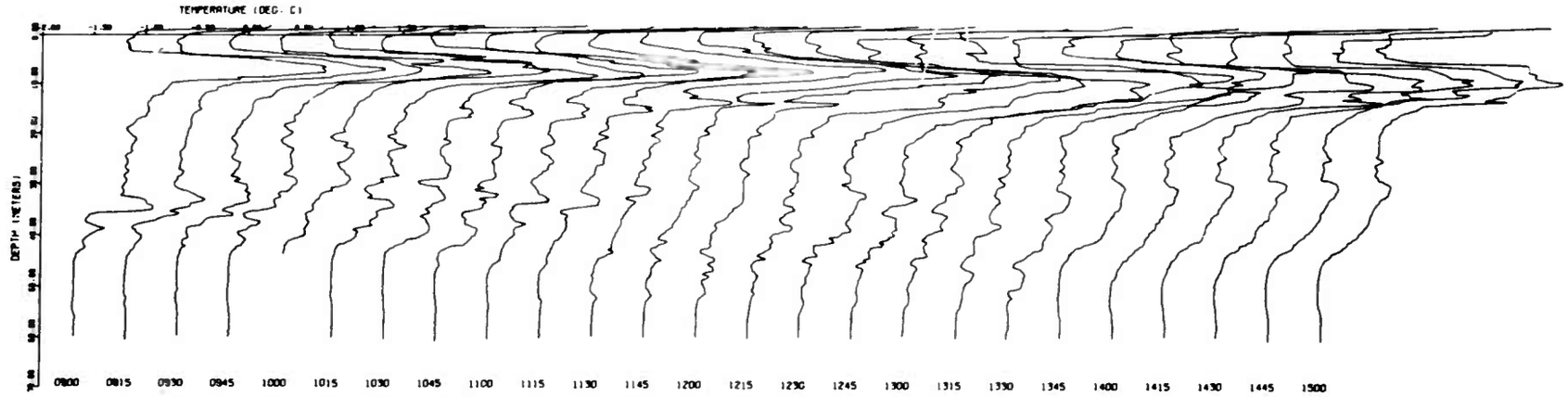

Camp 4

Figure 53. Temperature profiles for Camps 1-4, 9 August 1972, cont. (inaccuracies in the pressure transducer account for the error in depth at the surface)

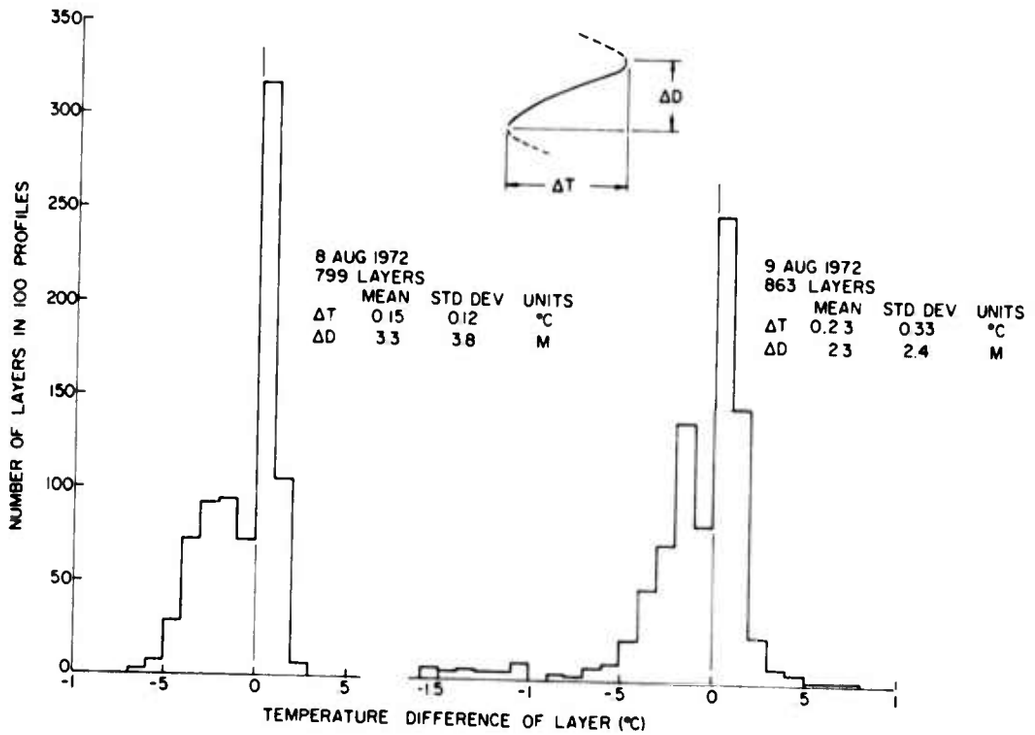

Figure 54. Distribution in temperature difference of thermal layers.

The layers appear to be very irregular and attempts to determine the shape and size of an individual layer have been unsuccessful. Therefore we have concentrated on studying the layers statistically to determine general characteristics. The relative movement of the floe with respect to the water is an important factor. Compare, for example, 8 and 9 August, when the situation differed considerably.

On 8 August the floe moved very slowly, 0.15 kn at 130° true bearing. The relative current was 0.14 kn at 146° true with an 8-kn head wind, indicating that the water carried the floe in a southeasterly direction but the head wind slowed its progress. On the average, each layer was identified for nine successive profiles (135 minutes). Considering the relative current and assuming that the floe was moving past layers fixed in the water, the average layer length would then be 600 m.

On 9 August, the floe moved much faster, 0.42 kn at 96° true, with a relative current of 0.36 kn at 41° true. A 3-kn tail wind probably had little effect. On the average, each layer was identified for eight profiles (120 minutes), indicating an average length, considering the relative current, of 1300 m.

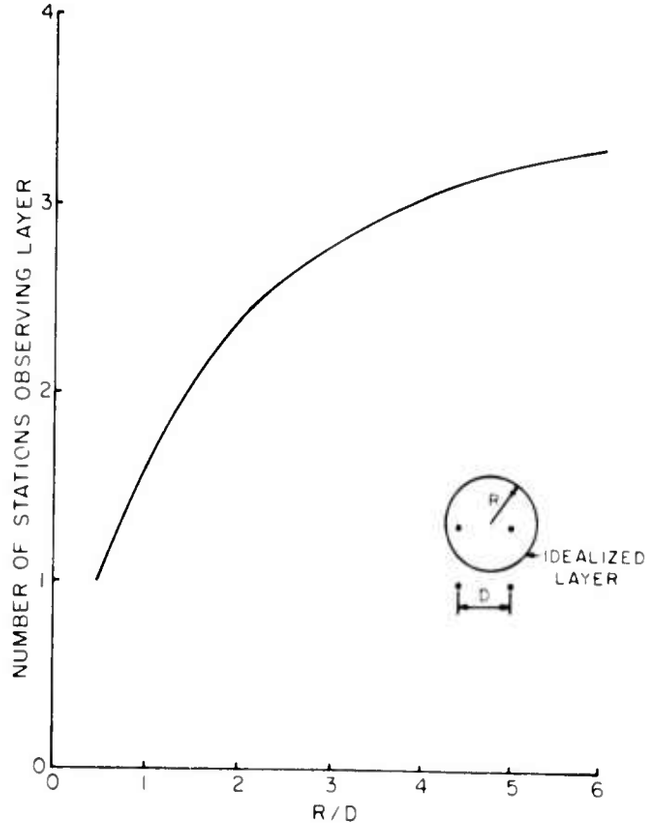

Figure 55. Number of stations that would observe random layers with a ratio of layer radius to station spacing of R/D.

These calculations assume that the floe is moving over fixed, pre-existing layers. The large difference in layer size (600 m vs 1300 m) indicates that this assumption is incorrect. On the other hand, a hypothesis that the layers are formed in the vicinity, decay slowly because of mixing, and should therefore be observed for a fairly constant time (assuming the floe stayed in the vicinity of the layer long enough) would mean that the layers, which were observed for about two hours on both days, were larger than 1300 m. The true picture is perhaps somewhere between these two hypotheses--some layers deteriorate and others move out of view.

Another indication of layer extent can be obtained by assuming that the temperature difference of a layer decreases linearly with distance. By comparing the observed difference at two camps one can compute the distance to the end of the layer. Doubling this distance gives a rough estimate of the horizontal extent of the layer. This procedure yields layer

lengths starting at 1000 m and scattering to three times that size for both dates.

Considering the spread in the various estimates of layer size made above, it appears that the observed layers were very irregular in shape and varied widely in size, from about 250 m to 1500 m. In this study no noticeable correlation between size and any other characteristic of the layer or of the MIZ was detected.

VI. ACOUSTIC PROPAGATION

The short range transmission of acoustic pulses in the 10-100 kHz range is important for submarine operation in the marginal ice zone. The prevalent thermal microstructure, especially when it consists of horizontal layering, results in considerable distortion to low angle transmissions. In order to measure and study the effect of the thermal layers, a transmitter was installed at one station on the ice floe and a receiver at another. The transmitting transducer was held at a fixed depth while the receiving transducer was raised or lowered to obtain a sound level-depth profile. At the same time a thermistor and Vibrotron pressure transducer attached just above the receiving transducer obtained a temperature profile. These measurements were taken hourly from 4 to 9 August. During the last two days on the floe some additional measurements were taken at other depths and ranges.

Instrumentation

The acoustic transmission equipment consisted of an electronic transmitter, an electronic receiver, two identical ring-stacked transducers (each on 60 m of cable), and three precision pulsers. The receiver output had a frequency proportional to the log of the input level and was fed to a paper-tape punch. An oscilloscope was used to monitor the receiver. A block diagram of the acoustic transmission equipment is shown in Figure 56.

The precision pulsers were portable units which contained their own batteries, used oven-stabilized crystal oscillators, and had rated drift rates of less than one part in 10^8 per hour after a 1-hour warmup. In practice, the difference between two units was less than 200 μsec in a 24-hour period. In order to obtain 2-day operation of the pulsers, external lead acid batteries were used at the receiving and transmitting units. The third pulser was used to carry the synchronization from one pulser to the other at the initiation of the experiment and when batteries were changed.

The transmitter's pulse width was 4 msec and the output voltage was 44 V rms, giving an acoustic output of 85 dB per volt (ref. 1 μbar at 1 m) in the center of the transducer beam.

A block diagram of the receiver is shown in Figure 57. The dynamic range of the input voltage was -100 dBV to -60 dBV (i.e., 10 μV to 1 mV) with the attenuator set at zero. The attenuator range was 38 dB in 2-dB steps, and thus the full range of the receiver was -100 dBV to -22 dBV. The 0 dB setting was used exclusively for all profiles taken on this trip. The output of the amplifier was sampled for 1 msec at a time determined by a delayed gate. The peak value was held and applied to the logarithmic amplifier. The output of this amplifier, presented on a panel meter for

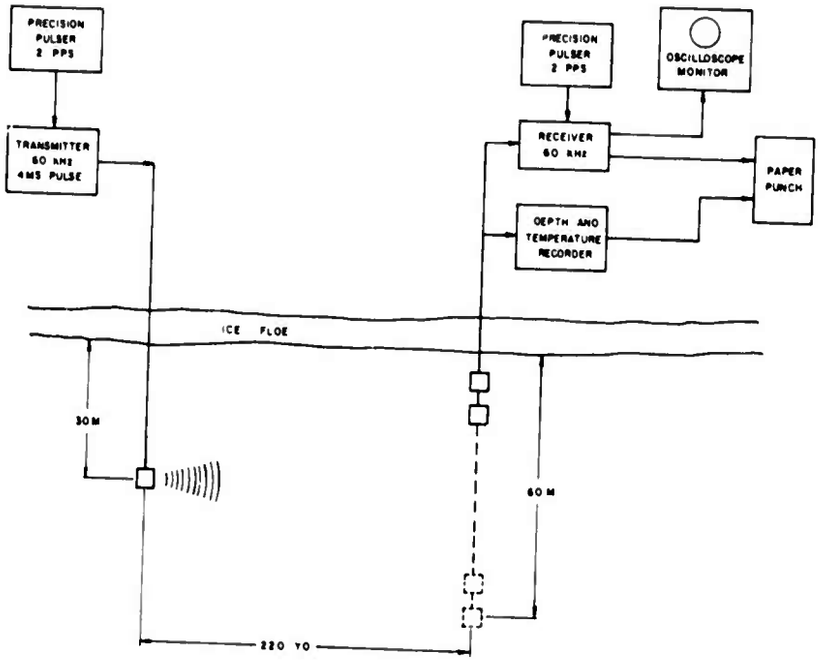

Figure 56. Block diagram of the acoustic transmission equipment.

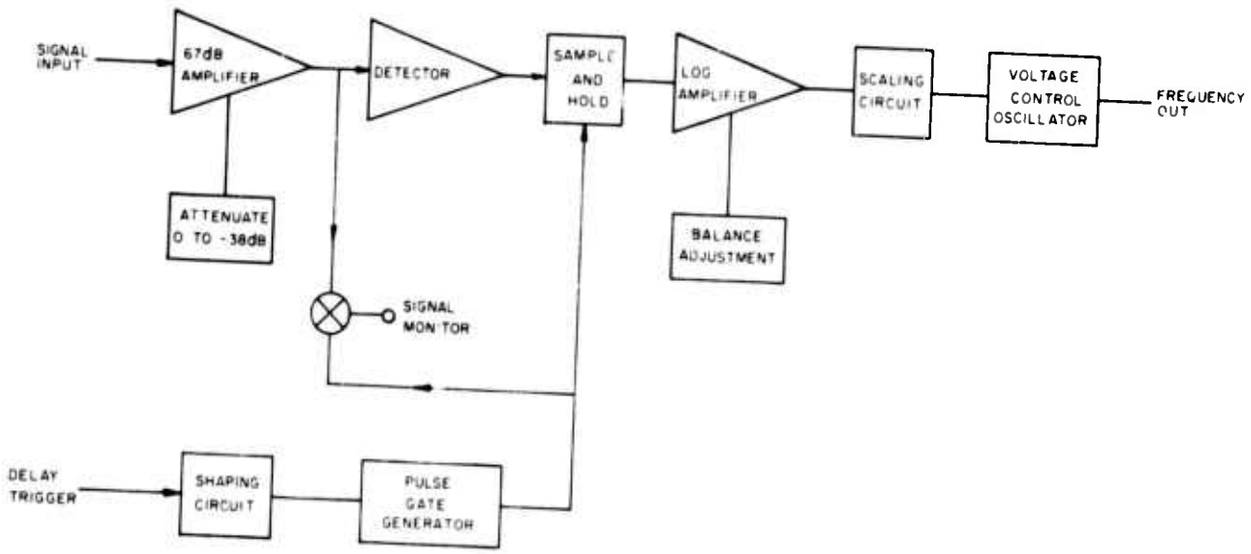

Figure 57. Block diagram of the acoustic receiver.

monitoring purposes, was applied to a voltage-variable oscillator which operated in the range of 12-25 kHz. The output of the amplifier was also summed with the gating pulse to provide an oscilloscope monitor output so that the gate could be adjusted to coincide with the received pulse.

The transducers were 60-kHz, ring-stacked magnetostrictive units having omnidirectional (within ±0.5 dB) patterns in the horizontal plane and a 26 degree pattern (half-power points) in the vertical plane. Their open circuit receiving sensitivity was -99 dBV/μbar; their transmitting output was 52 dB per volt (ref. 1 μbar at 1 m); and their impedance at the cable connector was 80 + j0 ohms. The transducers were identical within a small tolerance and were used interchangeably for transmitting and receiving.

Data recording instrumentation included a data signal converter and a paper-punch unit (see Figure 58). The signal converters used for the TD and CTD systems were capable of converting each of three frequency-modulated input signals to four-character BCD numbers. The converters utilized a BCD counter that stores the number of 1-MHz clock pulses generated during 255 complete cycles of the sensor processor output signal. The output of the BCD counter is gated by the functional timing controls and at the appropriate time is supplied to the paper tape unit for recording. The input sensor signals are sequentially multiplexed to produce a data sample that consists of three BCD outputs, a time code-word used to represent the relative time of the sample from the start of the drop, and an externally set 12-bit identification code. A data sample was obtained in approximately 0.8 sec

The punched-paper-tape output for each profile was about 25 ft long. The tape was usually fed into a box and rolled up after lowering the probe. Although it was necessary to keep the tape dry, it was possible to operate the punch in the open on many days.

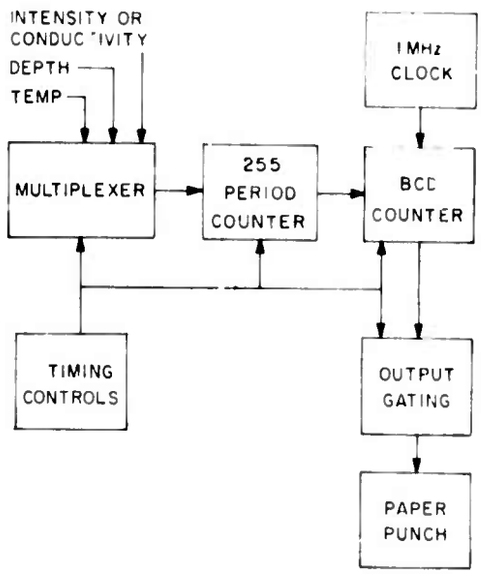

Figure 58. Block diagram of the data recording instrumentation.

A data reduction system was provided in the field to convert the punched-tape data to a plot of temperature and salinity versus depth. Occasionally, sound velocity and density were also included. This system consisted of a Hewlett-Packard tape reader, desk calculator, printer and plotter. A 50-m profile was plotted in about 15 minutes. The calculator rapidly performed the lengthy calculations of salinity, sound speed and density. The system was quite flexible since the plotter could be set to plot each variable at any desired scale. The plotter was the slowest link in the system, with the tape reader only slightly faster.

Transmission Measurements

Underwater transmissions were made from one station on the ice floe to another to study the effect of the thermal microstructure on short range transmissions. The transmitter was set at a depth of 33 m about 200 m away from Camp 1 and on a line extending beyond Camp 2 so that the transmission path could be monitored by both the temperature-salinity profiler at Camp 2 and the temperature profiler at Camp 1. A receiving transducer was attached to the temperature probe at Camp 1 and sound level profiles were measured routinely at the camp at the same time as the temperature profiles. Over 200 intensity profiles were measured during the 8 days the equipment was installed on the ice floe. Each profile consisted of sound level measurements at 200 successive depths as the receiving transducer was raised or lowered. A profile was taken each hour, except that on 2 days a 6-hour series was obtained with an interval of 15 minutes.

An example of a large variation in the received acoustic intensity is presented in Figure 59, which shows the salinity and temperature profiles at each end of the transmission path, and the intensity profile at the receiver. In this case the large anomaly in the intensity profile can be related to a warm layer which bends the sound down, causing a decrease in intensity at the depth of the layer and an increase below it. For most of the measurements the thermal layers were smaller and more numerous, and the resulting intensity profiles were more complex (see Figure 60).

The transmission measurements taken during the 8-day period are presented in detail in the data summary report (Ref. 2). The two 6-hour series taken on 8 and 9 August are of special interest because of the short interval (15 min) between measurements. These sound level profiles are plotted in Figures 61 and 62 alongside the corresponding series of sound velocity profiles at Camp 2. The decrease in sound level fluctuations during the afternoons of both days is easily attributed to the decrease in the amount of thermal structure at that time.

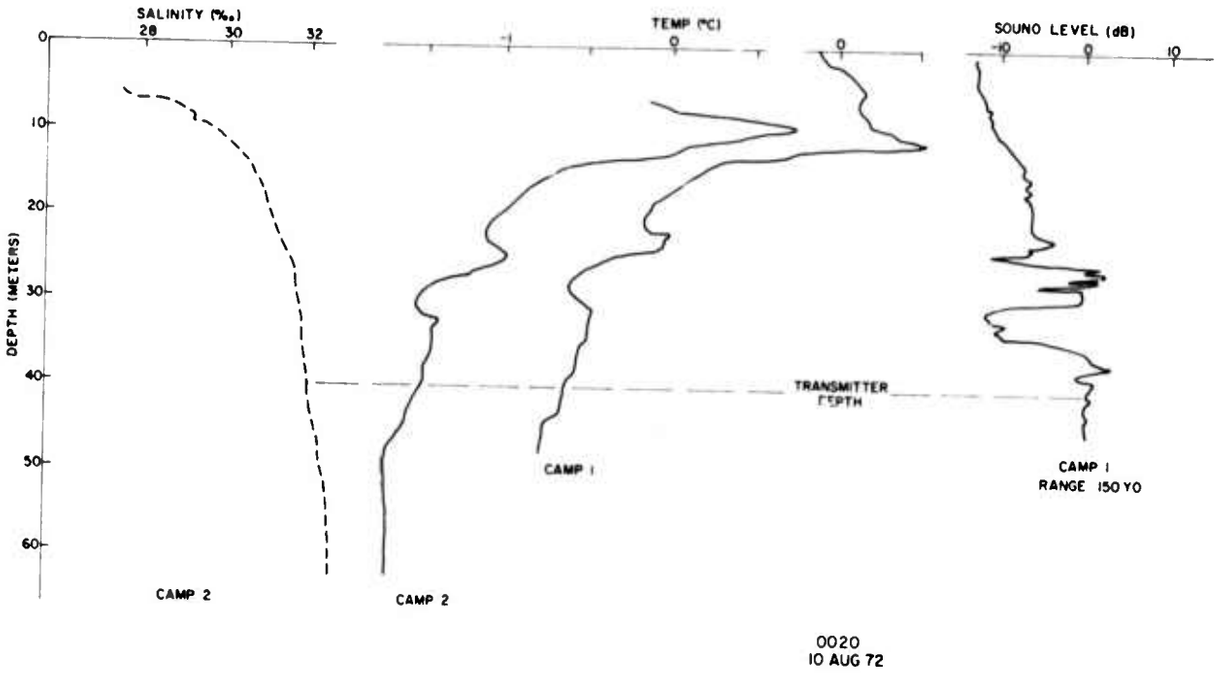

Figure 59. Sound intensity variation resulting from a large thermal layer.

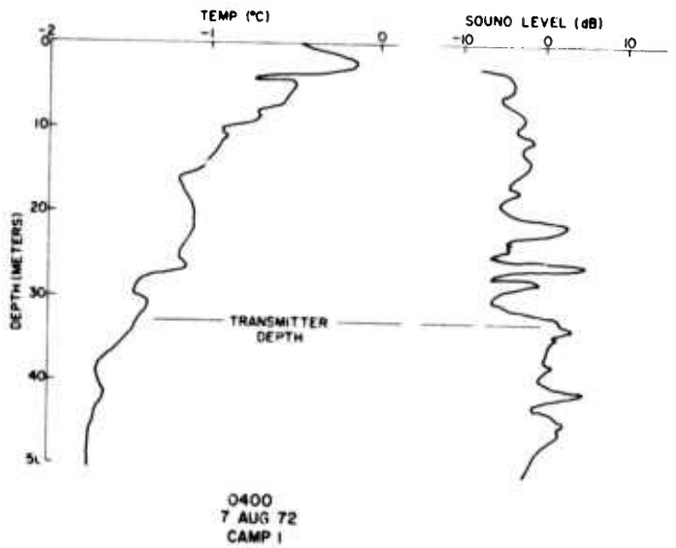

Figure 60. Sound intensity variation resulting from several small thermal layers.

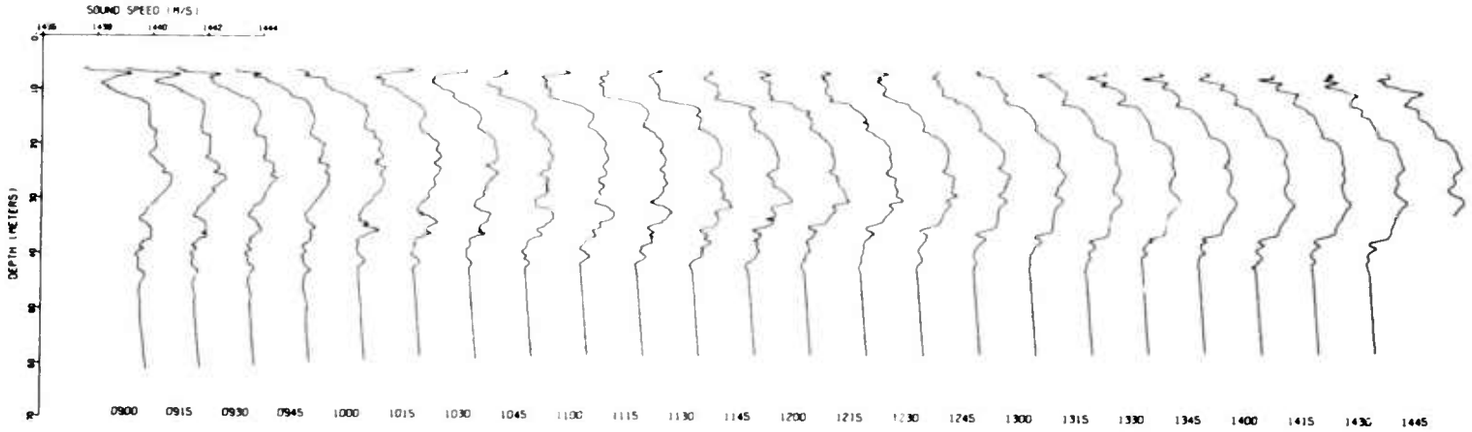

Figure 61a. Sound velocity profiles at Camp 2, 8 August 1972.

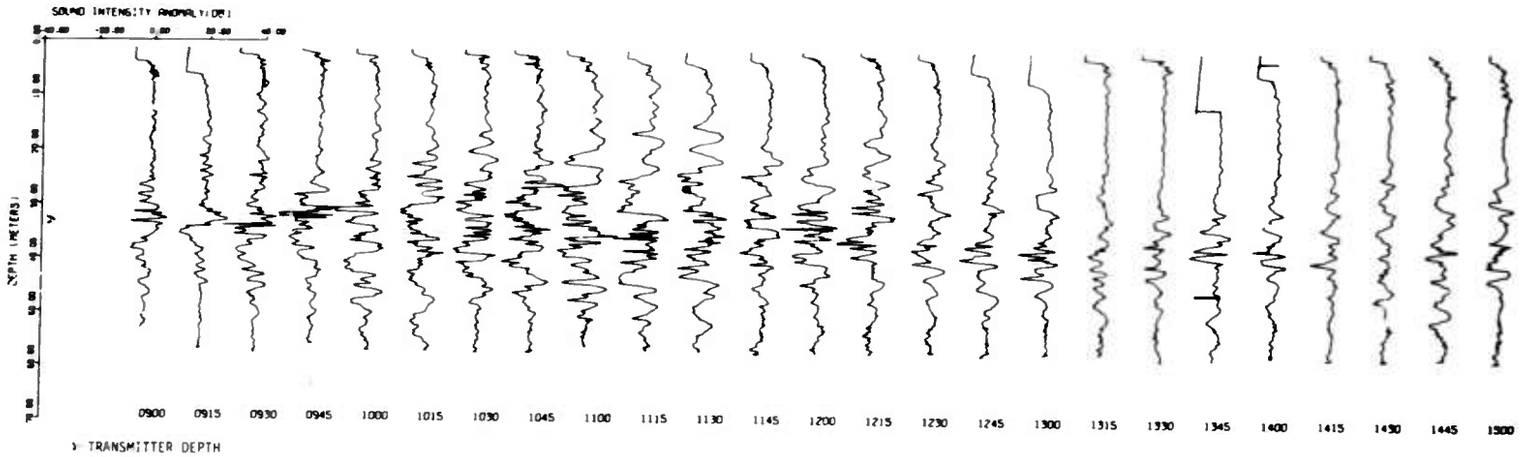

Figure 61b. Intensity profiles at Camp 1, 8 August 1972.

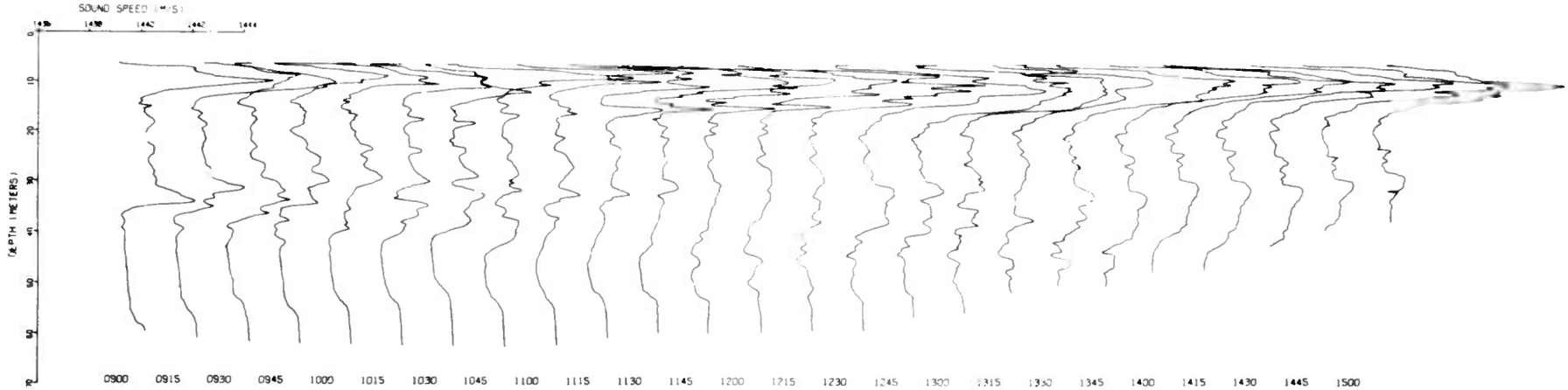

Figure 62a. Sound velocity profiles at Camp 2, 9 August 1972.

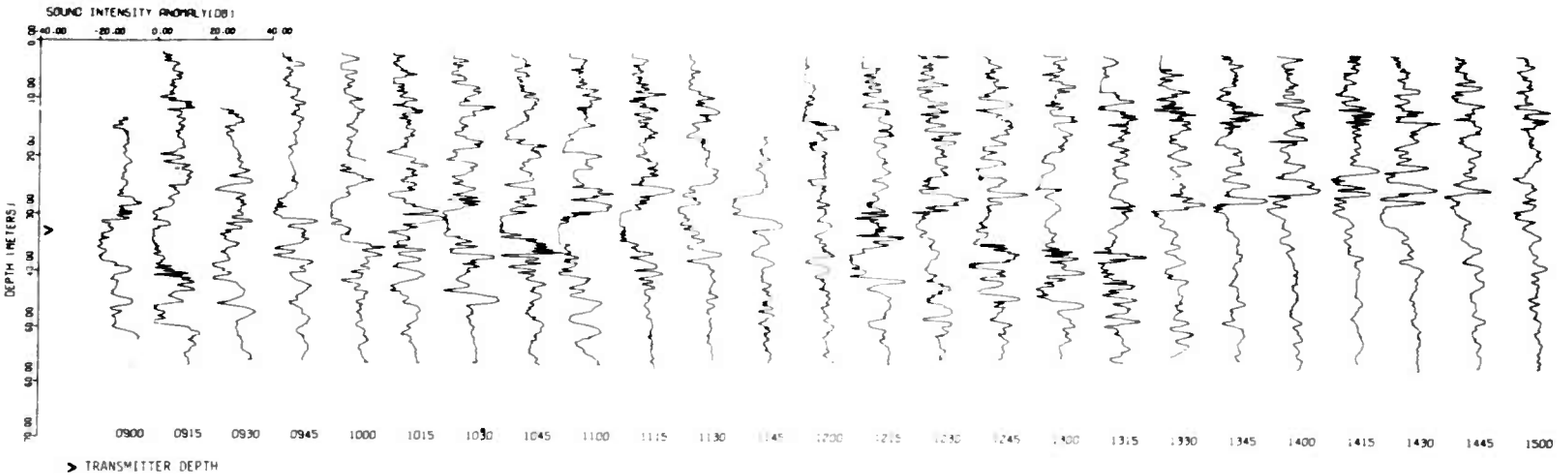

Figure 62b. Intensity profiles at Camp 1, 9 August 1972.

Effect of Layers

If the layers extend throughout the transmission path with little change in shape, a set of sound rays can be readily computed along with the intensity levels along the ray paths. A ray trace computer program obtained from Naval Undersea Center, San Diego, (Ref. 3) was used to calculate the ray paths and the sound level along each ray. An additional computer program was written to determine by interpolation the sound level for each ray at a prescribed range and to plot sound level versus depth at this range. These calculated profiles are compared to the measured profiles in Figure 63. The measurements selected for comparison were those with the best correlation between the temperature profile at Station 2, about one-third of the way along the transmission path, and the temperature profile at Station 1, at the receiving end. Profiles with pronounced layers near the transmitter depth were also favored.

The results indicate that the intensity variations can be roughly predicted through the use of sound ray computations. The failure of the computations to predict the variations in detail is assumed to result from a change in the sound velocity profiles along the transmission path.

Examination of the measured sound level profiles shows that there is often an unpredicted 3 to 5 dB fluctuation at depths considerably removed from the source depth. These fluctuations could be caused by a wobble of 6-8° in the transducer, but the short-range measurements show a variation of only about 1 dB (see next section), indicating a stable transducer configuration. These unpredicted fluctuations may be caused by horizontal bending of the sound rays and the resulting interference.

Some of the measured sound level profiles show violent fluctuations at depths near the transmitter depth. These fluctuations are usually in a region where two or more ray paths intersect. If rays intersect at angle P (see Figure 64) and are in phase at A, they will also be in phase at B if s is a multiple of a wavelength. For s equal to one wavelength, we have

$$\sin P = \frac{s}{h}$$

from which

$$h = s \csc P \quad .$$

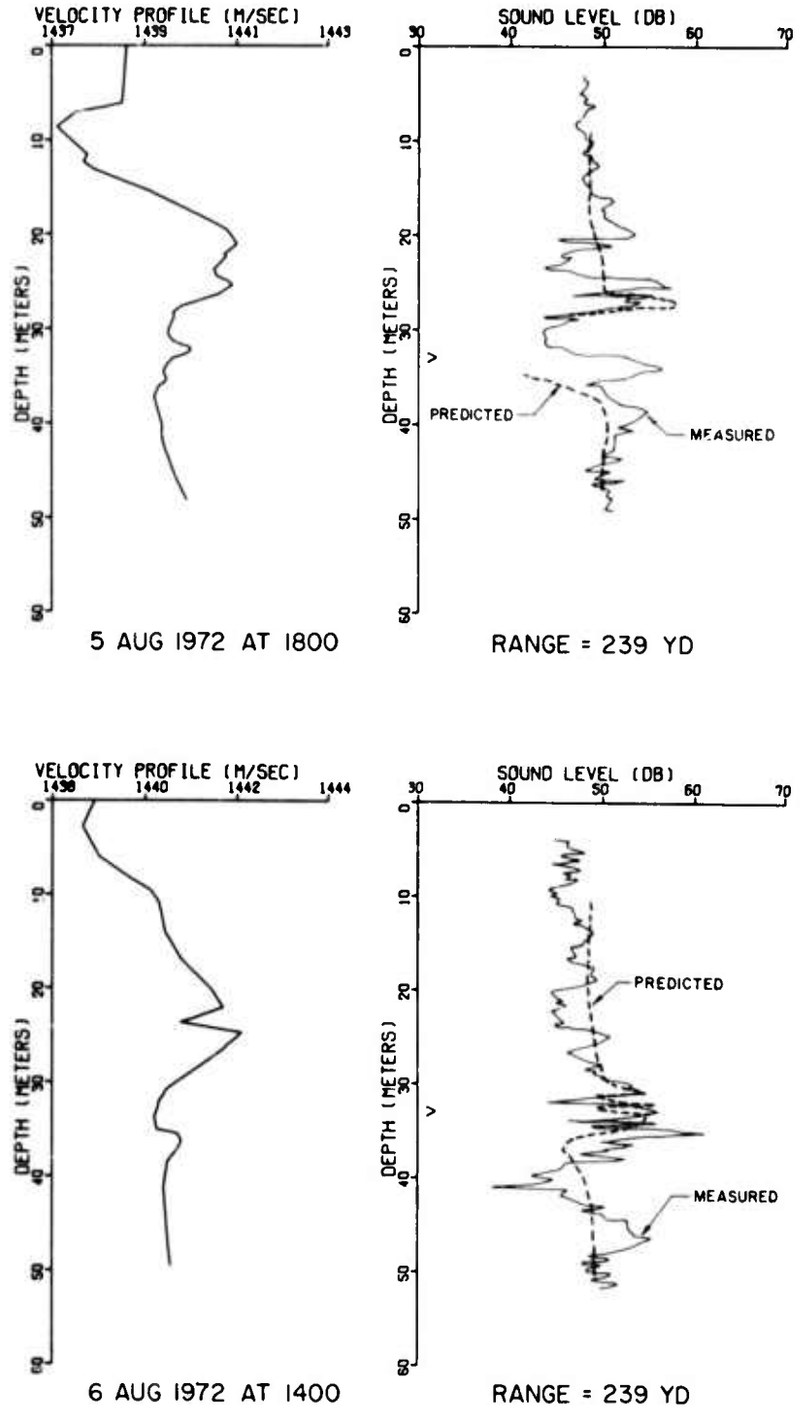

Figure 63. Comparison of measured to predicted sound level profiles.

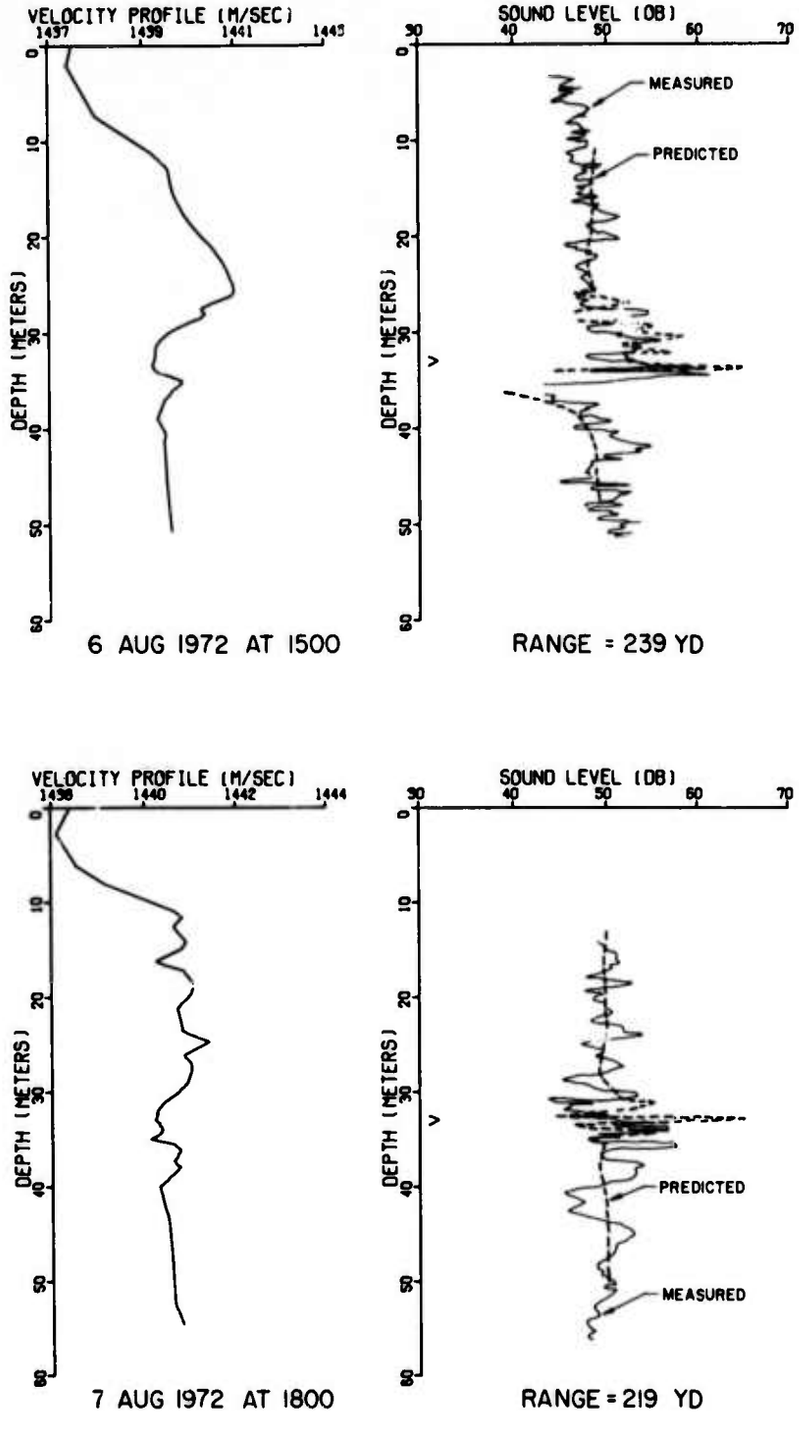

Figure 63. Comparison of measured to predicted sound level profiles, cont.

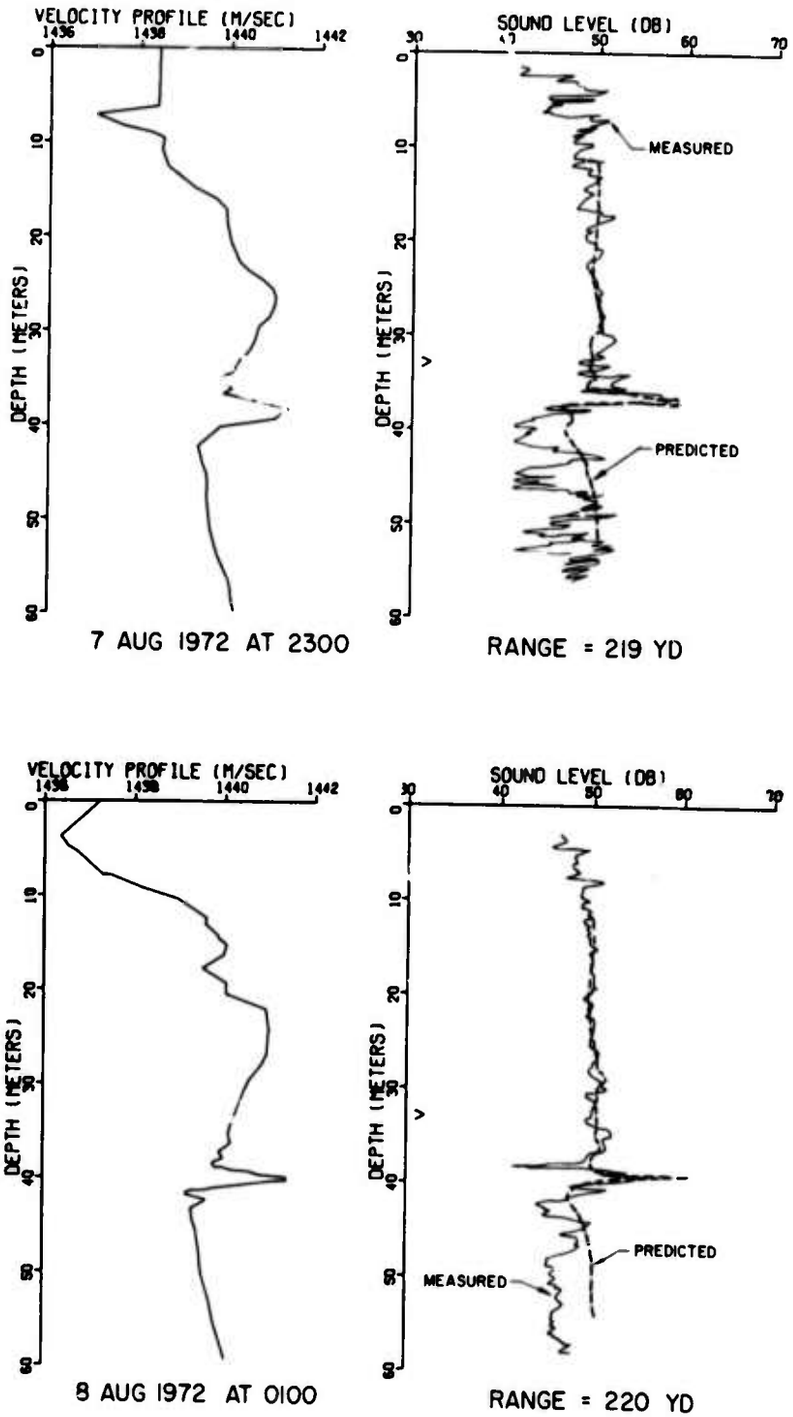

Figure 63. Comparison of measured to predicted sound level profiles, cont.

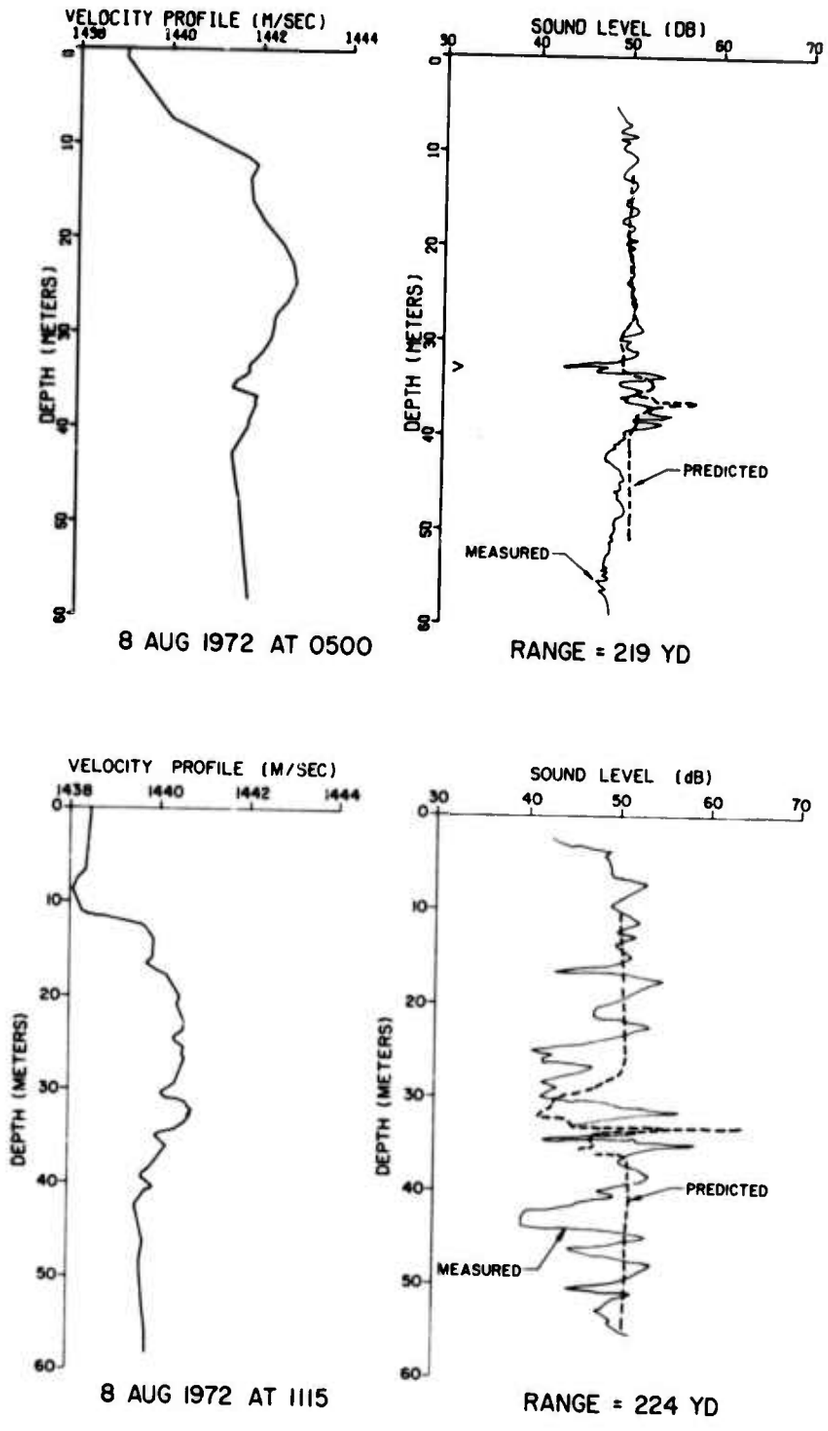

Figure 63. Comparison of measured to predicted sound level profiles, cont.

Values of h for small angles of intersection are given in Figure 64. In regions where rays intersect, the sound level should fluctuate through a cycle when the receiver is moved vertically from A to B. If the two rays are of equal amplitude the receiver would record a sound level with a peak of +6 dB when in phase and a minimum value representing noise when 180° out of phase.

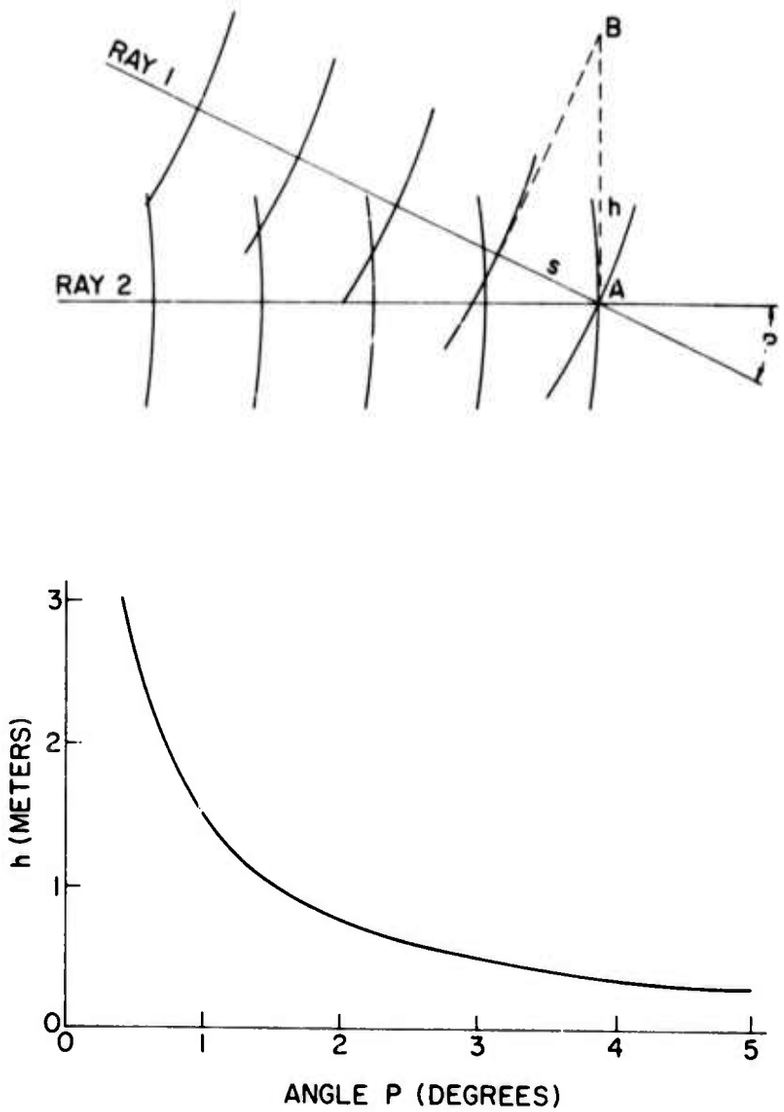

Figure 64. Intensity fluctuation when rays intersect (wave front curvature exaggerated).

Some of the sound ray diagrams were checked for intersecting rays. Where rays intersected there was usually a fluctuation with depth with a period somewhat similar to that given by the equation for h above.

Sound level measurements were made for several different source depths and ranges to obtain some indication of the variation of intensity fluctuations with range. These measurements are plotted in Figures 65, 66, and 67 along with the sound level profile predicted from sound ray diagrams for the measured sound velocity profile. The sound velocity profile varied so much during the 5 hours required to complete the measurements that an accurate range dependence could not be determined. (A very small change in the sound velocity profile near the transmitter will produce large changes in the sound level profile several hundred meters away.) However, it appears that the very large fluctuations that large, sharp layers would be expected to produce at long ranges are not likely to be observed if the range exceeds the layer dimension. Therefore, in the Chukchi Sea MIZ, the maximum sound level fluctuation may level off at about 10 dB when the range is increased beyond 200 m.

Another method of predicting the acoustic effect of thermal layers was derived by Potter and Murphy (Ref. 4). A perturbation calculation on the eikonal equations by Bergmann (Ref. 5) was extended to apply to acoustic transmission in a medium with a single horizontal layer in which the deviation of the index of refraction from unity was very small. Their results applied only to a layer with a temperature variation shaped like the Gaussian error curve. The effect on sound level predicted by this method is shown in Figure 68 for three locations of the sound source with respect to the layer. Letting σ be the standard deviation of the error curve and r the range, the predicted sound level variation is given by

$$L = -0.0109\ \Delta T\ \frac{r^2}{\sigma^2}\ R\ ,$$

where R is the value given on the curve in Figure 68, and ΔT is the magnitude of the error curve in degrees Celsius.

A comparison of measured sound level variations with those predicted by the equation above shows that the measured variation is usually much larger than the predicted one, probably because temperature layers are not usually as smoothly shaped as the Gaussian error curve. The dependence on the square of the range-to-σ ratio should be noted when predicting fluctuations for ranges longer than those reported here. However, this increase with range would only occur if the layer continued throughout the transmission path.

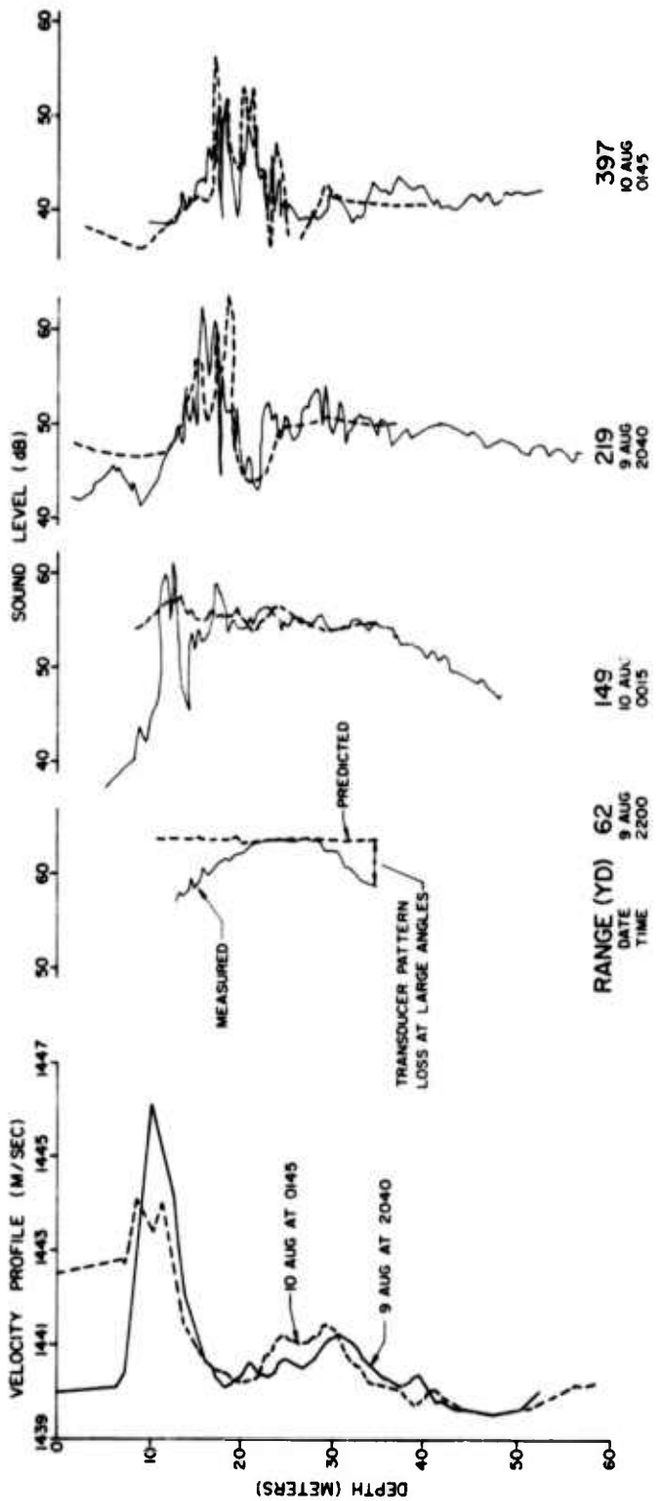

Figure 65. Measured and predicted sound level profiles at several ranges, source at 20 m.

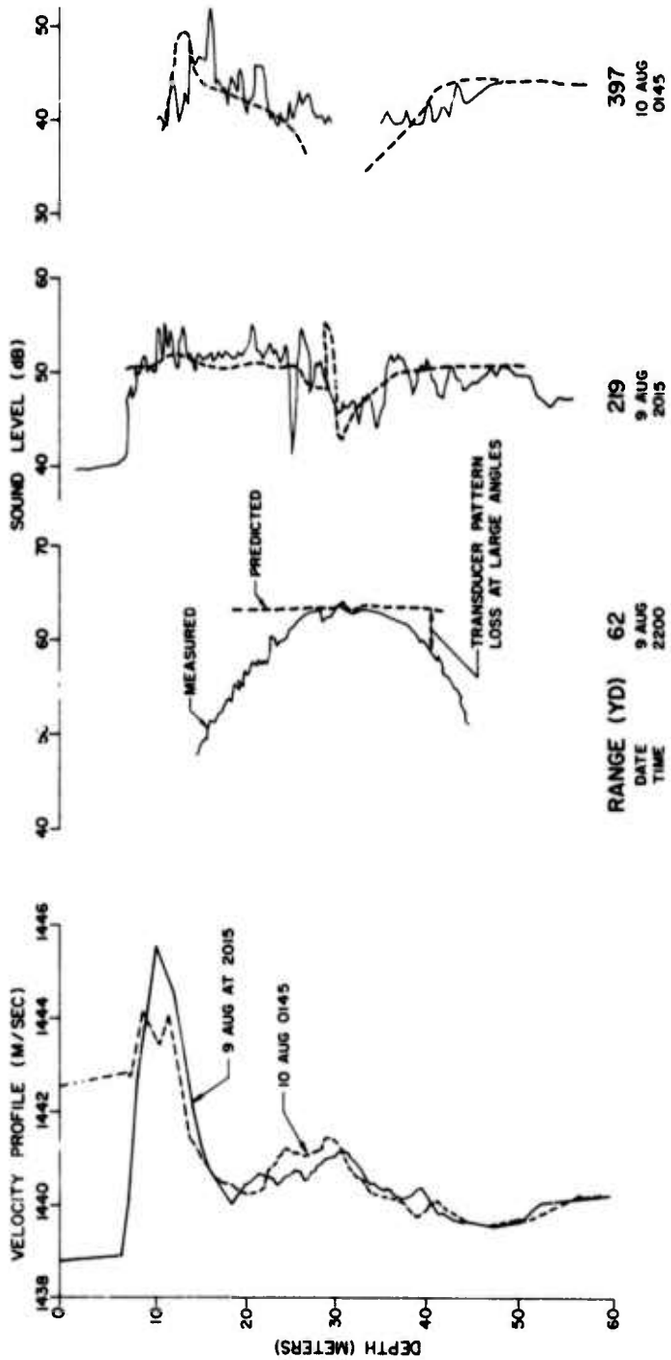

Figure 66. Measured and predicted sound level profiles at several ranges, source at 30 m.

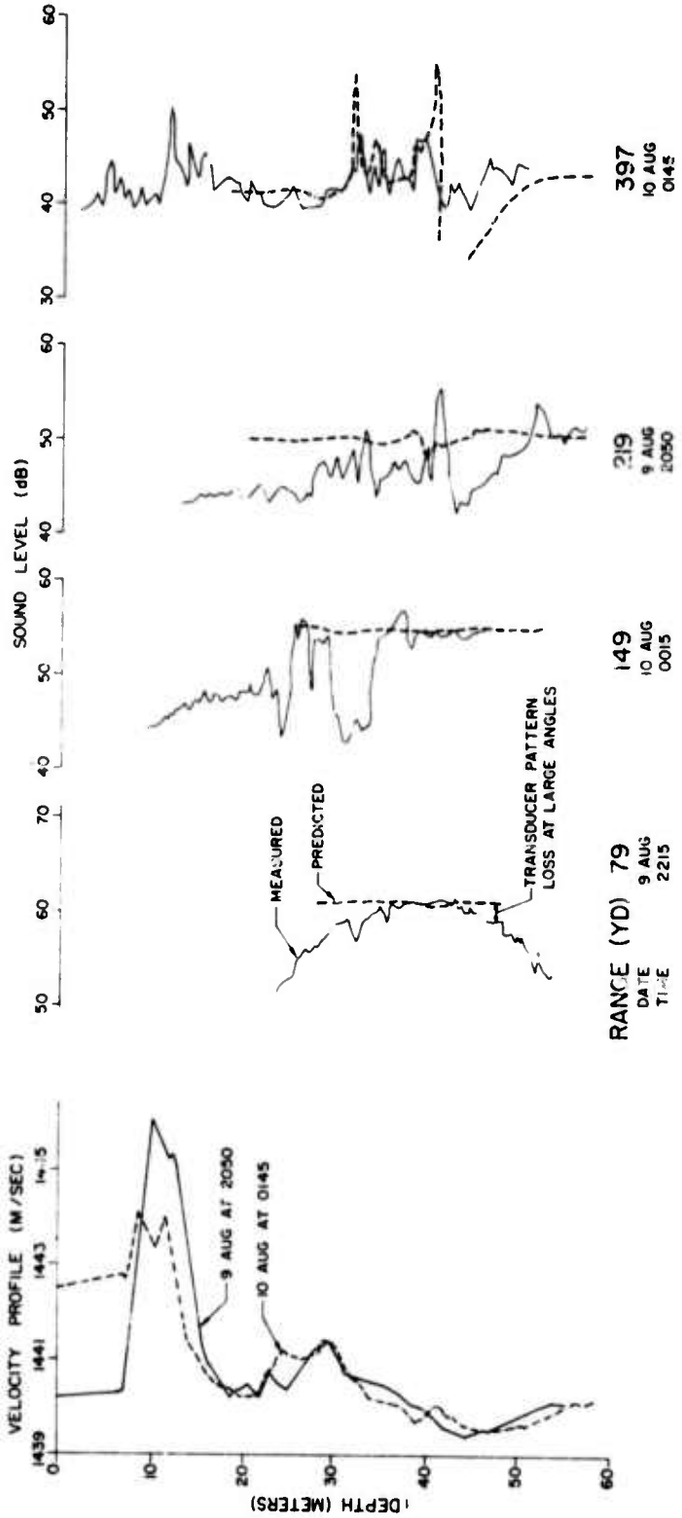

Figure 67. Measured and predicted sound level profiles at several ranges, source at 40 m.

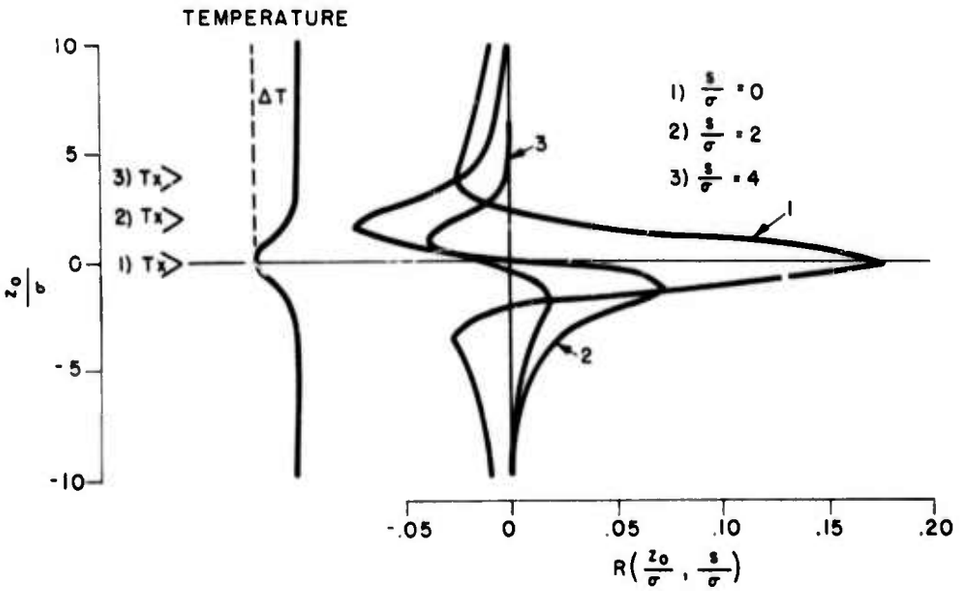

Figure 68. Sound level variations predicted by Potter and Murphy.

Statistical Relationship

When many small thermal layers exist it is not possible to relate each intensity anomaly to a certain thermal layer. Instead, we sought a statistical relationship between the average size of the thermal layers and the resulting average intensity variation.

Using the data taken on 8 and 9 August, when temperature profiles were measured at 4 stations on the floe every 15 minutes for 6 hours, the profiles were examined to determine the magnitude and horizontal extent of each layer. Layers with a temperature difference of less than 0.03°C were ignored Figure 54 on page 82 shows the distribution of the layers, the average magnitude of their temperature difference, and their average depth dimension for each day. Because of the large spread in these values, little more can be stated than that the layers were 1 to 2 meters thick with a temperature difference of one- to two-tenths of a degree Celsius.

During this 2-day period a transmitter was placed at a depth of 33 m about 200 m from Camp 1 on a line extending beyond Camp 2 so that the transmission passed directly under Camp 2. A sound intensity profile was measured simultaneously with each temperature profile at Camp 1. Each profile consisted of sound-level measurements at 200 successive depths as the receiving transducer was lowered or raised. The pressure amplitude was computed for each reading, and the average and the standard deviation of the amplitude were computed for each profile.

The results are shown in Figure 69, which plots the standard deviation of the amplitude divided by the average amplitude for the profile. The figure shows a greater variation on 9 August, which corresponds to the larger number of thermal layers and the smaller depth dimension of the layers on that date.

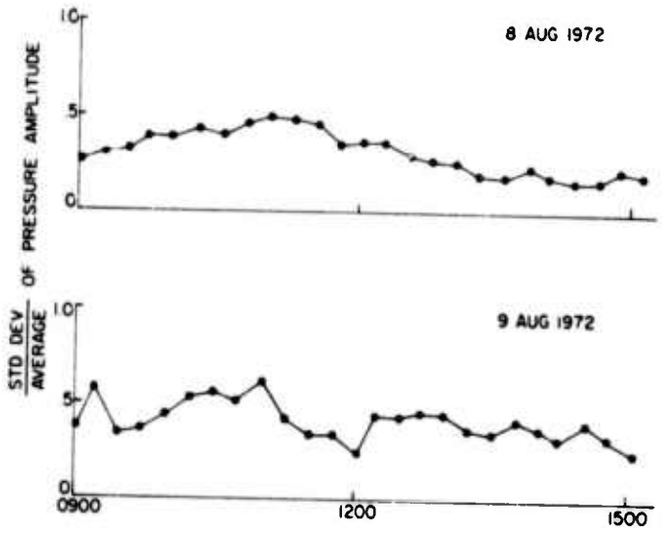

Figure 69. Statistical variation in pressure amplitude for each profile.

The thermal layers varied greatly in size and shape. The sound intensity variation depended greatly on the proximity of the acoustic source to a large, sharp layer. Therefore, the effect of the layers on acoustic transmissions can only be stated in general terms; namely, that layers 1 to 2 m thick with a temperature difference of one- to two-tenths of a degree Celsius produce intensity anomalies averaging +3 dB for increases in intensity and -6 dB for decreases in intensity at a range of 200 m.

VII. VOLUME REVERBERATION

General

A knowledge of how the acoustic scattering strength in a given region of the sea is distributed in space and time and the relationship between the scattering strength and the biological scatterers causing it is important in two ways. First, the more direct goal: if we know the acoustic scattering strength in a given region, we can predict to what extent active acoustic systems such as military sonars or fish-monitoring equipment may be limited by volume reverberation. Second, if the relationship between the biological parameters and the measured scattering strength of a region is known, it should be possible to monitor the biological activity in the region with relatively simple acoustic measurements, and to build, improve and test biological models of the region. The accomplishment of this second, more long-range goal, would enable us to assess more accurately the effects of man's activities on the local ecosystem.

The direct goal is clearly attainable. The MIZ studies have already contributed sufficient data to enable reasonable estimates of the effects of volume reverberation on some particular acoustic systems in a given region at a given time, viz., in the Marginal Ice Zone in summer (Ref. 6). However, the present work is only a beginning toward the second goal. The relationship between the acoustic measurements and the various organisms obtained in the biological samples is now being studied. We are also studying biological production models of the Arctic. This work is discussed further in Appendix B, a paper presented to the 1973 IEEE International Conference on Engineering in the Ocean Enivornment.

The first measurements in the ongoing study reported here were made by Moose and Shah in August of 1971 (Ref. 1). Measurements of the acoustic volume scattering strength were made at 35 locations in the MIZ at 105 kHz. All measurements were within 100 miles of Pt. Barrow, mostly to the east in the Beaufort Sea.

In 1972 the program was expanded to include measurements at 38 kHz as well as 105 kHz. During two cruises in the Chukchi Sea in July and August, measurements of volume scattering strength were made at 98 different locations with the 105 kHz system. Data were taken with the 38 kHz system at 79 of these sites and at two other locations. CTD measurements were made at most of the sites, and at 35 locations some biological sampling was also performed. A large area of the Chukchi Sea was covered: as far north as 73°00'N at 169°14'W, as far west as 173°58'W at 71°22'N (about 30 miles east of Herald Island), and as far south as 66°50'N at 169°03'W (about 60 miles north of the Diomedes) (see Figure 22).

Although most of the 1972 measurements were taken from the ship, seven of the 105-kHz measurements were taken from helicopters--the first such measurements so taken in the Arctic (or anywhere else to our knowledge). These data were taken as the helicopter hovered about 8 to 10 ft above open water, leads or polynyas. The gear was the same 105-kHz gear used for the shipboard measurements and was run from an inverter powered by the 28-Vdc supply in the helicopter. The technique proved quite feasible. The use of helicopters has enabled us to extend our range of operations into regions of heavy ice where ship operations would be slow and difficult.

Experimental Procedure

The experimental method has been described previously (Refs. 1 and 7) and will be reviewed only briefly here.

Both the 105- and 38-kHz systems operated in essentially the same manner. Acoustic pulses 0.1 to 0.6 msec long were directed downward in about a 10° wide conical beam for the 105-kHz system and a beam about 7° by 14° for the 38-kHz system. The returning echoes were amplified, beat down to 5 kHz, and recorded on magnetic tape. They were also rectified and displayed on paper echogram charts. The tape recordings were then digitized and analyzed to determine the average acoustic volume scattering strength in up to 10 selected depth intervals (Refs. 8 and 9). The depth intervals selected for each measurement site were those that the echogram charts indicated would best disclose any layered structure. The processing of each data file involved the averaging of some 100-500 pings. Thus, statistical errors were negligible (Ref. 9) compared to other, systematic, uncertainties. We estimate the uncertainty in the volume scattering strength of any given layer is ±3 dB at -50 to -75 dB (ref. 1 m^{-1}).

Figures 70 through 84 are 15 echogram charts accompanied by bar graphs showing the average volume scattering strength in the corresponding depth intervals. Each figure also shows the temperature profile at that location. Although these figures were chosen specifically to illustrate the more interesting layered structures, they are also representative of the variety in the results obtained.

Table III lists the 15 data files presented, the location at which the data were taken, the frequency, the lowest depth analyzed, the maximum volume scattering strength in any layer below 10 m, the weighted average volume scattering strength in all layers below 10 m, and the figure displaying the data file. The weighted average, S, is given by

$$S = 10 \log \left(\sum_i \delta_i \, 10^{d_i/10} \Big/ \sum_i \delta_i \right)$$

where d_i is the strength in decibels (ref. 1 m^{-1}) in the i^{th} layer, δ_i is the depth interval of the i^{th} layer, and the summations are taken over all layers below 10 m.

The top 10 m of data (the top 11-12 m of the ocean, since the transducer was generally 1-2 m below the surface) have been eliminated from consideration because of possible interference from the ship's hull or from bubbles caused by the ship. This interference was most noticeable in the 38-kHz data, presumably because of the higher sidelobes in the beam pattern of the 38-kHz transducer.

Table III

Date (1972)	Tape & File	Lat. N.	Long. W.	Freq. (kHz)	Lowest Depth Analyzed (m)	Maximum Sound Scattering in Any Layer Below 10 m (dB ref. 1 m^{-1})	Average Sound Scattering in All Layers Below 10 m (dB ref. 1 m^{-1})	Figure No.
7/28	5-2	70°51'	159°34'	105	28	-71	-77	82
7/28	5-3	70°57'	159°46'	105	53	-77	-80	83
7/28	5-4	71°01'	159°55'	105	52	-80	-81	81
7/28	5-10	71°31'	159°02'	105	51	-75	-80	80
7/28	5-10a	71°31'	159°02'	105	51	-71	-80	80
8/13	6-4	71°32'	157°09'	38	110	-56	-66	76
8/15	6-19	71°47'	165°02'	38	40	-58	-60	77
8/15	6-20	71°54'	165°24'	38	40	-60	-63	78
8/13	7-3	71°29'	157°02'	105	112	-84	-89	72
8/13	7-4	71°32'	157°09'	105	110	-57	-68	73
8/13	7-5	71°37'	157°18'	105	70	-63	-73	70
8/13	7-6	71°40'	157°26'	105	63	-65	-68	71
8/14	7-12	71°00'	159°49'	105	62	-66	-73	84
8/15	7-16	71°35'	162°34'	105	42	-78	-83	79
8/15	7-19	71°47'	165°02'	105	40	-61	-65	74
8/15	7-20	71°54'	165°24'	105	40	-62	-65	75

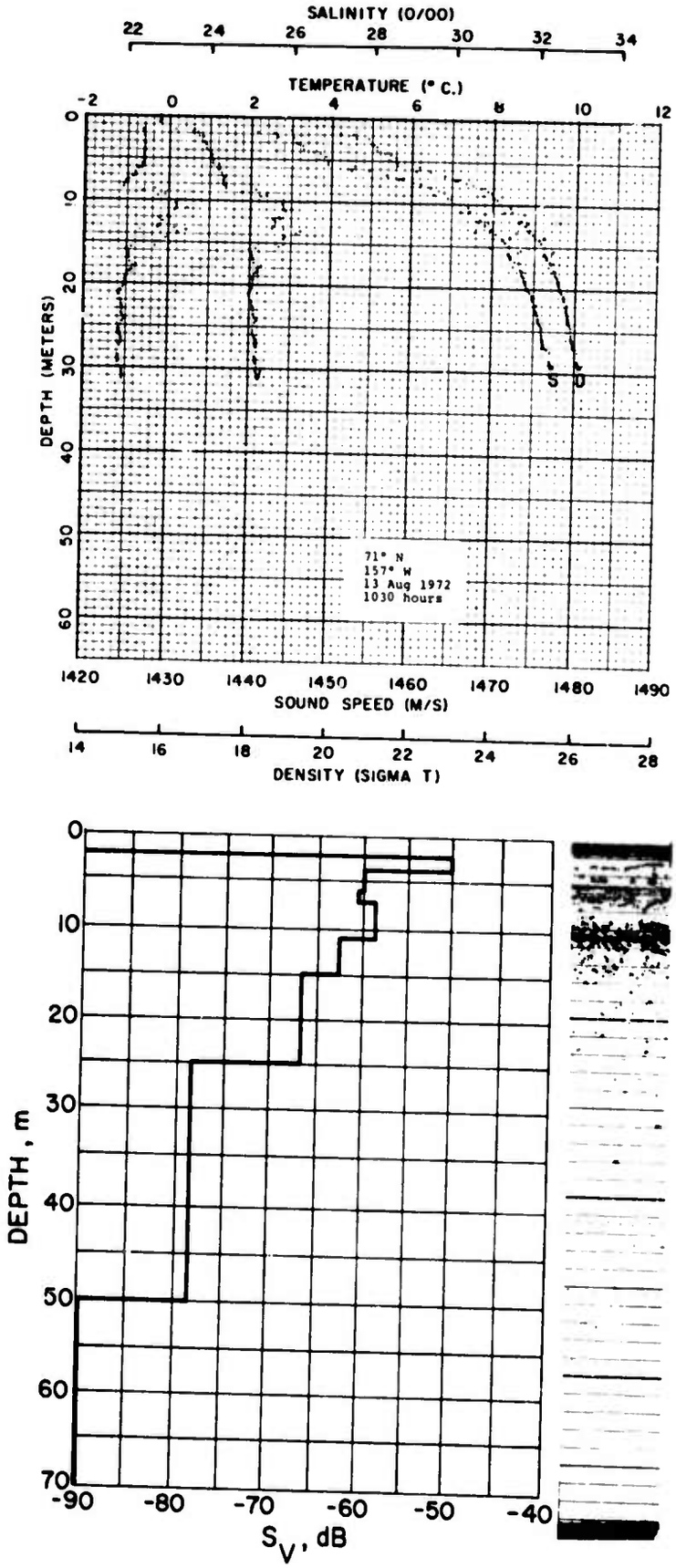

Figure 70. Tape 7 File 5, 105 kHz, 13 August 1972.

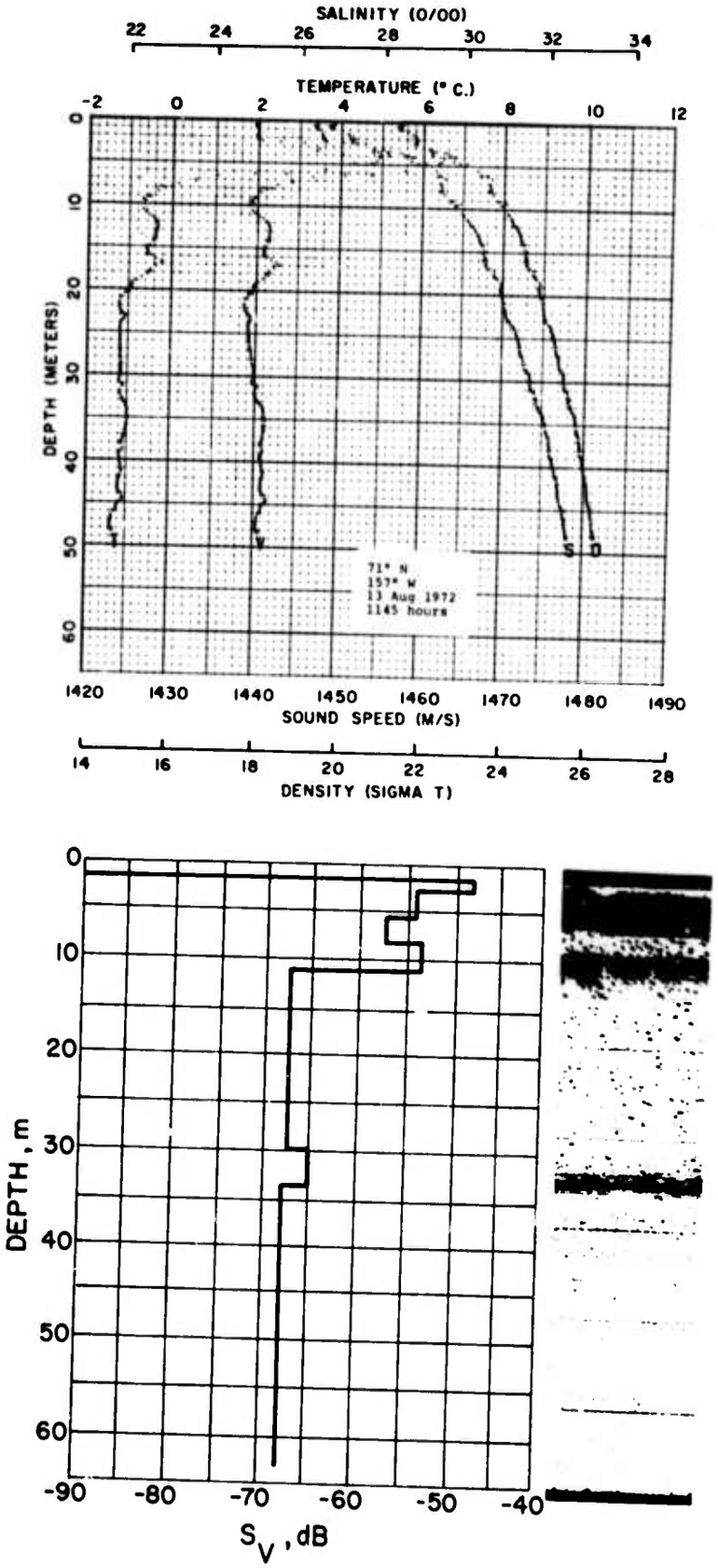

Figure 71. Tape 7 File 6, 105 kHz, 13 August 1972.

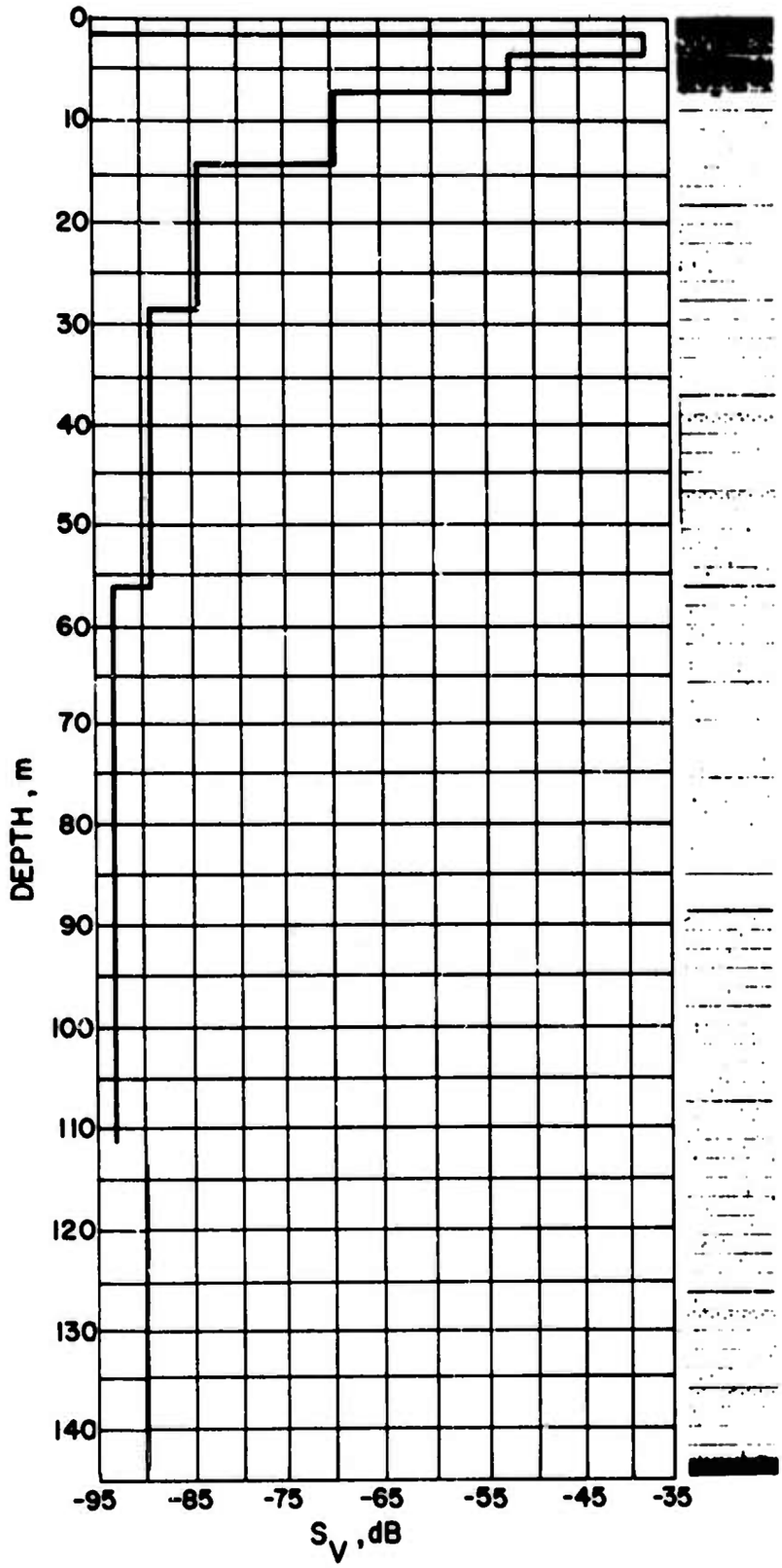

Figure 72. Tape 7 File 3, 105 kHz, 13 August 1972.

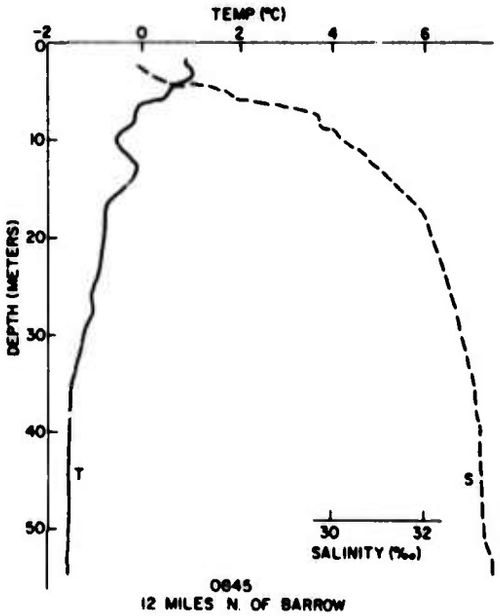

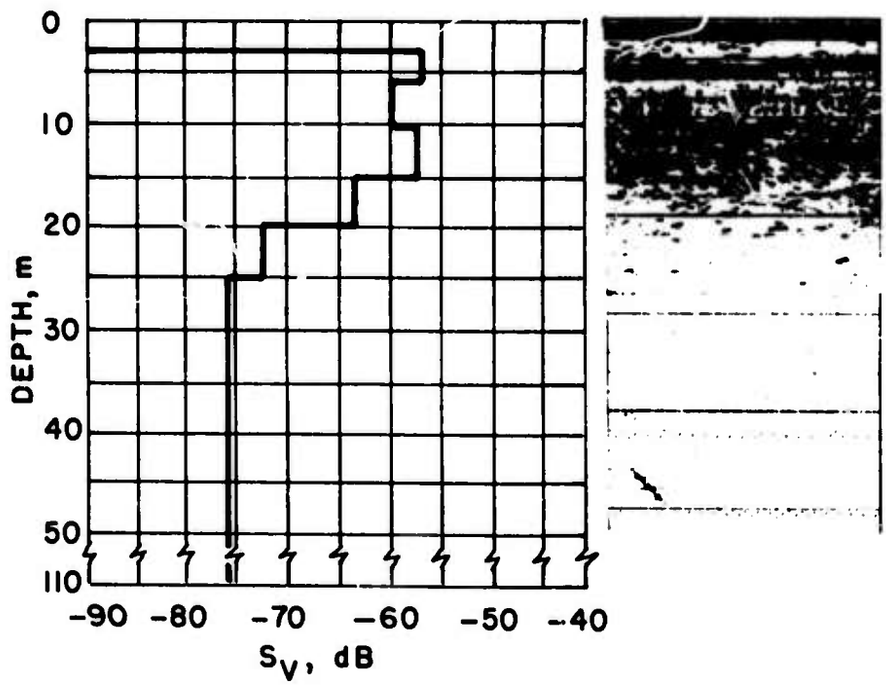

Figure 73. Tape 7 File 4, 105 kHz, 13 August 1972.

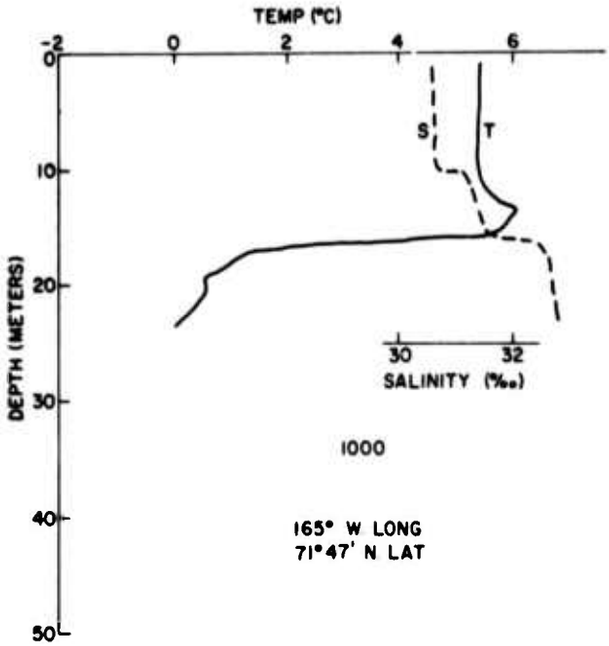

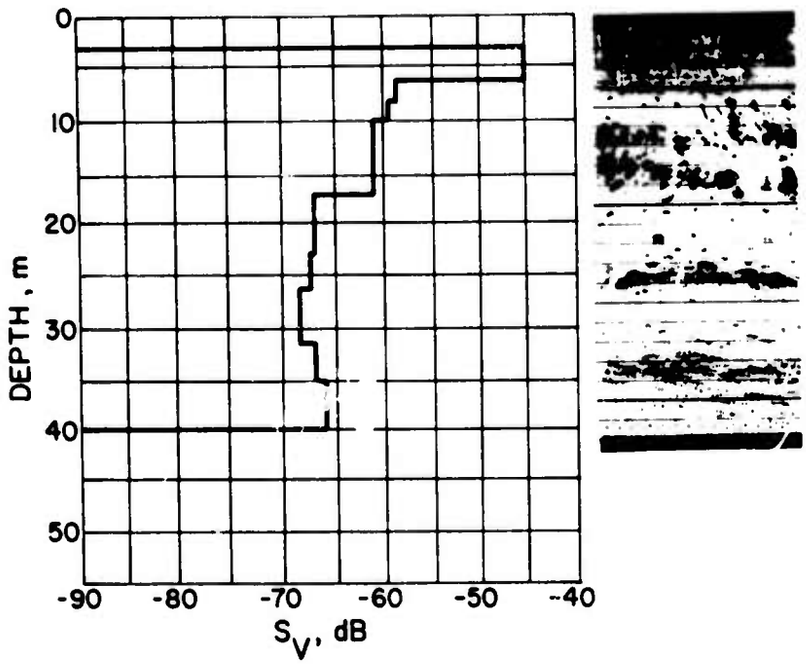

Figure 74. Tape 7 File 19, 105 kHz, 15 August 1972.

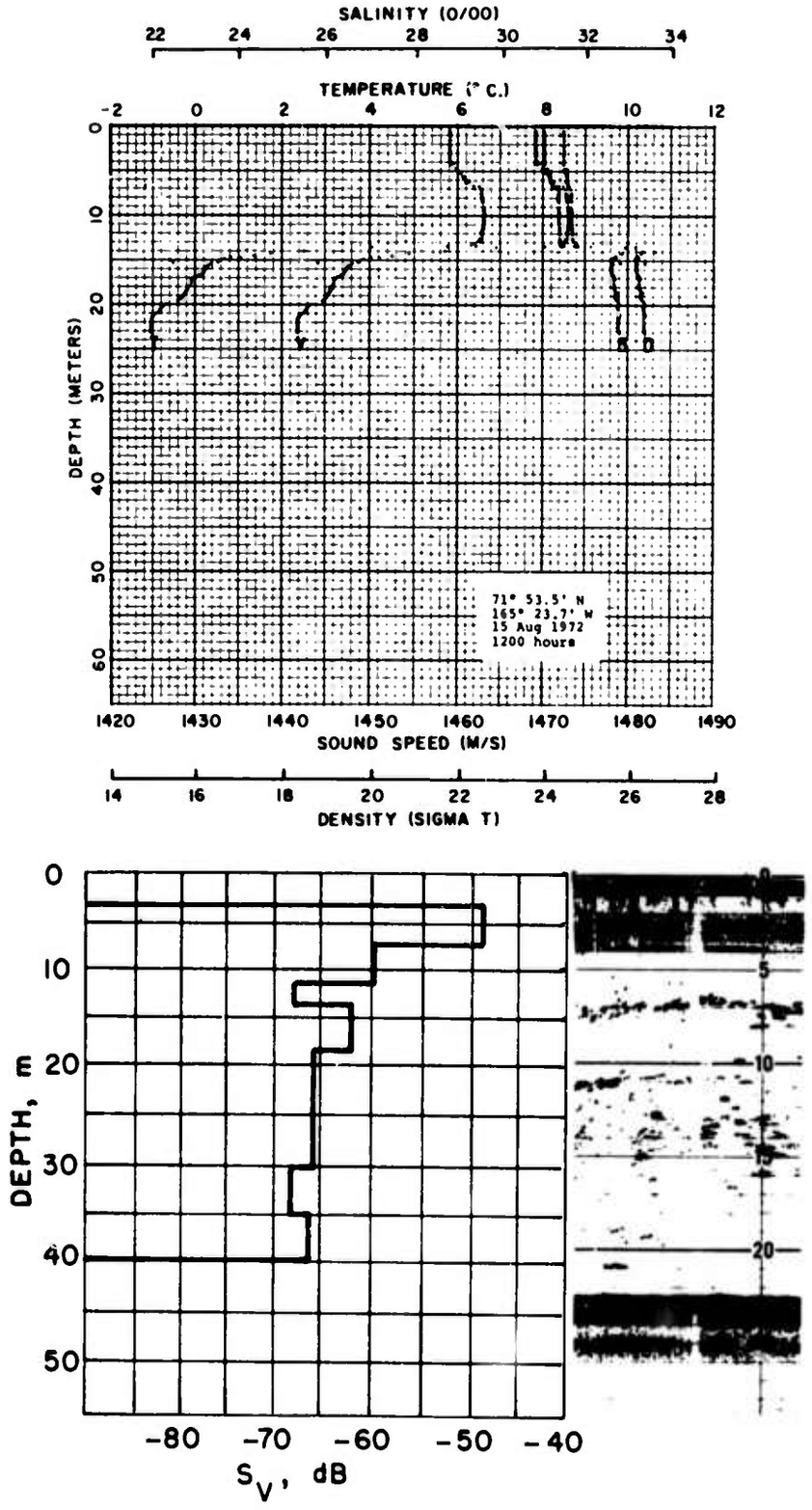

Figure 75. Tape 7 File 20, 105 kHz, 15 August 1972.

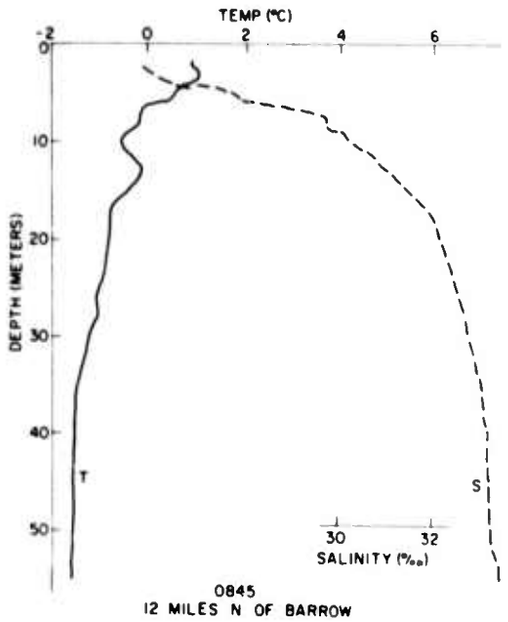

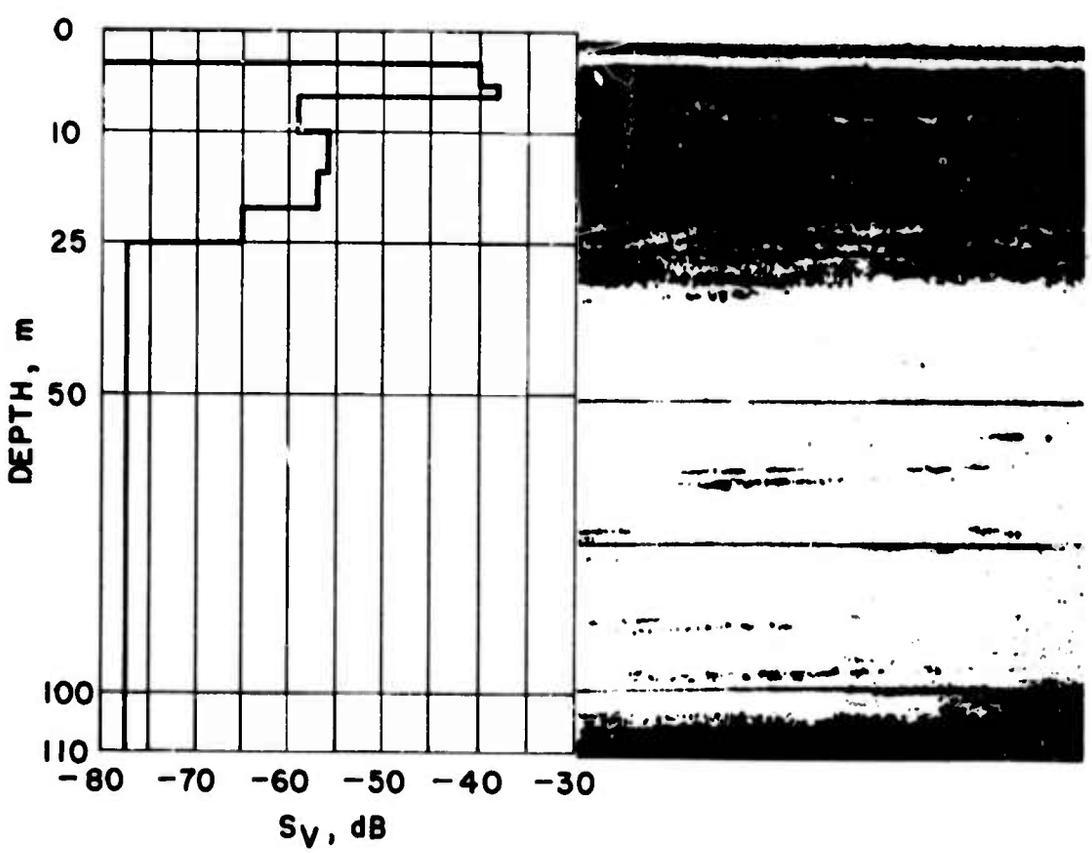

Figure 76. Tape 6 File 4, 105 kHz, 13 August 1972.

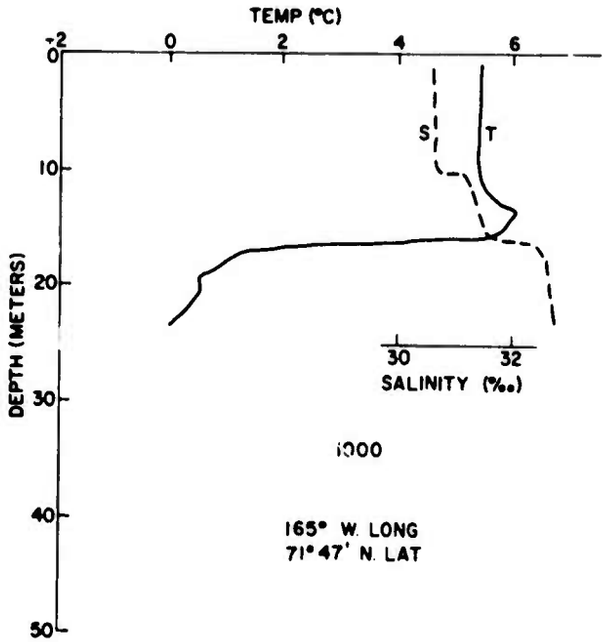

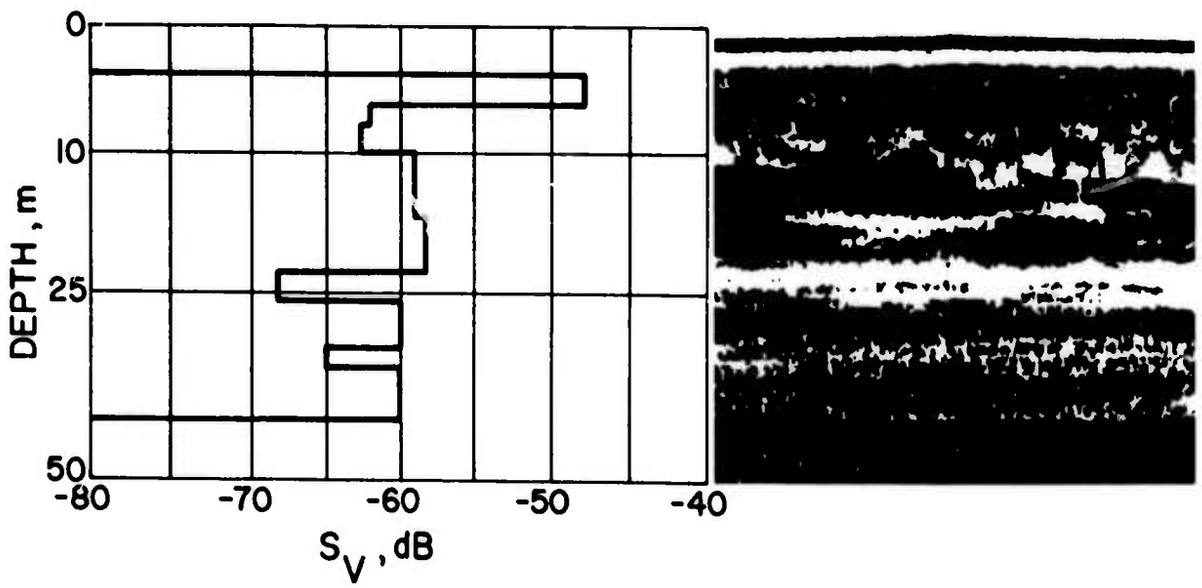

Figure 77. Tape 6 File 19, 38 kHz, 15 August 1972.

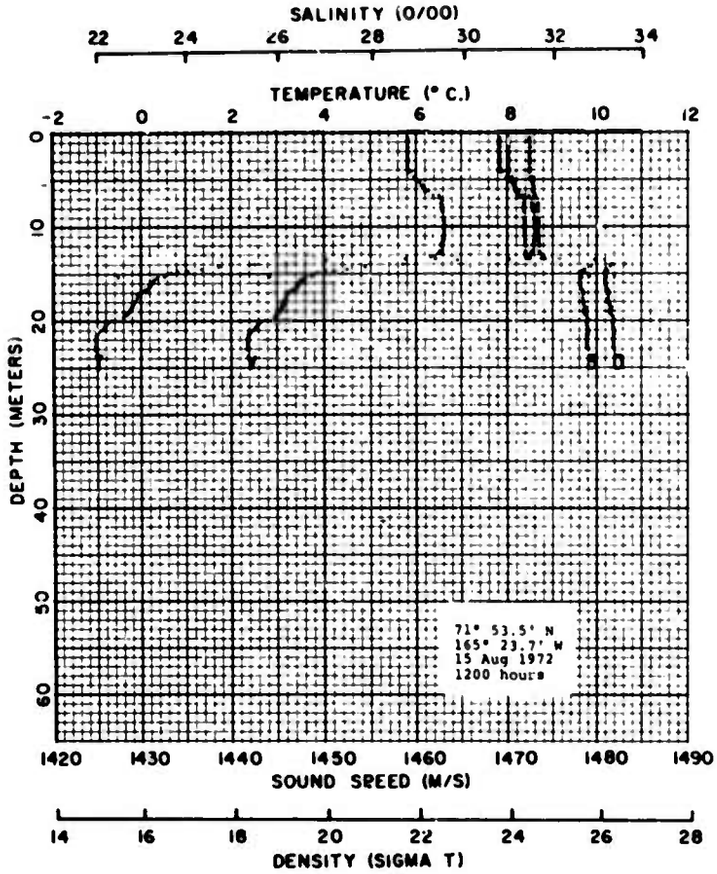

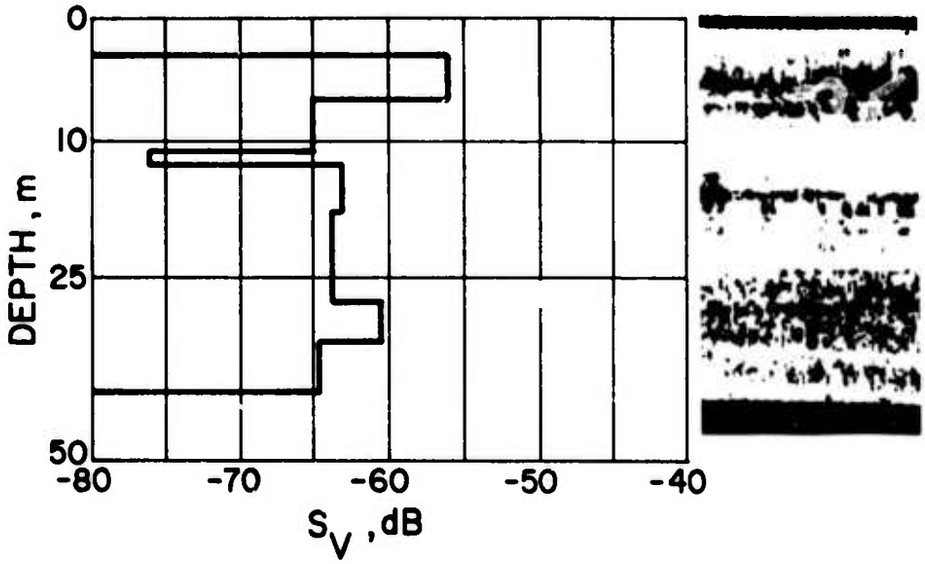

Figure 78. Tape 6 File 20, 38 kHz, 15 August 1972.

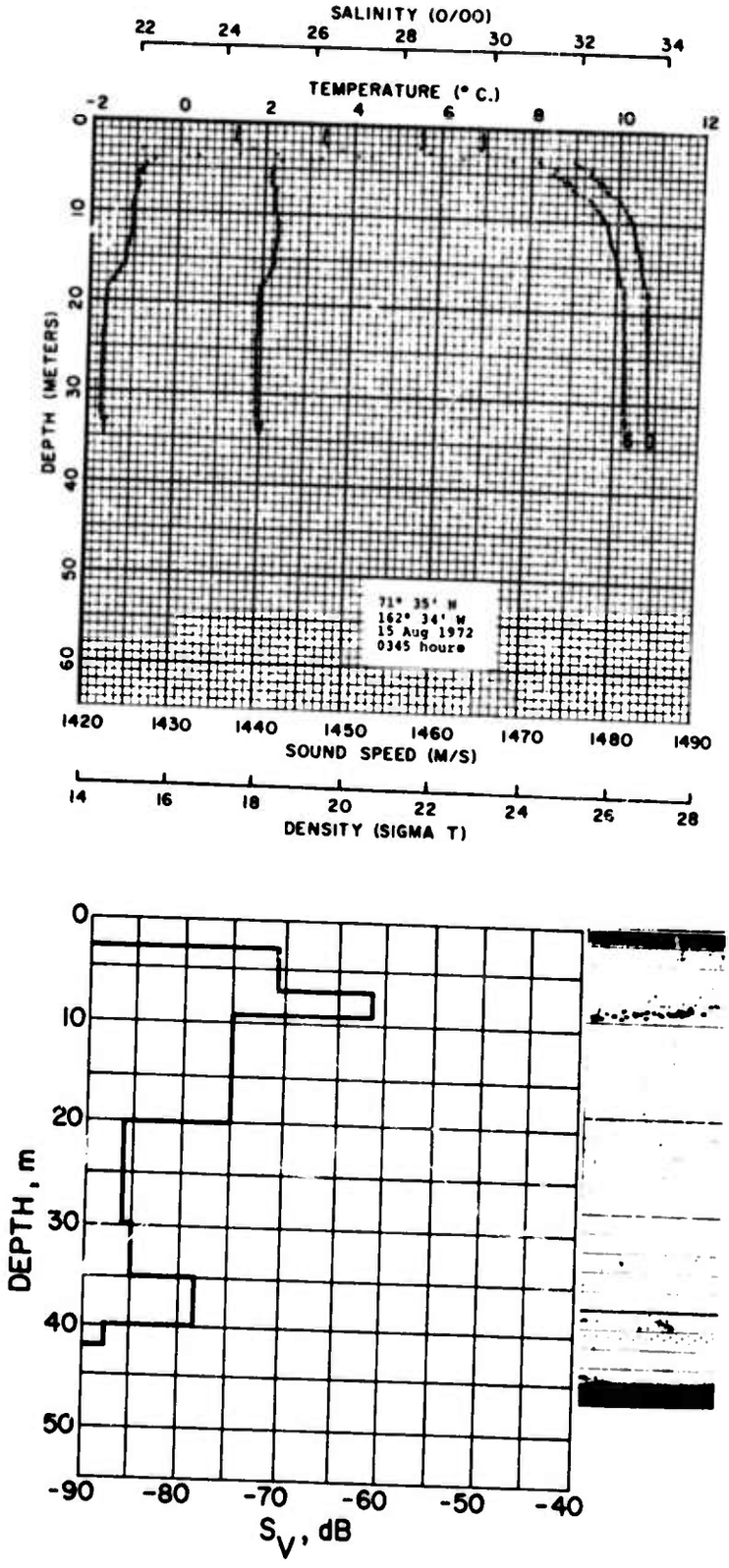

Figure 79. Tape 7 File 16, 105 kHz, 15 August 1972.

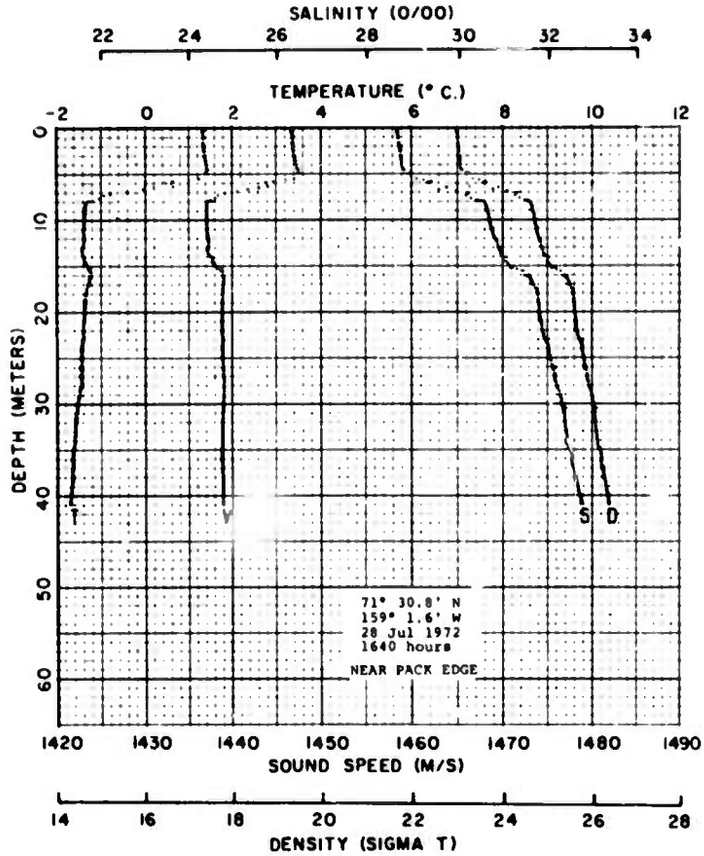

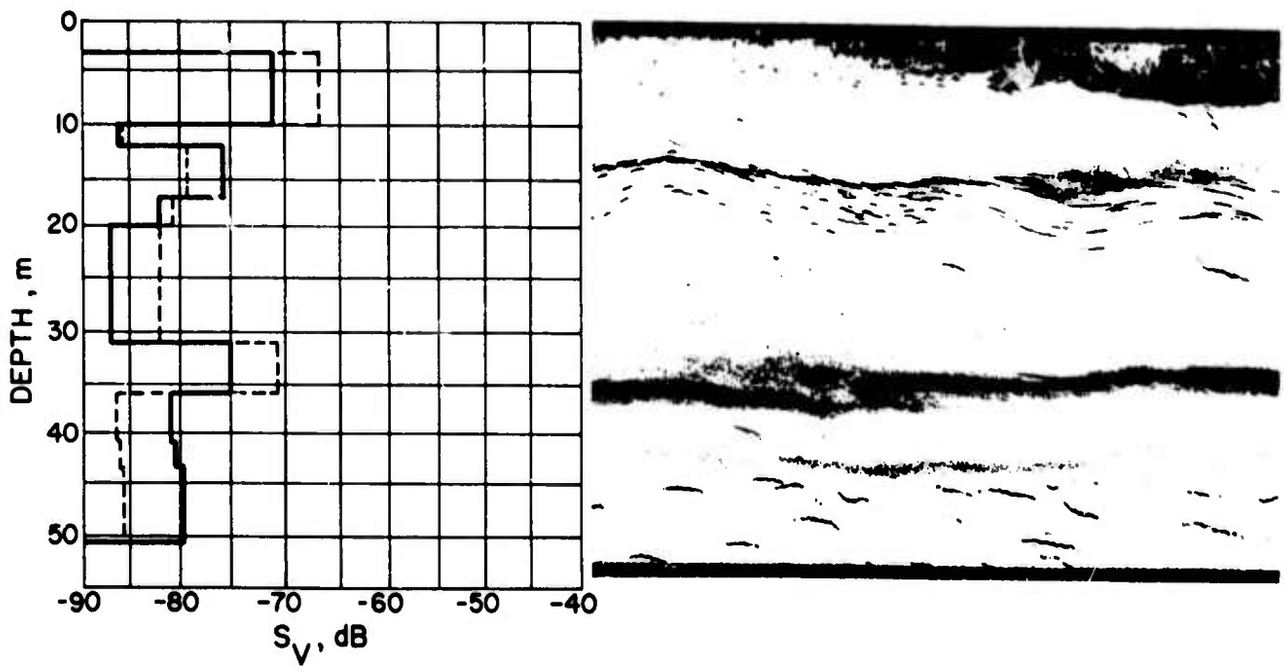

Figure 80. Tape 5 File 10, 105 kHz, 28 July 1972 (--- last 206 pings of run only).

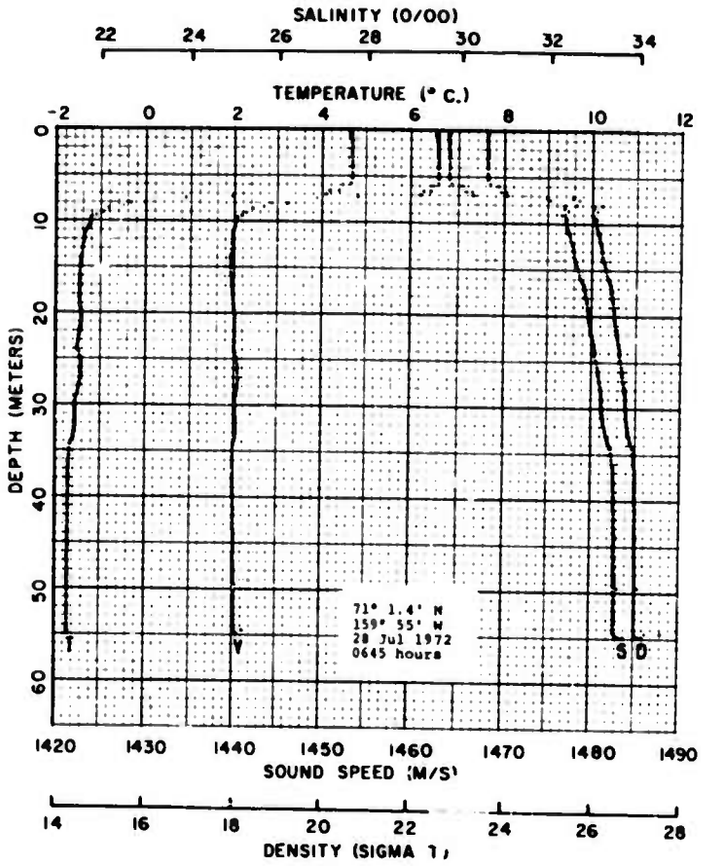

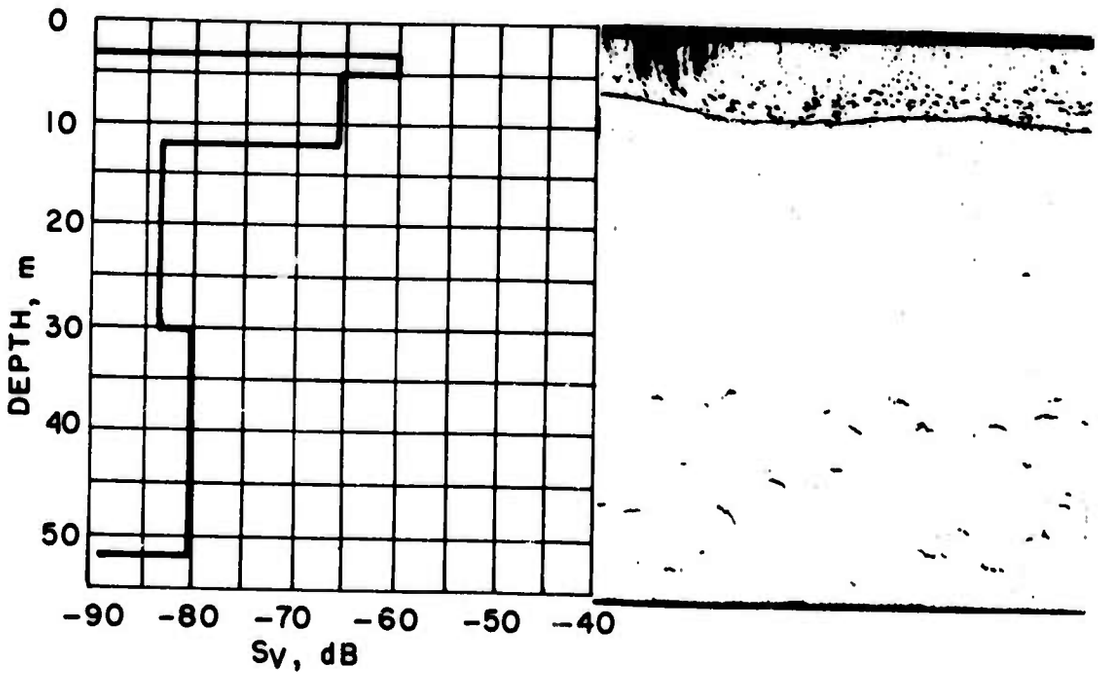

Figure 81. Tape 5 File 4, 105 kHz, 28 July 1972.

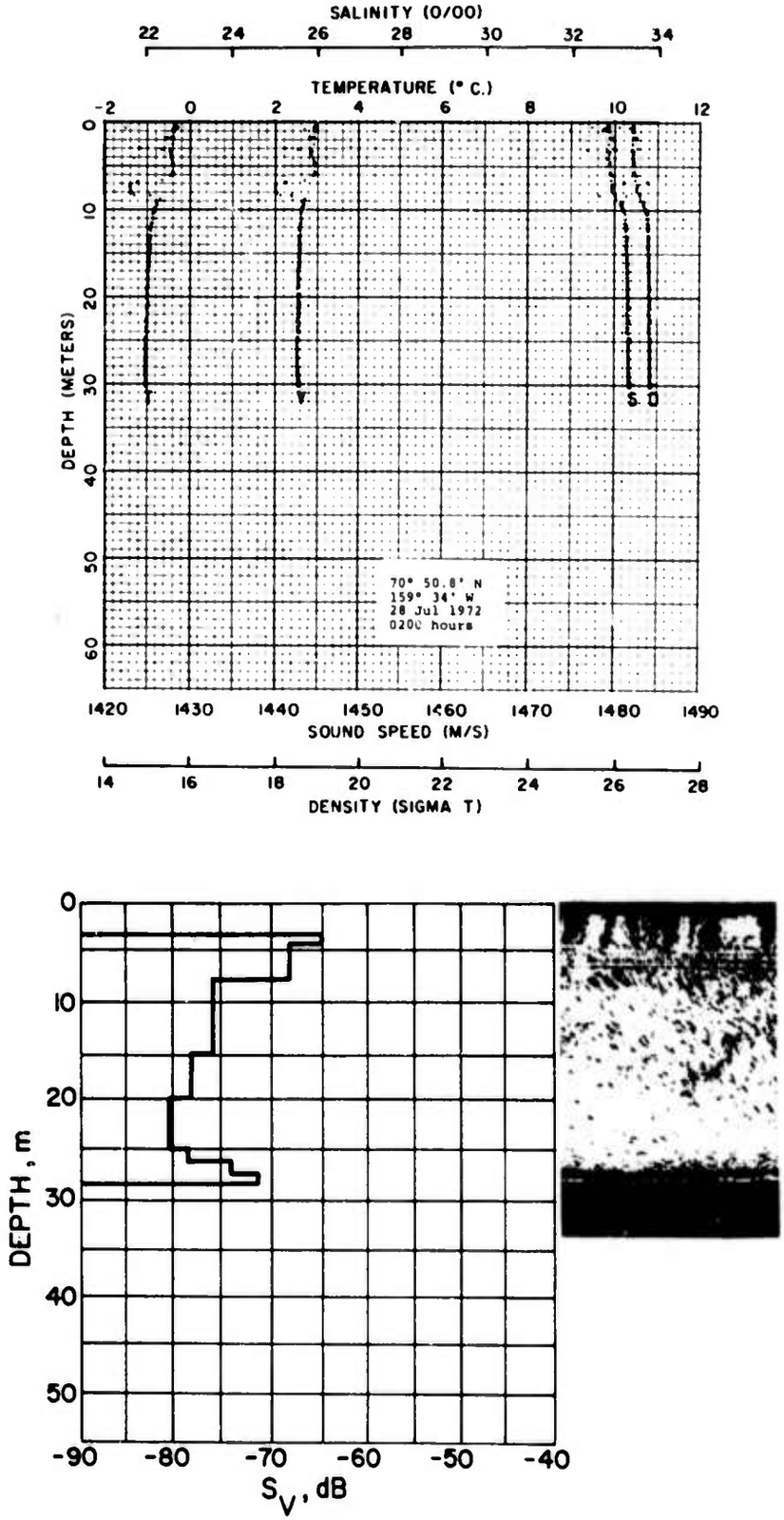

Figure 82. Tape 5 File 2, 105 kHz, 28 July 1972.

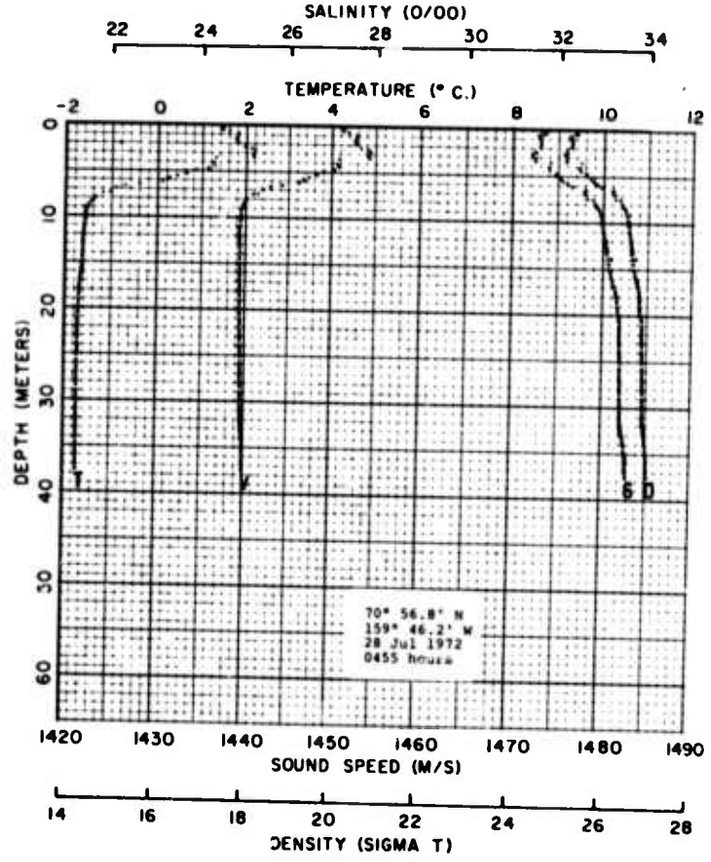

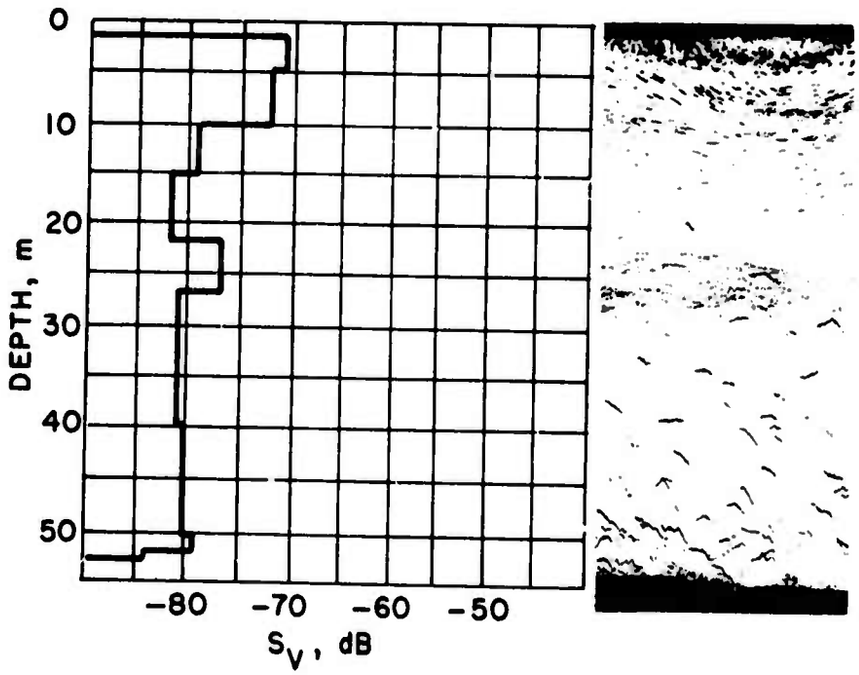

Figure 83. Tape 5 File 3, 105 kHz, 28 July 1972.

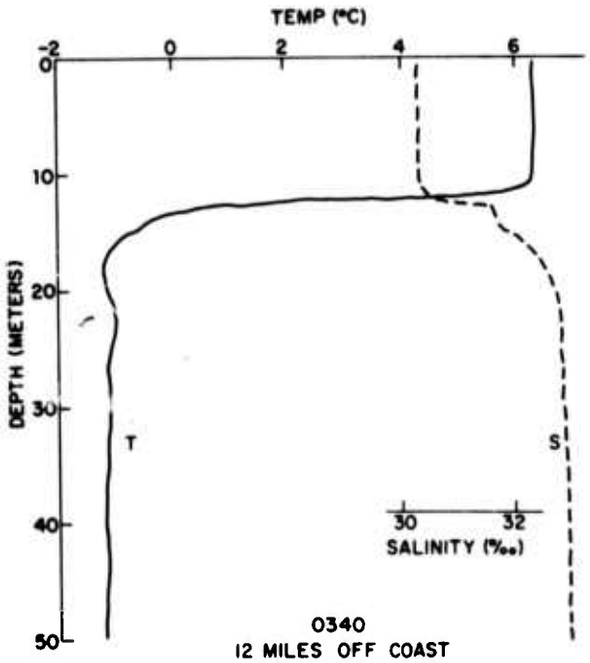

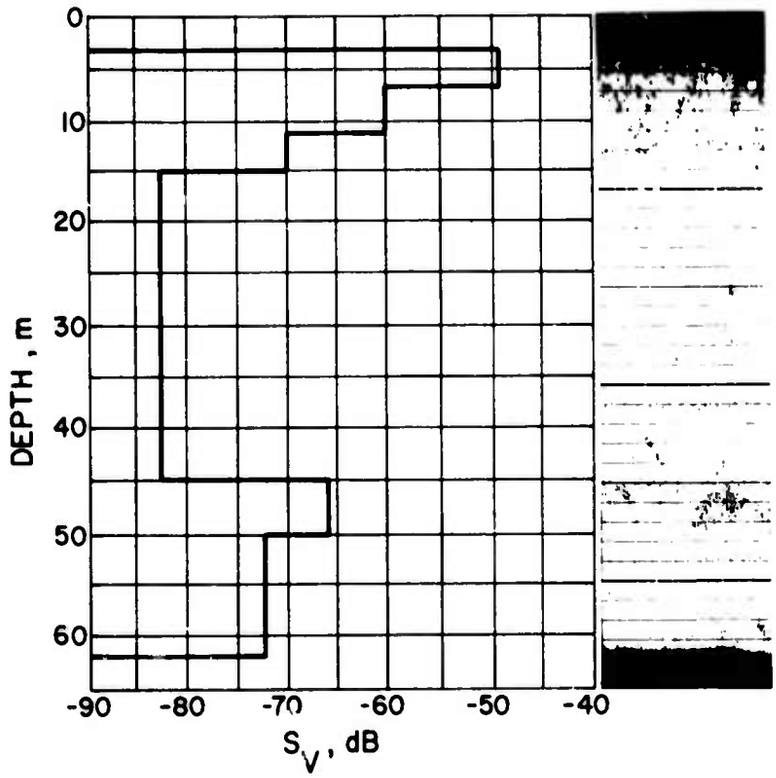

Figure 84. Tape 7 File 12, 105 kHz, 14 August 1972.

Results

Figures 70 and 71 are typical of many data files obtained on the cruises and help to give an accurate picture of the average overall results. The average results, however, are not as interesting as several specific features of the data obtained on these cruises.

The data varied greatly over very short distances. A good example of this variation can be seen by comparing Figures 72 and 73. These measurements were taken only 3.8 n. mi. and 2 hr apart, with little change in depth or ice conditions (about 6 oktas); yet there was a tremendous increase, about 21 dB, in acoustic scattering because of a dense, shallow layer at the latter site. Clearly, a great deal of averaging must be done to get a good estimate of the biological activity in an area.

Data taken at 38 kHz and at 105 kHz at the same location showed practically the same scattering strength. (Compare Figures 73, 74 and 75 with Figures 76, 77 and 78, respectively, which were taken at the same sites.) This was a surprising result. Most biological scattering was expected to come from organisms such as plankton, which are much smaller than the acoustic wavelengths employed. Therefore, Rayleigh's law should have applied, and the acoustic scattering strength at 38 kHz would be expected to be approximately 18 dB below that at 105 kHz. There are three possible explanations for this phenomenon: 1) the scatterers were large compared to typical plankton, 2) they were closely packed so as to scatter in agglomerations comparable to a wavelength (about 4 cm at 38 kHz), or 3) the scattering at 38 kHz was larger than normal because bubbles that resonate at 38 kHz were present in the medium, presumably attached to the biological species; such resonance would occur at a depth of 25 m for a bubble about 0.05 cm in diameter.

The air bubble hypothesis is an attractive one because the presence of air bubbles varying in size but including those resonant at 38 kHz would tend to equalize the relative effect of the Rayleigh scattering at the different frequencies. At 38 kHz, one 38 kHz-resonant bubble per cubic meter would produce a volume scattering strength of about -31 dB (ref. 1 m^{-1}). The possibility of scattering from gases thus would becloud any effort to determine the size of plankton and micronekton biomasses by comparing their acoustic scattering at two or more frequencies.

In general the 38- and 105-kHz results differed less than the combined uncertainty of the measurements. The scattering strength at 38 kHz was not always as large as that at 105 kHz. For example, the definite scattering layer at about 8 m in Figure 79, which was taken at 105 kHz, shows a volume scattering strength of -61 dB; the same layer had a strength of -67 dB at 38 kHz. The theoretical Rayleigh difference of 18 dB was never observed.

It should be noted that the measurements at the two frequencies were usually made within a few minutes of each other, but they were not made simultaneously because of mutual interference (reception of the output pulse of the other system). Figure 80 emphasizes the need to make comparative measurements on a specific biomass simultaneously. The dotted line shows the average acoustic volume scattering strength in the last 206 pings of the recording when, as can be seen on the echogram, the scattering layer at about 34 m concentrated and stabilized. In these last 206 pings, the average scattering strength in the depth interval from 32 to 36 m jumped 4 dB over the average for the recording as a whole. There was also an increase of 5 dB in the interval from 20 to 32 m, probably because of the single dark object at about 23 m near the right edge of the echogram. Meanwhile, the layer near 15 m became less pronounced and yielded about 5 dB less. In the future, we intend to synchronize the outputs of the two systems so that simultaneous measurements are possible.

Figure 81 is of particular interest because of a sharp echo at about 8 m on the echogram that corresponds to a sharp thermal layer. We do not know whether the sharp echo was caused by the sudden velocity change at the thermal interface (that is, by simple partial reflection from a rho-c discontinuity) or by organisms that congregated at the interface. A rough calculation indicates that the physical discontinuity was extreme enough to produce the observed scattering. Another feature of Figure 81, one typical of areas where there were warm surface intrusions, is the congregation of biomass in the warm surface water and the relatively little biomass in the deeper cold water.

Figure 82 (very shallow water, about 30 m, just off Pt. Belcher) is one of the few data files where the biomass was distributed more or less evenly throughout the volume. This relatively homogeneous distribution was not observed farther from shore and was probably due to in-shore mixing of the shallow water. Figure 83, 7 n. mi. farther away from Pt. Belcher in water about 55 m deep, shows the development of definite layering, particularly if the returns that appear to be layers of plankton and those that appear to be single targets are considered separately. Another 4.6 n. mi. away from shore, in water 57 m deep, was the extreme surface thermal and biolayer previously discussed (Figure 81).

Figure 84 is unusual in that it shows a substantial scattering layer (-66 dB) around 48 m. Typically, scattering layers above -70 dB were not found in the lower half of the volume. The large temperature discontinuity (the top 12 m are 7.5°C warmer than the rest of the volume) and the usual accompanying concentration of biomass near the surface in the warm water make the presence of this deep scattering layer all the more unusual. We do not know its composition.

Biological Sampling

During the two cruises, 89 net hauls and net trawls were made. Of the 89 samples, 31 were taken with a 3/4-m diam. ring net (216-μ mesh) at 6 sites and 58 were taken with a 1-m square NIO midwater trawl net (1000-μ mesh) at 22 sites.

The contents of the hauls were preserved in unbuffered formalin to which eosin dye had been added and were returned to Seattle by ship. Three samples were lost because of net breakage or spillage and four NIO trawls that crashed on the bottom yielded dubious contents. The contents of one haul were given to a scientist from the Smithsonian Institution.

Because of interference from the ice floes, only the ring net was used while the ship was operating in the ice. In open water, the NIO trawl net was used almost exclusively because for most of the cruise it was the only net available that could be closed. At the last two ring net sites the net was jury-rigged to give at least some control over the depths sampled, but this arrangement did not close completely.

The ring net became clogged with diatoms whenever used. All in all, it was too small and too slow to take adequate samples. However, since a replacement net with larger mesh missed the ship in Barrow, the smaller-meshed net was used throughout the trip.

The NIO trawl net performed admirably throughout the cruise once a method was found for launching and recovering it without lifing it over the rail. Trawls were standardized at 10 min and were timed from when the desired length of wire was paid out until the net was tripped. Small time deviations were not recorded since they were insignificant compared to errors in the estimation of ship speed. During the tows, the speed was maintained as close to 2 kn as possible.

Because plankton sampling slowed down the entire operation, plankton samples were not taken at every sonic station. An effort was made to sample at at least every third station, and more often if possible--especially if interesting layers showed up on the sonic gear. Attempts were made to trawl both in and out of definite sonic layers, but it was hard to predict from the ship's estimated speed and the observed sea conditions exactly how the net would behave at large wire angles. At wire angles greater than 65° (over 80 m of paid-out cable), difficulty was also experienced in tripping the net.

The biological sampling was performed by Mr. Miles J. Furnas, a student in the Department of Oceanography at the University of Washington.* A cursory examination of the samples shows a large number of various species, and, in particular, a large concentration of copepods in certain layers (see Table I in Ref. 6). A few individual fish were found, arctic cod and sculpin, but most of the single acoustic targets could not be caught efficiently by the method used.

Other than the very few fish, the strongest acoustic scatterers found in the 1972 net samples were euphausiids. The only known measurement of the scattering cross section of an individual zooplankton was done on euphausiids by Beamish (Ref. 10). Beamish found that euphausiids typically have a backscattering cross section of about $1.4 \cdot 10^{-4}$ cm^2 at 102 kHz. Thus it would take 60 to 600 euphausiids per cubic meter to produce an acoustic layer with a volume scattering strength of -60 to -50 dB (ref. 1 m^{-1}) at 105 kHz--if the scattering were caused mainly by these organisms.

Discussion and Future Work

A comparison of the 105-kHz results with those of 1971 does not show any differences that can be attributed to an annual change. Some of the very dense, relatively deep layers observed in 1971 were missing in 1972. However, the 1971 data were taken, on the average, closer to shore and under less ice cover; also, a considerable part of the 1971 data was taken to the east of Barrow in the Beaufort Sea instead of to the west in the Chukchi Sea. It is therefore impossible to tell whether the changes observed in the scattering were caused by annual differences in the climate or oceanographic and ice conditions.

Although many different organisms were found in the samples collected in 1972, information as to the volume swept, catching efficiency, and catching depth was too uncertain to warrant any attempt to use the data quantitatively. More accurate sampling methods are being prepared in connection with the biological modeling work described in Appendix B. This improvement should complement the reverberation work by enabling us to collect samples from a specific acoustic scattering layer more efficiently. In addition to improving our biological sampling capability, we plan to add a 250-kHz system to collect acoustic data on the smaller zooplankton observed in the samples.

Because of the great local variability in the data, any quantitative conclusions will have to be based on a large number of measurements.

*Now a graduate student at the University of Rhode Island.

There were 179 data files taken in the Chukchi Sea in July and August 1972. Since then, August 1973 measurements have added 126 data files. Analysis of the data taken in the Chukchi Sea in August 1973 should enable us to make an appropriate quantitative comparison of the scattering levels.

More data will be obtained in July and September 1974 from the same region. Statistical analyses of these data will be made and correlated with environmental variables. In addition, the volume reverberation data taken in August 1971 in the Beaufort Sea and in March 1973 in the Bering Sea will provide comparisons with other regions. As more data on the region are collected and analyzed, we will be able to gain more insight into the relationship of the acoustic scattering strength to the season, water temperature, and ice cover.

VIII. REFERENCES

1. APL-UW 7223, "Studies in the Marginal Ice Zone of the Chukchi and Beaufort Seas: A Report on Project MIZPAC-71B," Applied Physics Laboratory, University of Washington, by G.R. Garrison and E.A. Pence, January 1973.

2. APL-UW 7309, "Studies in the Marginal Ice Zone of the Chukchi Sea: Acoustic and Oceanographic Data for 1972," Applied Physics Laboratory, University of Washington, by G.R. Garrison, E.A. Pence, and H.R. Feldman, July 1973.

3. NUC TP 164, "Digital Computer Programs for Analyzing Acoustic Search Performance in Refractive Waters, NUC Programs 800000 and 800001," Vols. 1 and 2, Naval Undersea Research and Development Center, December 1969.

4. "Propagation of Acoustic Waves in a Medium with Experimentally Determined Inhomogeneities," by S.R. Murphy, Doctoral Thesis, University of Washington, 1959.

5. "Propagation of Radiation in a Medium with Random Inhomogeneities," by P.G. Bergmann, Phys. Rev., 70, p. 486, 1946.

6. "Volume Scattering Measurements in the Marginal Ice Zone," by P.H. Moose and H.R. Feldman, Proceedings of the 29th Navy Symposium on Underwater Acoustics, New London, 1972.

7. "Measurements of the Volume Scattering Strength in the Beaufort and Chukchi Seas," by H.R. Feldman, P.H. Moose and S.R. Shah, Proceedings of the IEEE Conference on Engineering in the Ocean Environment, Seattle, 1973.

8. "Electronic System and Data Processing Techniques for Estimating Fish Abundance," by P.H. Moose, et al., Proceedings of the IEEE Conference on Engineering in the Ocean Environment, 33-36, Newport, 1972.

9. "An Expression for the Variance of Abundance Estimates Using a Fish Echo Integrator," by P.H. Moose and J.E. Ehrenberg, J. Fish. Res. Bd. Canada, Vol. 28, No. 9, 1293-1301, 1971.

10. "Acoustic Scattering from Zooplanktonic Organisms," by P. Beamish, Proceedings of an International Symposium on Biological Sound Scattering in the Ocean, 474-5, Warrenton, Virginia, 1970.

AUTOMATIC PROFILER

The automatic profiler was developed as a prototype unmanned system for gathering conductivity-temperature-depth data. Basically it is an automated CTD profiler that can be deployed at a remote site and left unattended to record data at a preprogrammed rate.

The profiler utilizes the same types of sensors as the CTD system used in the MIZ and records data in the same format. All winch operations, punch control and drop timing functions are internally controlled by the system. The duration of unmanned profiler operation is limited primarily by the consumption of battery power and the capacity of the recording system.

System Operation

A functional description of the automatic profiler is shown in the block diagram in Figure A1. The operation of the system is controlled by the master control unit, which can program profiling at a rate of one per hour or two per hour. A manual override control also allows activation of the system at any time. The control unit performs all data processing and tape formating operations for the system in the same manner as in the CTD system (see Ref. 1).

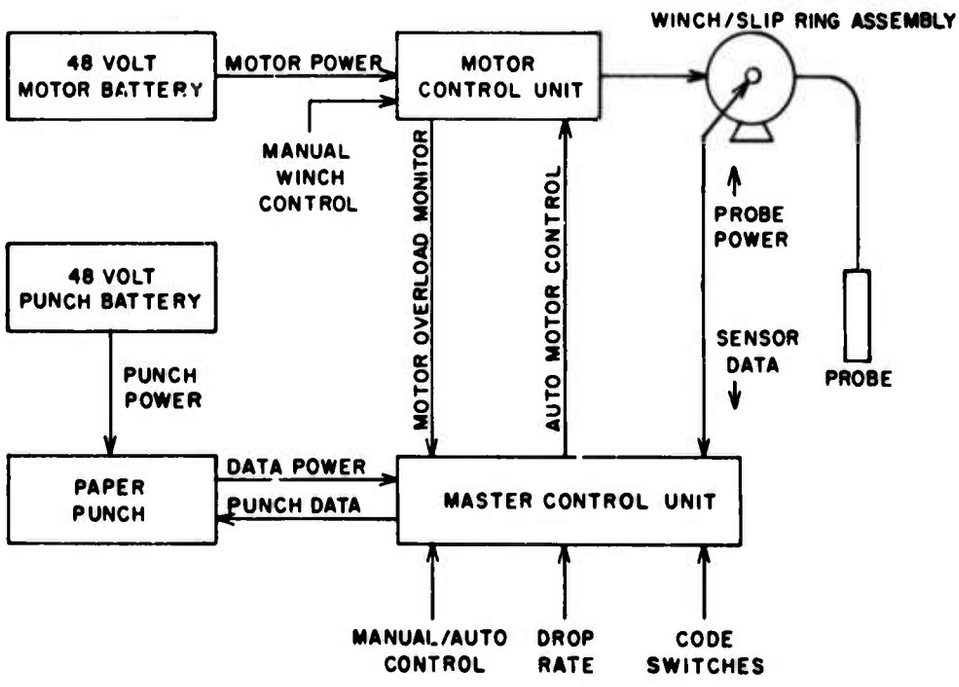

Figure A1. Block diagram of the automatic profiler.

When the control unit starts a drop sequence, power is automatically supplied to the sensors for a 1-min period before the data system is activated. During this time a 2-ft length of spacer tape is punched to separate the new data record from the previous one. After the initial 1-min delay, data samples are recorded for 15 sec with the probe in its starting position. This data is used to provide a constant starting depth reference. A signal from the master control unit to the motor control unit then applies power to the winch motor and the probe is lowered at a rate of 1/3 m/sec.

Lowering is continued until the probe touches the bottom or exceeds a preset depth (80-m maximum). At this time, data sampling is stopped, the winch motor is reversed, and the probe is raised at the same rate to its initial position. A second 2-ft length of spacer tape is punched to complete the record and all functions are reset to await the next drop command.

System Description

The winch assembly and probe are shown in Figures A2 and A3, respectively. The winch is mounted on one leg of an 8-ft tripod, carries 100 m of cable, and includes a module with a 48-volt dc motor, gear box, drum and slip ring.

The probe contains the sensors, the bottom detector, the depth-limit switch, and a data multiplexer and its control electronics. The probe has an overall length of 50 in., a maximum outer diameter of 8.5 in. and an in-water weight of 26 lb.

To deploy the profiler, a hole at least 9 in. in diameter must be made through the ice. The ice thickness must be sufficient to support the total system weight of 600 lb but not exceed the hole drilling capability. The tripod and winch assembly are then mounted over the hole and the probe is dropped through it. In normal operation the probe is left just below the bottom of the ice to reduce the possibility of damage if the probe should rise automatically when the hole has refrozen.

The batteries, paper punch and control units are placed on a sled or pallet next to the tripod and covered with a canvas. The whole system can be assembled and tested in less than 1 hour after the ice hole has been cut. The deployed profiler is shown in Figure A4.

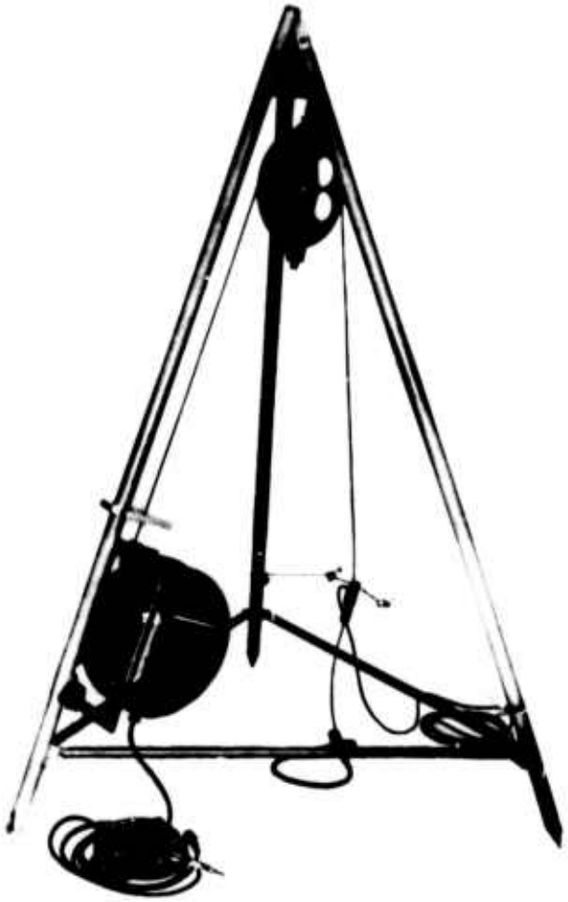

Figure A2. Automatic profiler winch assembly.

Figure A3. Automatic profiler CTD probe.

Figure A4. Automatic profiler installed on an ice floe.

Operational Limitations

The primary limitations on the unmanned operation of the profiler are the capacity of the recording unit and the battery power supplied to the system. The paper tape recorder can handle 1000 ft of tape. The take-up system, however, is only 90% efficient. At the profiler drop rate of 1/3 m/sec, the capacity of the take-up system is approximately 55 minutes of profile data, or 20 drops to a depth of 50 m.

Power for the profiler is presently supplied by two 48-V packs of lead acid batteries. A separate battery pack is used for the data system to isolate it from noise generated by the dc winch motor. When the profiler is not in operation, the power drain from the punch battery is less than 10 mA. The motor battery has no power loss since it is gated out of the system until the drop is started. During the drop, the average battery drain by the punch is 2.5 A, of which approximately 2 A are used by the recording system. The motor current during the drop varies from 3 to 4 A, depending on the ambient temperature and the drop frequency. A 150-ft drop drains approximately 0.1 A-h of charge from the punch battery and 0.4 A-h from the motor battery. At an ambient temperature of approximately 0°C, and a rate of one 50-m drop per hour, the motor battery will provide 40 drops before recharging is necessary and the punch battery more than 100 drops.

System Improvements

The weakest feature of the profiler system proved to be recording the data on paper tape. Not only did the tape take-up and supply capacity limit the number of unattended drops but the punch was also susceptible to jamming and paper tearing. In addition, the punch consumed relatively large amounts of power.

The method best suited for data recovery of this type would appear to be data telemetry. This method would eliminate the capacity and power supply problems of an on-site recording system and, in addition, would allow transmission of data relating to any profiler equipment problems that might require attention. The addition of a radio link would enable the profiler to be interrogated from the recording site at any time.

To achieve real-time transmission, the telemetry system and the recording system would both have to be capable of operating at a data rate of 250 bits/sec or, alternatively, a suitable memory system could be included in the profiler to store the data for transmission at a later time and the data telemetry rates could be adjusted as desired. The latter method would also prove useful in recovering data if more than one profiler were being controlled by the data recording station.

EVALUATION OF A TECHNIQUE FOR PREDICTING VOLUME REVERBERATION FROM BIOLOGICAL SCATTERERS IN THE OCEAN

ABSTRACT

This paper describes a technique for predicting the scattering strengths of biological scatterers in the ocean. An attempt was made to predict the seasonal variations in the biomass and volume reverberation (at various frequencies) in the Arctic. A dynamic biological population production model has been constructed which converts environmental input parameters into a prediction of the density and size distributions of the biological population as a function of space and time. This output is then converted to a prediction of the volume scattering strength by use of theoretical and empirical relationships between organism size and distribution and acoustic scattering phenomena. We have used a simple model to describe the intertrophic population dynamics of the biological scatterers. The model simulates relationships between the nutrient concentration and the population density of the various organisms. The feasibility of monitoring the biomass by acoustic techniques coupled with computer simulation is also discussed.

INTRODUCTION

The major source of volume reverberation in the oceans has been established as biological organisms [1]. Non-biological sources such as dust and sand particles, thermal gradients, and turbulence of natural or man-made origin are usually insignificant contributors to the volume scattering strength observed at sea.

Many studies have been done to identify the biological organisms responsible for sound scattering, as well as to determine the scattering properties of an individual organism. Love [2] and Cushing and Richardson [3] have made measurements of the target strength of fish. Love has determined a description of the target strength of an individual fish as a function of its length and the acoustic wavelength.

During the last decade, much interest has been shown in the acoustic assessments of fish stocks [4,5]. The recent developments in high-speed processing of sonar information render the task of measurement and estimation of the volume reverberation easier. However, we are far from knowing the volume scattering strength in different oceans, at various seasons, depths and frequencies.

Figure 1 is a simplified block diagram of the dynamics of the marine ecosystem. The principal biological components are phytoplankton, and herbivorous and carnivorous zooplankton, with nutrients and visible radiation as the driving forces.

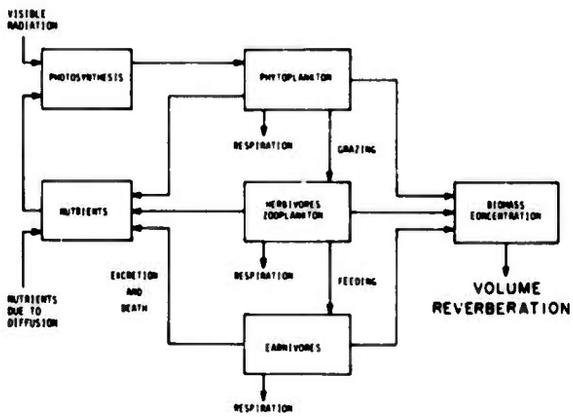

Figure 1. Marine Ecosystem.

There is interaction among the biological components, which collectively form biomass to produce volume reverberation. Successful prediction of the bioacoustic environment can lead to confident prediction of mean volume scattering strengths. The volume scattering strengths are estimated from the predicted distribution of biological scatterers; therefore, it is necessary to know the average body size, mass and the number of different scatterers. Based on the body size, the target strength for various scatterers can be estimated at different frequencies.

Since 1971, the Applied Physics Laboratory of the University of Washington has been actively involved in the measurement of volume reverberation in the Arctic as part of the Marginal Ice Zone Pacific Project (sponsored by the Arctic Submarine Laboratory, Naval Undersea Center, San Diego) [6].

In addition to making quantitative measurements of volume scattering strength, biological samples were taken to identify the type and relative numbers of the scatterers. As a result of the measurements taken in the Arctic (Chukchi Sea and Beaufort Sea), and because of the apparent simplicity in biological annual cycles, the lower Arctic in the vicinity of Barrow was chosen as the initial area of investigation.

PRELIMINARY POPULATION MODEL

Plankton population dynamics is influenced by many complex biological and physical phenomena. It is necessary, therefore, to idealize and simplify the conceptual model so that the result can be manageably simulated. Referring to Figure 1, the state variables of the system are concentrations of:

phytoplankton (p)

herbivorous zooplankton (h)

carnivorous zooplankton (c)

nutrient (n)

The visible radiation intensity (with temporal variations) is the forcing function.

The model simulates relationships between the state variables in a fixed volume of water (for a homogeneous area). The simulation consists of the solution of a system of coupled partial differential equations, one for each of the state variables.

Our simulation of the model is based on the following assumptions:

1) The photosynthesis rate is proportional to the light intensity at low intensity, but is limited when the saturation rate is reached according to Steele's [7] expression

$$P_h = P_h(\max)(I/I_{opt})\exp(1-I/I_{opt}),$$

where P_h is the photosynthesis rate, I is the incident light intensity and I_{opt} is the light intensity which gives maximum photosynthesis rate $P_h(\max)$.

The light intensity I at depth z as a function of incident surface radiation I_o may be expressed by the Beer-Lambert law as

$$I = I_o\exp(-k\,z)$$

where k, the coefficient of extinction, is assumed constant. Self-shading effects may be included by making k a function of phytoplankton concentration; that is, extreme increases in phytoplankton would inhibit the sunlight and reduce photosynthesis production.

2) Inorganic nitrogen is considered to be the limiting nutrient affecting the photosynthetic assimilation of carbon [8]. The ratio of photosynthetic assimilation of carbon to nitrogen is assumed to be 6 [9].

3) The Ivlev [10] predator-prey relationship describes the grazing and predation rates. The Ivlev expression for grazing is

$$W = W_{max}[1-e^{-kp}],$$

where M_{max} is the maximum grazing rate, p is the phytoplankton (prey) concentration and k is a constant.

4) The fractional loss of phytoplankton biomass due to sinking is constant.

5) Respiration, excretion and mortality rates are constant for each trophic level.

6) A euphotic zone exists from the surface down to 20 meters (based on 50% light level at 10 meters), with homogeneous distribution of the bio-concentrations in this zone.

7) Water temperature is constant at 0°C.

8) Assimilation efficiency of herbivores is 60% [11], and for carnivores is 85%.

9) Nutrient flux is described by the Fickian expression for diffusion,

$$\text{flux} = -k_z \cdot dn/dz,$$

where k_z is a vertical eddy diffusivity constant, and dn/dz is the nutrient vertical gradient [12].

The coupled partial differential equations used in the simulation are:

$$\partial p/\partial t = p(P_h - RP - SINK) - W_1 \cdot h$$

$$\partial h/\partial t = h(0.6\,W_1 - RH - MOLT) - W_2 \cdot C$$

$$\partial c/\partial t = c(0.85\,W_2 - RC - MORT)$$

$$\partial n/\partial t = h \cdot EXC1 + c \cdot EXC2 - k_z \cdot dn/dz - (p \cdot P_h)q$$

The symbols are:

RP - respiration rate of phytoplankton

RH - respiration rate of herbivores

RC - respiration rate of carnivores

SINK - sinking rate of phytoplankton

MOLT - mortality rate of carnivores

W_1 - grazing rate of phytoplankton by herbivores

W_2 - predation rate of herbivores by carnivores

EXC1 - excretion rate of ammonia by herbivores

EXC2 - excretion rate of carnivores

q - conversion factor between the amount of carbon assimilated and equivalent amount of inorganic nitrogen consumed.

The simulation of this simple model consists of solving the four partial differential equations, by the elementary forward time-step method. That is, if we represent the four equations by

$$\frac{\partial F_i(t)}{\partial t} = f_i\ [F_j(j=1,\ldots,4),\phi(t)];\ i = 1,\ldots,4$$

(where the F_i are the four concentrations and $\phi(t)$ represents the driving functions); then,

$$F_i(t+\Delta t) = \Delta t \cdot \frac{\partial F_i(t)}{\partial t} + F_i(t);\ i = 1,\ldots,4.$$

In this way, given the initial concentrations of inorganic nitrogen, phytoplankton, herbivorous and carnivorous zooplankton and their functional interdependence, we can project their concentrations forward in time.

The stability and accuracy of the method are preserved if the changes in the variables during time Δt are small enough so that the first order term in Taylor's expansion is adequate. This elementary method of solution has proven sufficient.

PRELIMINARY ACOUSTIC MODEL

The acoustic volume scattering strengths are obtained using the biological scatterer density predicted by the population model simulation. It is therefore very important to know the target strengths of individual scatterers as a function of frequency. The target strength of a distribution of organisms which scatter incoherently relative to one another is given by [1]

$$T = 10 \log \int_0^\infty N(S)\sigma(S,\lambda)dS,$$

where $\sigma(S,\lambda)$ is the average scattering cross section at acoustic wavelength λ and $N(S)dS$ is the number of organisms per unit volume whose length is between S and S+dS.

Computation of the Target Strengths

Cooney's [13] expression was used for the small targets (<1 cm in length) and Love's expression was used for fish.

Cooney's expression for the target strength of very small targets based on Rayleigh scattering for the individual plankton is

$$TS = 10 \log \frac{\pi^2 T^2}{\lambda^4} (1 + \frac{3}{2}\mu)^2,$$

where TS is the target strength in decibels, T is the volume of the "ideal" animal, λ is the wavelength of the incident sound, and μ is the cosine of the angle between the scattering direction and the reverse direction of the incident wave; $\mu = 1$ for backscattering.

Love [2] has developed an empirical equation that approximates the dorsal-aspect target strength (T_D) of an individual fish in the L/λ range of interest for most sonar application, where L is the length of fish, and λ is the acoustic wavelength.

Love's expression for the dorsal-aspect target strength of an individual fish is

$$T_D = 19.1 \log L + 0.9 \log \lambda - 23.88,$$

where L and λ are in meters, and T_D is in decibels. The equation is a good approximation to the dorsal-aspect target strength of an individual fish for $0.7 \leq L/\lambda \leq 90$.

SIMULATION OF THE MODEL AND THE RESULTS

The model was simulated to predict the concentrations of phytoplankton, herbivorous and carnivorous zooplankton (in milligrams carbon/meter^3) and inorganic nitrogen (in μg At N/liter) from spring to fall on a daily basis. The volume reverberation is predicted at a frequency of 100 kHz, the frequency used for the measurement of volume reverberation in the Arctic in 1971 and 1972.

Results

Figure 2 shows some of the results for a typical set of inputs as shown in Table I. There are early spring phytoplankton blooms which are limited by the inorganic nitrogen concentrations. The blooms are depleted by the herbivorous zooplankton stock, which in turn is consumed by the carnivores. The typical predator-prey relationship is exemplified by the oscillatory behavior of the plankton variables. The volume scattering strength varies between -85 dB and -70 dB. The peaks in scattering strength coincide with peaks in carnivore concentration. The scattering data at 105 kHz obtained experimentally in 1971 are also shown. An elementary parameter sensitivity analysis resulted in the following observations:

1) A 10% variation in inorganic nitrogen concentration does not have a significant effect on the scattering strength.
2) Increasing the respiration rates of the plankton by 10% also affects the scatering insignificantly.
3) Increasing the grazing or feeding rates by 10% increases the scattering by about 2 dB at the peak.
4) Doubling the initial concentration of the state variables resulted in an increase in scattering of about 5 dB during the first 4 weeks, after which the model stabilized with only slight variations in scattering.

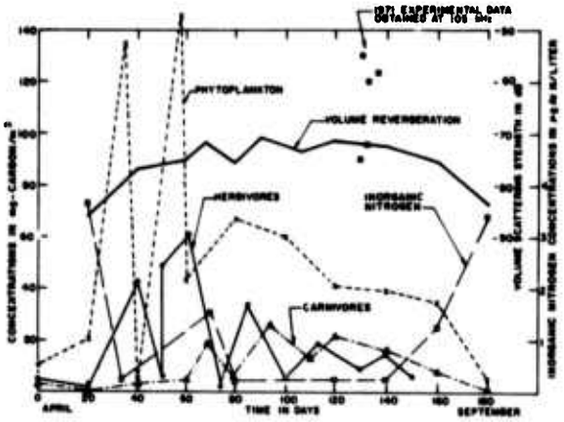

Figure 2.

DISCUSSION

The simulation of this simple model has shown that with the knowledge of certain biological parameters, volume reverberation can be predicted with confidence. Accuracy of the model is dependent upon a) the validity of the model and b) the accuracy in the knowledge of the biological rate parameters.

Though the acoustic scattering strengths obtained from the simulation fall within the range of the experimental data, this must be viewed critically, and not as an indication of the success of the model. Experiments should be designed to obtain the critical data needed for operation and verification of this model and its simulation. This would entail biological sampling and acoustic and physical measurement procedures to be performed over sufficient time and averaged over sufficient area to be a critical test of the biological mode, its simulation, and its acoustic consequences.

The current interest in modeling the oceanic upwelling regions of the world has resulted in large-scale simulation programs under the International Biological Program. These involve a team of specialists simulating and verifying models on-site. These long-term programs should provide better understanding of the population dynamics and more accurate rate parameters. Studies should be carried out which entail a biological and acoustic investigation in a small oceanic area, conducted over a period of time, to obtain a better understanding of the relationships between biological, acoustic and physical oceanographic variables. The knowledge and experience gathered from investigations in one area should lead to prediction models for other areas of interest.

Table I.

Initial Concentration	Quantity	Unit
phytoplankton	10	mg carbon/m^3
herbivores	5	mg carbon/m^3
carnivores	3	mg carbon/m^3
inorganic nitrogen	3	µg At N/liter

Respiration Rates (fraction per day) [14]:

phytoplankton	0.15
herbivores	0.13
carnivores	0.05

Maximum photosynthesis rate = 1.00 per day

I_{opt} = 0.5 gm-cal/cm^2/min

Extinction coefficient of sea water = 0.05/m

Sinking rate = 0.05 per day

Mortality rate of carnivores = 0.10 per day

Molting rate of herbivores = 0.05 per day

Maximum grazing rate = 1.5 per day[a]

Maximum predation rate = 0.6 per day[a]

Ivlev constant for herbivores = 0.015[a]

Ivlev constant for carnivores = 0.029[a]

	Individual [14]		
	Average length (mm)	Average mass (mg carbon)	Target strength (dB)
Herbivores	5	0.039	-110
Carnivores	15	1.0	-85

Light data were obtained from English's measurements in the Arctic [15].

(a) Unpublished data, M. Jawed, Dept. of Oceanography, University of Washington

REFERENCES

1. Urick, R.J., 1967: *Principles of Underwater Sound for Engineers;* McGraw-Hill, 204.

2. Love, R.H., 1971: *Dorsal-Aspect Target Strength of an Individual Fish*; J. Acoust. Soc. Am., Vol. 49, #3, 816-823.

3. Cushing, D.H. and I.B. Richardson, 1955: *Echo Sounding Experiments on Fish*; Brit. Min. Agr. Fisheries Invest., (2) & (4).

4. Moose, P.H. et al. 1971: *Electronic System and Data Processing Techniques for Estimating Fish Abundance*; IEEE 1971 Eng. in the Ocean Environment, 33-36.

5. Ehrenberg, J.E. and D.W. Lytle, 1972: *Acoustic Techniques for Fish Abundance*; IEEE Trans, Vol. GE-10, 138-145.

6. Garrison, G.R. and E.A. Pence, 1973: *Studies in the Marginal Ice Zone of the Chukchi and Beaufort Seas--A Report on Project MIZPAC-71B*; Applied Physics Laboratory, University of Washington, APL-UW 7227, 127-141.

7. Steele, J.H., 1962: *Environmental Control of Photosynthesis in the Sea*; Limnol. Oceanogr., 7, 137-50.

8. MacIsaac, J.J. and R.C. Dugdale, 1972: *Interactions of Light and Inorganic Nitrogen Uptake in the Sea*; Deep-Sea Res. 19, 209-232.

9. Dugdale, R.C. and J.J. Goering, 1967: *Uptake of New and Regenerated Forms of Nitrogen in Primary Productivity*; Limnol. Oceanogr. 12, 196-206.

10. Ivlev, V.S., 1945: *The Biological Productivity of Seas*; Usp. Sovren. Biol., 19(1), 88-120.

11. McAllister, C.D., 1969: *Aspects of Estimating Zooplankton Production from Phytoplankton Production*; J. Fish. Research Board of Canada, Vol. 26, No. 2, 1969.

12. Jawed, M., 1973: *Ammonia Excretion by Zooplankton and its Significance to Primary Productivity during Summer*; Contribution No. 000, Dept. of Oceanography, U. of Washington, Seattle, Washington.

13. Cooney, R.T., 1971: *Zooplankton and Micronekton Associated with a Diffuse Sound-Scattering Layer in Puget Sound, Washington*; PhD Thesis, University of Washington, Seattle, Washington.

14. Ikeda, T., 1970: *Relationship between Respiration Rate and Body Size in Marine Plankton Animals as a Function of the Temperature of Habitat*; Bul. of the Faculty of Fisheries, Hokkaido Univ., Vol. 21, No. 2, 91-112.

15. English, T.S., 1961: *Some Biological Oceanographic Observations in the Central North Polar Sea Drift Station Alaska*; Arctic Inst. of N. Am., Scientific Rpt. No., 15, 1957-58.

UNCLASSIFIED

Security Classification

AD779856

DOCUMENT CONTROL DATA - R&D

(Security classification of title, body of abstract and indexing annotation must be entered when the overall report is classified)

1. ORIGINATING ACTIVITY (Corporate author)

Applied Physics Laboratory, University of Washington, 1013 NE 40th, Seattle, Wash. 98195

2a. REPORT SECURITY CLASSIFICATION: Unclassified

2b. GROUP

3. REPORT TITLE

STUDIES IN THE MARGINAL ICE ZONE OF THE CHUKCHI SEA: ANALYSIS OF 1972 DATA

4. DESCRIPTIVE NOTES (Type of report and inclusive dates)

5. AUTHOR(S) (Last name, first name, initial)

Garrison, Gerald R.
Pence, Elbert A.
Feldman, Henry R.
Shah, Shashikant R.

6. REPORT DATE	7a. TOTAL NO. OF PAGES	7b. NO. OF REFS
14 March 1974	142	25

8a. CONTRACT OR GRANT NO.: N00014123-71-C-1333

b. PROJECT NO.:

c. ARPA Order No. 1782

d.

9a. ORIGINATOR'S REPORT NUMBER(S): APL-UW 7311

9b. OTHER REPORT NO(S) (Any other numbers that may be assigned this report)

10. AVAILABILITY/LIMITATION NOTICES

The distribution of this report is unlimited.

DISTRIBUTION STATEMENT A
Approved for public release;
Distribution Unlimited

11. SUPPLEMENTARY NOTES

12. SPONSORING MILITARY ACTIVITY

Arctic Submarine Laboratory, Code 90
Naval Undersea Center
San Diego, California

13. ABSTRACT

This report is a summary and analysis of studies in the Marginal Ice Zone of the Chukchi Sea in 1972 by the Applied Physics Laboratory of the University of Washington. A camp on an ice floe was established and occupied for 2 weeks during the summer. Temperature profiles of the water under the floe were taken simultaneously at four stations every hour to measure the character and change of the thermal microstructure in the water. At the same time, acoustic pulses were transmitted from one station to another to determine the effect of the thermal microstructure on acoustic propagation. Two 1-week cruises across the Chukchi Sea were made, one before and one after the ice floe occupancy, to study the intrusion of warm Pacific water which occurs every summer and to measure acoustic scattering from biological layers.

The intrusion of Pacific water appeared as a 6 to 8°C, 10-m thick surface layer extending across the western portion of the Chukchi Sea. In the transition zone between the intrusion and the existing winter water, thermal microstructure with variations as high as 0.3°C appeared in horizontal layers averaging 3 meters in thickness and several hundred meters in extent. These layers caused variations of 5 to 10 dB when acoustic pulses were transmitted through them. Biological acoustic scatterers were found to be more prevalent in the warmer water of the intrusion.

DD FORM 1 JAN 64 1473

UNCLASSIFIED

Security Classification

14. KEY WORDS	LINK A		LINK B		LINK C	
	ROLE	WT	ROLE	WT	ROLE	WT
Chukchi Sea Marginal Ice Zone, Studies in						
Marginal Ice Zone of the Chukchi Sea						
Thermal Microstructure						
Volume Reverberation						
Sound Transmission						

INSTRUCTIONS

1. ORIGINATING ACTIVITY: Enter the name and address of the contractor, subcontractor, grantee, Department of Defenae activity or other organization *(corporate author)* issuing the report.

2a. REPORT SECURITY CLASSIFICATION: Enter the overall security classification of the report. Indicate whether "Restricted Data" is included. Marking is to be in accordance with appropriate security regulations.

2b. GROUP: Automatic downgrading is specified in DoD Directive 5200.10 and Armed Forces Industrial Manual. Enter the group number. Also, when applicable, show that optional markings have been used for Group 3 and Group 4 as authorized.

3. REPORT TITLE: Enter the complete report title in all capital letters. Titles in all cases should be unclassified. If a meaningful title cannot be selected without classification, show title classification in all capitals in parenthesis immediately following the title.

4. DESCRIPTIVE NOTES: If appropriate, enter the type of report, e.g., interim, progress, summary, annual, or final. Give the inclusive dates when a specific reporting period is covered.

5. AUTHOR(S): Enter the name(s) of author(s) as shown on or in the report. Enter last name, first name, middle initial. If military, show rank and branch of service. The name of the principal author is an absolute minimum requirement.

6. REPORT DATE: Enter the date of the report as day, month, year; or month, year. If more than one date appears on the report, use date of publication.

7a. TOTAL NUMBER OF PAGES: The total page count should follow normal pagination procedures, i.e., enter the number of pages containing information.

7b. NUMBER OF REFERENCES: Enter the total number of references cited in the report.

8a. CONTRACT OR GRANT NUMBER: If appropriate, enter the applicable number of the contract or grant under which the report was written.

8b, 8c, & 8d. PROJECT NUMBER: Enter the appropriate military department identification, such as project number, subproject number, system numbers, task number, etc.

9a. ORIGINATOR'S REPORT NUMBER(S): Enter the official report number by which the document will be identified and controlled by the originating activity. This number must be unique to this report.

9b. OTHER REPORT NUMBER(S): If the report has been assigned any other report numbers *(either by the originator or by the sponsor)*, also enter this number(s).

10. AVAILABILITY/LIMITATION NOTICES: Enter any limitations on further dissemination of the report, other than those imposed by security classification, using standard statements such as:

(1) "Qualified requesters may obtain copies of this report from DDC."

(2) "Foreign announcement and dissemination of this report by DDC is not authorized."

(3) "U. S. Government agencies may obtain copies of this report directly from DDC. Other qualified DDC users shall request through _____."

(4) "U. S. military agencies may obtain copies of this report directly from DDC. Other qualified users shall request through _____."

(5) "All distribution of this report is controlled. Qualified DDC users shall request through _____."

If the report has been furnished to the Office of Technical Services, Department of Commerce, for sale to the public, indicate this fact and enter the price, if known.

11. SUPPLEMENTARY NOTES: Use for additional explanatory notes.

12. SPONSORING MILITARY ACTIVITY: Enter the name of the departmental project office or laboratory sponsoring *(paying for)* the research and development. Include address.

13. ABSTRACT: Enter an abstract giving a brief and factual summary of the document indicative of the report, even though it may also appear elsewhere in the body of the technical report. If additional space is required, a continuation sheet shall be attached.

It is highly desirable that the abstract of classified reports be unclassified. Each paragraph of the abstract shall end with an indication of the military security classification of the information in the paragraph, represented as *(TS)*, *(S)*, *(C)*, or *(U)*.

There is no limitation on the length of the abstract. However, the suggested length is from 150 to 225 words.

14. KEY WORDS: Key words are technically meaningful terms or short phrases that characterize a report and may be used as index entries for cataloging the report. Key words must be selected so that no security classification is required. Identifiers, such as equipment model designation, trade name, military project code name, geographic location, may be used as key words but will be followed by an indication of technical context. The assignment of links, roles, and weights is optional.